UNIVERSITY OF OKLAHOMA

GRADUATE COLLEGE

A REGIONAL MODELING STUDY OF CLIMATE CHANGE IMPACTS ON

WARM-SEASON PRECIPITATION IN THE U.S.

A DISSERTATION

SUBMITTED TO THE GRADUATE FACULTY

in partial fulfillment of the requirements for the

Degree of

DOCTOR OF PHILOSOPHY

By

MELISSA SUE BUKOVSKY
Norman, Oklahoma
2009

A REGIONAL MODELING STUDY OF CLIMATE CHANGE IMPACTS ON
WARM-SEASON PRECIPITATION IN THE U.S.

A DISSERTATION APPROVED FOR THE
SCHOOL OF METEOROLOGY

BY

_____

Dr. David Karoly, Co-Chair

_____

Dr. Frederick Carr, Co-Chair

_____

Dr. Jack Kain

_____

Dr. Susan Postawko

_____

Dr. Michael Richman

_____

Dr. Baxter Vieux

Acknowledgements

Data are available from the following websites:

CPC	http://www.cdc.noaa.gov
ERA-40	http://dss.ucar.edu/pub/era40
NARR	http://wwwt.emc.ncep.noaa.gov/mmb/rreanl/
NCEP Reanalysis 2	http://www.cdc.noaa.gov
NNRP	http://dss.ucar.edu/datasets/ds090.0/data/pgbf00-grb2d/
Environment Canada	http://www.climate.weatheroffice.ec.gc.ca
CMIP3 Dataset	https://esg.llnl.gov:8443/home/publicHomePage.do
CCSM at ESG	http://www.earthsystemgrid.org

Table of Contents

List of Tables

List of Figures

Abstract

Changes in the character of precipitation have already been observed over much of the United States. In a warming climate, the impacts of these changes will likely be felt most strongly through changes in the intensity and frequency of climate extremes. With precipitation, this has potential to be highly disruptive to the environment and the economy. However, while current global climate models may provide acceptable simulations of precipitation on a continental scale, they are lacking when it comes to properly portraying the characteristics of warm-season precipitation over the U.S., creating uncertainty in the projections of future precipitation in this area of the world. Because predicting climate change is essential for mitigation, adaptation, and planning purposes, assessing the uncertainty associated with climate change projections and producing adequate simulations of present climate is important.

This study proceeds in several parts to address this issue. It asks the overarching question of how climate change will impact warm-season precipitation over the U.S., focusing on precipitation extremes and the central U.S. region. To do so, the Weather Research and Forecasting (WRF) model is employed as a nested regional climate model to dynamically downscale output from the National Center for Atmospheric Research's (NCAR) Community Climate System Model (CCSM) version 3 and the National Center for Environmental Prediction (NCEP)/NCAR global reanalysis (NNRP). The latter is used for verification of late 20th century climate simulations from the WRF. In theory, the increase in horizontal resolution and sophistication of physical parameterizations in the WRF should improve the simulation of warm-season precipitation over the U.S., allowing a better representation of present climate and more reliable projections of future climate. As background, warm-season precipitation over the U.S. from current global climate models is assessed, as well as precipitation from current reanalyses in order to provide a basis for the comparison of model precipitation of the late 20th century.

This study finds that the WRF is able to produce precipitation that is more realistic than that from the sources of its forcing (the CCSM and NNRP). It also diagnoses potential issues with and differences between all of the simulations completed. Specifically, the magnitude of heavy 6h average precipitation events and the frequency distribution of precipitation over the central U.S. is greatly improved. Projections from the WRF for late 21st century precipitation show decreases in average May-August (MJJA) precipitation, but an increase in the intensity of both heavy precipitation events and rain in general when it does fall. A decrease in the number of 6h periods with rainfall accounts for the overall decrease in average precipitation. The WRF also shows an increase in the frequency of very heavy to extreme 6h average events, but a decrease in the frequency of all events lighter than those over the central U.S. Overall, projections from this study suggest an increase in the frequency of both floods and droughts during the warm-season in the central U.S.

1. Introduction

As stated in the Intergovernmental Panel on Climate Change's (IPCC) Summary for Policymakers (SPM) for the Fourth Assessment Report (AR4), "[w]arming of the climate system is unequivocal, as is now evident from observations of increases in global average air and ocean temperatures, widespread melting of snow and ice, and rising global mean sea level" (IPCC 2007). Warming, of course is not the only atmospheric consequence of increases in greenhouse gas concentrations, as many other variables are physically related to temperature. With this warming also comes increases in saturation vapor pressure; as, by the Clausius-Clapeyron relationship, at typical lower troposphere temperatures, the saturation vapor pressure increases by about 7% for every 1°K rise in temperature (Held and Soden 2006). If there is more water vapor in the atmosphere at warmer temperatures, it follows that changes in the hydrologic cycle would occur as temperatures increase, and observations along these lines have already been made (e.g. Kunkel et al. 1999, Groisman et al. 2001, Peterson et al. 2006, Pryor et al. 2009). This study is particularly concerned with changes in the hydrologic cycle manifested through changes in the character of precipitation. Naturally, changes are not and will not be uniform globally, so this study will focus on regional responses of precipitation to climate change.

Why focus on precipitation? Water resources are governed largely by it, and water is essential to life, so changes in the hydrologic cycle may have very significant impacts across many sectors. "If society is not well prepared for such changes and fails to monitor variations in the hydrologic cycle, large numbers of people run the risk of living under water stress or seeing their livelihoods devastated by water-related hazards such as floods" (Oki and Kanae 2006), and this is not to mention the consequences faced by natural ecosystems.

Climate change, however, is just one of many factors applying a stress on water. For example, population growth and economic development will likely have a much greater influence on water supply and demand than climate change (Vorosmarty et al. 2000), but changes of this nature are outside the scope of this study. All systems reliant on water avail-

ability and quality would be impacted by changes in precipitation; these include wetlands, other marine and terrestrial ecosystems, agriculture, industry, transportation, and development, among others. Changes in the character of precipitation are particularly important (e.g. intensity and frequency) as they will also impact the intensity and frequency of flooding, flash flooding, drought, and other precipitation-related extremes which, in turn, would affect erosion amounts, pollutant transport, structural planning, etc. (Arnell et al. 1996). Thus, they can be very disruptive to the environment and the economy (Easterling et al. 2000b, Nearing et al. 2005, IPCC 2008). It is important, therefore, to examine the influence climate change will have on precipitation, especially at sub-global scales. Appropriately, Gleick (2000) concluded that "in many cases and in many locations, there is compelling scientific evidence that climate changes will pose serious challenges to our water systems."

a. Observed Changes in Precipitation

A number of studies have already documented changes in observed precipitation. Though changes in precipitation are less spatially coherent than the changes that have been documented in global temperature, most of the world has tended towards wetter conditions during the 20th century (Alexander et al. 2006). There has been a global decrease in the number of consecutive dry days, and an increase in the number of wet days (Kiktev et al. 2003). Frich et al. (2002) have also reported an increase in the frequency of heavy precipitation events in more areas of the world than have decreases. They also documented an increase in the maximum 5 day precipitation totals over much of the globe (an indication of more flood-producing events). That is, wet spells produced higher precipitation totals in the latter part of the 20th century than in earlier decades (Frich et al. 2002, Alexander et al. 2006).

Observed changes have been generally consistent with a warming climate. An increase in global mean temperature would be followed by an increase in saturation vapor pressure and, thus an increase in the overall content of water vapor in the atmosphere (Douville

et al. 2002, Trenberth et al. 2003). The latter has been observed over most of the Northern Hemisphere (Ross and Elliott 2001), globally over oceans (Santer et al. 2007), at the surface worldwide (Willett et al. 2007), and is attributable mainly to human influences.

Over the United States, there has been an increase in cumulonimbus clouds (Sun et al. 2001) and in the frequency of thunderstorms (Changnon 2001), both consistent with the increase in observed water vapor content. Furthermore, Karl et al. (1995), Karl and Knight (1998), and Easterling et al. (2007) have documented an increase in precipitation over the U.S., and others have documented increases in other countries (e.g. Suppiah and Hennessy 1998, Iwashima and Yamamoto 1993). This is not necessarily due to an increase in all categories of precipitation; in many cases, an increase in mean precipitation is manifested through an increase in heavy precipitation. For example, Groisman et al. (1999) observed that changes in mean monthly precipitation disproportionately occur in heavy precipitation in several countries with sufficient records, and Easterling et al. (2000a) found that extreme precipitation events have been occurring more frequently over the U.S. and southern Canada. Likewise, Kunkel et al. (1999) and Groisman et al. (2005) have reported tendencies toward increasing heavy precipitation events, and Pryor et al. (2009) have shown that of U.S. observation stations that do show trends in extreme precipitation metrics, most tend toward increases in the number and intensity of these events, especially for those above the 95th percentile. Additionally, Pryor et al. (2009) report that the largest increase in the magnitude of extreme precipitation events has been found for the central Great Plains and northern Midwest. This region has also seen an increase in the frequency of precipitation.

b. The Future of Precipitation

It is well documented that climate models project an increase in globally averaged precipitation totals in a warming climate (e. g. Hennessy et al. 1997, Houghton and coeditors 2001, Trenberth et al. 2003, Meehl et al. 2007). This predicted global increase also applies to precipitation intensity (to a greater extent, Kharin et al. 2007), and the opposite to

precipitation frequency (Sun et al. 2007). Globally, Hennessy et al. (1997) concluded that there must be a decrease in lighter rain events or less frequent rain events to compensate for an increase in heavy rainfall without an equivalent increase in evaporation. In essence, large-scale mean precipitation is controlled by the energy budget, but extreme precipitation is related to moisture content which is related non-linearly with temperature; therefore, extreme precipitation can increase more than the mean. Thus, for precipitation, impacts of a warming climate are likely to be felt more through changes in intensity and frequency than through changes in the mean.

Projections for future changes in precipitation follow along these lines. In the future, mean precipitation is generally projected to increase in the tropics and at high latitudes and decrease in the subtropics (with an overall globally averaged increase) - the result of a strengthening of the global hydrological cycle (Meehl et al. 2007). Similarly, Benestad (2006) found an increase in future simulated precipitation extremes, especially in middle and high latitudes. In that study, global warming produces enhanced tropical convection, enhanced stratiform precipitation in mid-latitudes, and a decrease in heavy precipitation in the subtropics. Watterson (2006) also indicated an increase in the mean and extreme rainfall intensities associated with extratropical cyclones, especially over Northern Hemisphere continents, using 2 global climate models. Furthermore, Kharin and Zwiers (2005) found an increase in extremes in almost all regions of the world, but a decrease in the mean in some places. As such, in some areas, an increase in precipitation extremes will come with an overall drier climate, as less lighter precipitation occurs between events and this may be augmented by an increase in evapotranspiration in a warmer climate (McGuffie et al. 1999, Allen and Ingram 2002, Kharin and Zwiers 2005, Meehl et al. 2005, Tebaldi et al. 2006). The studies of Tselioudis and Rossow (2006), Pall et al. (2007), and Stephens and Ellis (2008) also note the increase in the intensity of storms with longer periods of time between them.

The distribution of changes around the globe is not uniform. In general, global climate models project that areas that are already wet in the present climate will become wetter and those that are already dry will become drier (Held and Soden 2006, Seager et al. 2007, Sillmann and Roeckner 2008, Stephens and Ellis 2008). Patterns of change are sensitive to shifts in circulation, advection, and are related with areas that already experience mean moisture convergence or divergence.

Other related responses of the hydrologic cycle are likely. Held and Soden (2006), for instance, found a decrease in convective mass fluxes, an increase in the horizontal transport of moisture, an enhancement in the pattern of evaporation minus precipitation, and changes in the horizontal transport of sensible heat in model simulations produced for the IPCC AR4. The decrease in model convective mass fluxes, model vertical velocities (Vecchi and Soden 2006), and the shift projected in the frequency and intensity of heavy precipitation are all indicators of changes in the atmospheric component of the hydrologic cycle.

c. Precipitation Simulation Using Climate Models

Many of the potential consequences of climate change on water-related issues are based on predicted changes in the characteristics of precipitation; yet, on a global scale, precipitation prediction is still lacking, despite simulated trends that generally match observed trends in precipitation (Dai 2006). Warm-season deep convection is the main component of precipitation in many parts of the U.S., yet climate model simulations of warm-season, continental convection and associated precipitation do not compare well with observations. Errors in the distribution, frequency, intensity, and diurnal cycle of simulated precipitation then affect simulations of the hydrologic cycle. Much of the uncertainty involved in predictions of precipitation under climate change scenarios is rooted in model resolution and dependence on convective parameterization (Chaboureau et al. 2003, Duffy et al. 2003, Leung et al. 2003, Liang et al. 2004b, Sun et al. 2006). Uncertainty compounds in the prediction of precipitation at regional scales owing to resolution issues; coarse resolution

climate models have problems with topography, eddy processes, and subgrid parameter-izations, giving them little predictive ability at regional scales (Duffy et al. 2003). This creates additional error that will propagate through to the prediction of precipitation. Un-fortunately, higher resolution models have problems reproducing regional scale precipita-tion features as well, again due to their dependence on convective parameterization (Liang et al. 2006). Commonly-noted problems here and in coarser resolution models include a failure to represent the nocturnal maximum in convection that exists over the U.S. Great Plains, precipitation that is too early, too frequent, and too light, and an unrealistic diur-nal cycle in some regions (Randall et al. 1991, Garratt et al. 1993, Dai et al. 1999, Lin et al. 2000, Groisman et al. 2000, Zhang et al. 2003, Davis et al. 2003, Liang et al. 2004b). There is, however, some hope at higher resolutions, as results have been obtained that better match observations by high resolution climate models and nested regional climate models (Duffy et al. 2003, Leung et al. 2003, Leung and Qian 2009).

The prediction of convection in climate and numerical weather prediction models re-quires that both the initiation and evolution of convection be realistically captured (Kain and Fritsch 1992, Betts and Jakob 2002, Jakob and Siebesma 2003, Bechtold et al. 2004). Each convective parameterization scheme (CPS) uses a different combination of factors to describe the cause-and-effect relationship between convection and larger-scale processes, and there is little agreement on which factors are best. Portraying the evolution of con-vection is even more challenging, especially when the convection is organized. Orga-nized mesoscale convective systems produce most of the warm-season rainfall over the U.S. (Fritsch et al. 1986), and the failure of convective schemes to correctly portray them has been blamed for the serious deficiencies seen in simulated warm-season rainfall clima-tologies over the U.S. (Davis et al. 2003). In addition, convective parameterizations play a significant role in determining cloud and water vapor distributions and vertical profiles of temperature and moisture, all major uncertainties in climate models (NRC 2003).

Problems that exist with the simulation of warm-season convection over the central U.S. (a focus area for this study) are two fold - they encompass both the convective parameterization problem and the issue of model resolution. Not only do convective schemes have problems with the main type of convection over this part of the country, but at coarse resolutions, the necessary mesoscale processes that produce favorable conditions for mesoscale convective systems (MCS) may not be captured. That is, processes that converge moisture into the central U.S., produce a low-level jet, and then convert that converged moisture into precipitation near the northern terminus of the low-level jet (LLJ) must be simulated (Augustine and Caracena 1994).

Global climate models do not do well with this, partly because of their resolution. Though Cook et al. (2008) show that LLJs are produced in the Great Plains in the 18 global climate models (GCMs) run for the IPCC AR4 that they examined, most are not captured well; i.e., the position or magnitude is off. Precipitation in the models that more accurately simulate a LLJ is not necessarily better either.

d. An Introduction to Regional Climate Prediction

Regional climate modeling (or dynamic downscaling) has become increasingly popular and important as impacts from climate variability and change at regional levels cannot be diagnosed well using GCMs. To obtain higher spatial resolution data using dynamic downscaling, a regional model is generally used with initial and boundary conditions from a GCM or reanalysis (thus, it is also known as nested regional climate modeling). This approach allows regional climate features and extreme events to be more realistically simulated and, as mentioned above, has been shown to produce results that are more accurate than those from the driving GCM (Fowler et al. 2005, Frei et al. 2006, Liang et al. 2006). There are some immediate downsides to downscaling GCM output in this manner: it is computationally intensive and the regional model will also inherit biases from the GCM, which will only add to prediction uncertainty. A regional climate model (RCM) will usu-

ally have a different horizontal and vertical resolution and set of parameterizations than the global model driving it. This can contribute to inconsistencies within an RCM simulation as well.

Nesting a regional model with a global model is not a new concept. It has been done in numerical weather prediction for years. However, for climate, it is relatively new. One of the first applications of this concept for climate (if not the first, as it appears to be in the published literature), was done by Dickinson et al. (1989). They used the National Center for Atmospheric Research (NCAR) Community Climate Model version 1 (with a 500-km horizontal resolution) as forcing for the Pennsylvania State University/NCAR Mesoscale Model version 4 (MM4) (with a 60-km horizontal resolution) over the western U.S. for a 3 year simulation period. The goal of this study was to assess the ability of this approach to provide better characteristics of future climate, especially in regards to any change that might raise the water table near a potential high-level nuclear waste storage facility (Yucca Mountain, NV). The results of Dickinson et al. (1989) indicated that this method greatly improved winter precipitation patterns. Further outcomes of existing studies and more details regarding the challenges of region climate modeling will be reviewed in chapter 4.

There is also the option of statistically downscaling GCM output to gain regional detail. This is generally a much simpler method of downscaling. It is relatively cheap, computationally efficient, and many different methods have been developed to generate higher-resolution data from coarse GCM output. These range from simpler perturbation and regression methods to more complex weather typing and weather generator schemes. One of the greatest weaknesses of this method, however, is that statistical downscaling tends to underestimate variance and does not represent extreme events well (Fowler et al. 2007), though new methods have been applied successfully to extremes with strong links to large-scale variables (e.g. wintertime U.S. precipitation, Wang and Zhang 2008). Part of the problem with extremes exists because these methods assume that regional climates are purely a function of the large-scale atmospheric state, while this is only true for part

of a regional or local climate. It is also assumed, when using statistical downscaling, that relationships used to represent the present will hold in the future (Christensen et al. 2007).

e. Objectives

Because the prediction of climate change is vital for mitigation, adaptation, and planning in various sectors of society, the economy, and the environment, knowing the magnitude of uncertainty associated with different aspects of prediction is important.

This study proceeds in several parts in order to answer a host of questions. The overarching question is, of course: how will climate change impact warm-season precipitation over the United States?

In order to attempt an answer to this question, others will be addressed first.

To start, a dataset representing observed precipitation with an adequate spatial and temporal resolution over the time periods of the 20th century analysed in this study is necessary. Chapter 2 provides an overview and analysis of work done to find a reanalysis with a realistic representation of some of the climatological characteristics of summertime U.S. precipitation. Limitations of these datasets are also explored.

Next, this study provides a better understanding of how current climate models simulate U.S. warm-season precipitation. It investigates possible causes for differences between some of the 20th century climate model runs produced for the IPCC AR4 and what their limitations are when it comes to reproducing summertime precipitation characteristics. A brief analysis of some of the climate model projections for the future of precipitation over specific regions in the U.S. is also presented.

Finally, this study asks whether or not the Weather Research and Forecasting (WRF) model is useful for dynamically downscaling global climate model output, what it projects for precipitation changes in a warming climate, and why some of its simulations differ from others. As chapter 3 and other studies demonstrate, coarse resolution climate models are not able to accurately represent topography and other sub-grid scale features, making

it difficult to assess climate on a regional scale. Given that statistical downscaling requires strong ties between the variable to be downscaled and large-scale predictors and does not handle extremes well, and this work focuses on warm-season precipitation and precipitation extremes over the U.S., which is partly dependent on local and mesoscale circulations, dynamic downscaling is used. Dynamical downscaling also makes it possible to test the sensitivity of the precipitation climatologies to variations in setup of the WRF model, as done in chapter 4. In theory, the increase in resolution provided by the WRF model should improve the simulation of warm-season precipitation over the U.S. However, summertime convective precipitation is difficult to simulate to start, and the benefits from a change in resolution are sometimes masked by the sensitivity of the model physics to resolution (Giorgi and Marinucci 1996).

Chapter 5 addresses the use of the WRF as a nested regional climate model for the present to determine if it provides an improved simulation of climatological precipitation characteristics relative to that given by current climate models. Applied to future climate change scenarios, nested regional climate simulations give more detailed simulations of precipitation in a warmer climate and another possible outcome given a set of boundary and initial conditions from an existing global climate simulation.

Projections from the WRF are given in chapter 6. This is followed by a more in depth explanation of some of the differences seen in chapters 5 and 6. The latter is presented because a more detailed projection does not necessarily indicate that there is less uncertainty in it. Examining some of the underlying mechanisms responsible for the projected changes and differences between the different model simulations used, as done in chapter 7, helps quantify part of the uncertainty always involved in climate simulation and projection. The last chapter provides a summary and final discussion of the results presented in this dissertation.

.

2. Reanalysis Intercomparison

This chapter has been published in the Journal of Hydrometeorology under the title: "A Brief Evaluation of Precipitation from the North American Regional Reanalysis" (Bukovsky and Karoly 2007). Precipitation from observations and in reanalysis datasets has been compared to establish their validity and usefulness for comparison against the climate models. Some interesting results were found during this comparison, and led to this publication.

a. Introduction

Many studies utilize the combination of observations and model assimilation and integration known as "reanalysis" data as a benchmark for model comparison, while others employ it to create initial conditions for case studies or for regional climatology or hydrometeorological analysis (e.g. Hane et al. 2001, Betts 2004, Ruiz-Barradas and Nigam 2005). Reanalyses basically provide another data set for use in further understanding our environment. They are, however, only an estimate of the real state of the atmosphere. Using reanalysis data may inadvertently add inaccuracies to a study if the data are not used with caution, as they do not always match what is observed, particularly for precipitation (Higgins et al. 1996b, Betts et al. 1998, Kållberg et al. 2004, West et al. 2006). In this respect, precipitation reanalyses are in a different category relative to other available reanalysis variables. Identifying inaccuracies that reanalyses may contain is the first step towards correcting them. This chapter, therefore, aims to identify some strong and weak points in the precipitation field from the North American Regional Reanalysis (NARR, Mesinger et al. 2006) and several other available reanalyses.

In general, qualitative similarities and differences between the different reanalyses are identified in terms of precipitation in the North American region. This study concentrates on the NARR precipitation climatology over a domain encompassing the United States

with an emphasis on warm-season precipitation during the 1990s. The spatial distribution, intensity, diurnal cycle, and annual cycle of precipitation are explored in order to establish the reliability of the reanalyses. The goal is to identify the usefulness of the NARR versus the other precipitation datasets and to provide a warning to potential users about some of the inaccuracies the reanalyses may contain.

b. *Reanalyses and Methods*

Precipitation from three reanalyses and one objectively analyzed dataset are used in this study; their descriptions follow. The objectively analyzed dataset will be used to approximate the "truth". Unless otherwise noted, all results use the original horizontal resolution of the data. Interpolating reanalyses to matching grids does not change the qualitative results presented in the next section.

The National Center for Environmental Prediction (NCEP)/Department of Energy (DOE) Atmospheric Model Intercomparison Project (AMIP-II) global reanalysis (NCEP-DOE (also known as R-2), Kanamitsu et al. 2002), the European Center for Medium-Range Weather Forecasts' global reanalysis (ERA-40, Kållberg et al. 2004), and NCEP's NARR (Mesinger et al. 2006) were chosen because of their widespread use and potential for application in verification and diagnostic studies. The Climate Prediction Center's hourly U.S. objectively analyzed, gridded, observationally based precipitation dataset (hereafter referred to as CPC, Higgins et al. 1996a) was chosen for its time resolution, successful application in other studies (e.g. Trenberth 1998, Dai 1999), and full U.S. coverage.

These reanalyses were originally gathered and compared for use in climate model verification, but interesting results were found during the comparison which motivated this review. As data from the models at a high temporal resolution are only available from 1991-2000, that decade was used in the verification and will also be used for this study. Where precipitation rate data is referred to as being hourly, three-hourly, or six-hourly, it

has been averaged over that span of time, starting at a given hour (e.g. a value at 0300 UTC from three-hourly data would be the average precipitation rate from 0300-0600 UTC).

1) NCEP-DOE

The NCEP-DOE is an updated version of the NCEP/NCAR global reanalysis project (NNRP, Kalnay et al.1996). The assimilation system that produces the NCEP-DOE is an improved version of the system that created the NNRP. It utilizes a version of the NCEP global spectral model. The horizontal resolution is approximately 209-km (T62) and there are 28 vertical levels. Parameterizations of convective and large-scale precipitation, shallow convection, gravity wave drag, radiation, and boundary layer processes are included. The convective parameterization, is a version of the modified Arakawa and Schubert (1974, hereafter AS) scheme that was developed by Pan and Wu (1994). Observed precipitation is not assimilated in the NCEP-DOE; thus, all precipitation fields are based on physical parameterization and are calculated during the assimilation process. Data from the NCEP-DOE are available from 1979 to 2005, and this study uses the 6-hour daily precipitation fields (averaged to 6-hour monthly) from 1991-2000.

2) ERA-40

The ERA-40 system is based on the 1.125°x1.125° (T159, approximately 125 km), 60 level IFS CY23r4 atmospheric model[1] . As with the NCEP-DOE, the ERA40 does not assimilate any precipitation observations. Convective precipitation is produced by the bulk mass flux scheme described in Tiedtke (1989). Once again, 6-hour monthly average precipitation fields from the ERA-40 are used from 1991-2000.

---

[1]http://www.ecmwf.int/research/ifsdocs/CY23r4/index.html

3) NARR

The final reanalysis used in this study is the relatively new, higher resolution NARR from NCEP. Reanalysis fields are available from 1979 to the present every 3 hours at a 32-km/45 layer resolution. Data are also used in a 6h monthly averaged form to match the other reanalyses. The NARR system utilizes a version of the Eta Model and its 3D-Var Data Assimilation System (EDAS) similar to the version that was operational in April 2003 (Mesinger et al. 2006). Differences from the operational version include a lower resolution, a different microphysics parameterization, and an increased number of observational sources. The model utilizes the Betts-Miller-Janjić convective parameterization (BMJ, Betts 1986, Janjić 1994) which is a convective adjustment type scheme. Unlike the NCEP-DOE and ERA-40, however, the NARR system does assimilate precipitation observations as latent heating profiles, as described in Lin et al. (1999). The precipitation fields, therefore, are not purely determined by the assimilated large-scale variables and the model's physical parameterizations. Precipitation data for assimilation comes from the following sources: for Mexico and Canada, a 1° rain gauge analysis is used; over the continental United States, a 1/8° rain gauge analysis is included; the CPC merged analysis of precipitation (CMAP) global 2.5° analysis is used over oceans south of 27.5°N and land south of Mexico; no data are assimilated for oceans north of 43.5°N (Mesinger et al. 2006).

4) CPC

An objective analysis of precipitation from U.S. station reports from the NWS/Techniques Development Laboratory as described in Higgins et al. (1996a) is used to judge the validity of precipitation in the three previously described reanalyses. This analysis is available hourly from 1948 to 2002 on a 2° latitude by 2.5° longitude grid that extends from 140°W to 60°W and 20°N to 60°N. Some uncertainty is involved in the use of this analysis because it is based on station data and, therefore, influenced by changes in the density, configura-

tion, and temporal continuity of the observation sites, among other factors. As precipita-tion amounts are objectively analyzed onto grid points using a modified Cressman scheme (Cressman 1959) even if no rain gauge observations exist (for instance, over the oceans), comparisons using this information will only be done over land. To match the reanalyses, the CPC dataset is averaged to a 6-hour monthly time resolution.

Before comparison, it should be noted that the NARR and the CPC analysis are not independent datasets. They both include some of the same precipitation observations as in-put. Specifically, the HPD[2] dataset was incorporated into the CPC analysis and assimilated into the NARR over the continental U.S. Although the NARR and the CPC analysis are, therefore, expected to be similar, the ingestion of precipitation data into the NARR did not guarantee that the reanalysis would match the observations after assimilation (Mesinger et al. 2006). Any divergence of the CPC from observations would be due to the objec-tive analysis of the data., The CPC analysis is therefore used as a close and conveniently gridded approximation of the "truth".

c. Results

1) REANALYSIS PRECIPITATION

As illustrated in the left half of Fig. 1, there is a general agreement in the distribution of precipitation rate over the continental United States on an annual average basis between the NARR, ERA-40, NCEP-DOE, and the CPC dataset. Discrepancies between each of these, however, come out in the details, which are important when the data are used for weather, hydrological, and climate research. All of the datasets capture the average annual maximums in the southeast and northwest U.S. The NCEP-DOE, however, produces a slight excess of precipitation over the southeast, although this excess is improved compared to that in the NNRP (not shown, see Kalnay et al.1996, Trenberth and Guillemot 1998).

---

[2]Hourly Precipitation Data from U.S. observing stations (Hammer and Steurer 1997)
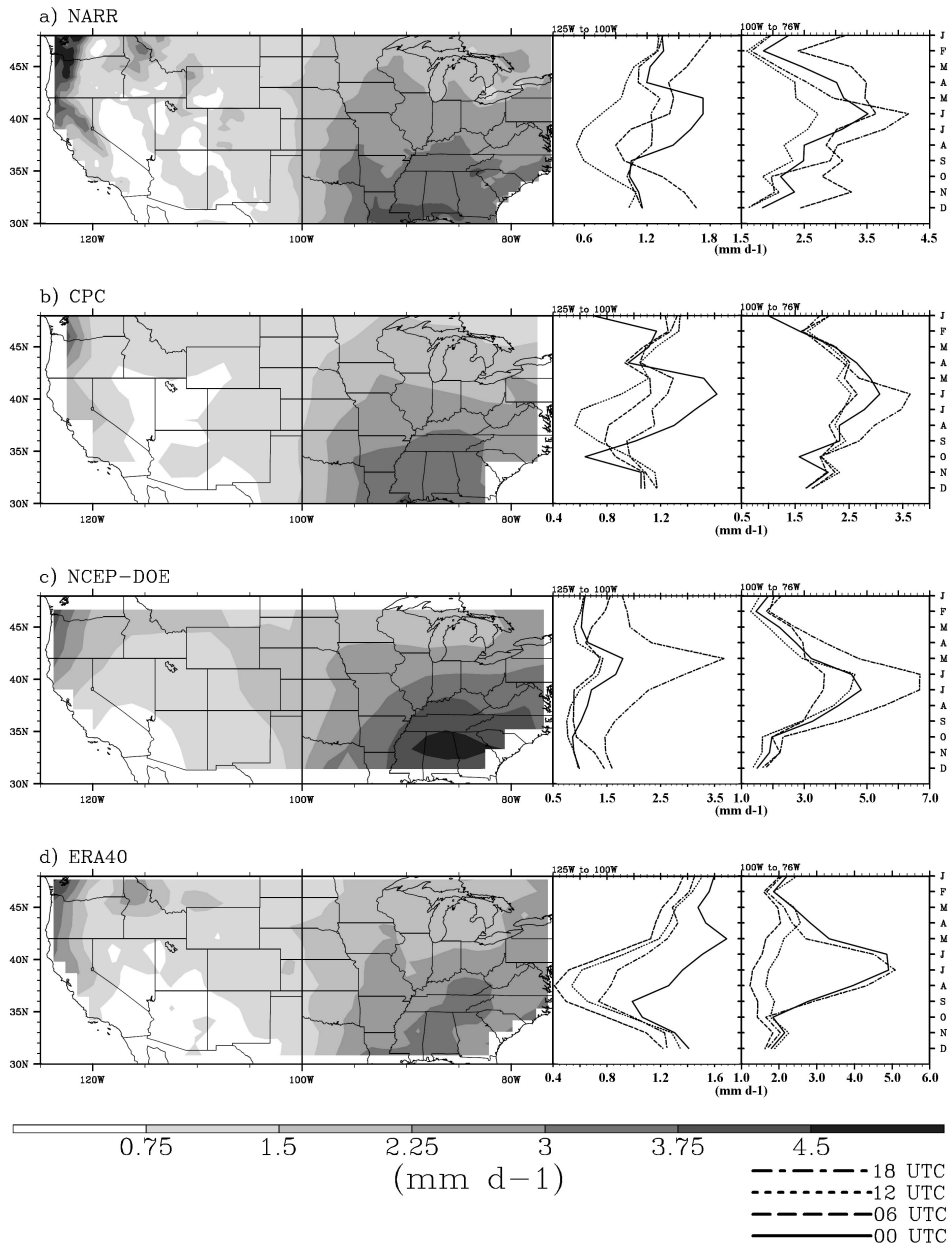
FIG. 1. 1991-2000 annual average precipitation rate (left column, mm/day) and 6h monthly average precipitation rate for the domain shown in the left column from 125°W to 100°W (center column, mm/day) and from 100°W to 76°W (right column, mm/day) excluding the oceans for: a) NARR, b) CPC, c) NCEP-DOE, d) ERA-40. Month of the year is noted on the right-most y-axis by the first letter of each month. The U.S. divide at 100°W is indicated on the images in the left column by the heavy black line. Note: every other grid point from the NARR dataset was used here, decreasing its resolution to 64-km, to prevent NARR data arrays from overflowing.

This surplus of precipitation primarily occurs during the June-August (JJA) season, but is strong enough to show up in the annual average. The NARR agrees well with the CPC dataset over the continental U.S., the slight differences are mostly due to the immense differences in resolution.

The right-hand side of Fig. 1 shows the annual cycle of precipitation for the western (center column) and eastern (right column) halves of the domain shown in the left half of Fig. 1 for 6h monthly averaged time periods over land only. The annual cycle figures were split to cover the domain from 125°W to 100°W and from 100°W to 76°W in order to remove some of the issues that arise when averaging the diurnal cycle in UTC over several time zones. Separated in this way, there are approximately two time zones per figure (a fact that should be kept in mind when interpreting them) and the areas of the country dominated by cool season and warm-season precipitation are somewhat divided. Over the eastern half of the U.S., all of the reanalyses correctly produce the summertime maximum in the annual cycle. It is, however, too pronounced in the NCEP-DOE (mostly because of the excessive precipitation in JJA over the Southeast). This is also the case in the ERA-40, but not to the same extent. Fall, winter, and spring average rates over the eastern half of the U.S. are much more reasonable in all of the reanalyses, as are the distributions of precipitation during these seasons (not shown).

There are disagreements in the average U.S. diurnal cycle over the eastern half of the country between all reanalyses. Regardless, all reanalyses, agree that the maximum in warm-season precipitation occurs around 1800 UTC[3], consistent with the timing of the climatological plethora of precipitation in the Southeast. There are also issues with the diurnal cycle of precipitation throughout the cool season, but the diurnal cycle is not as amplified at this time of year, so this is not as obvious. The NARR, for all other seasons, places a strong peak in the diurnal cycle around 0600 UTC; the root of this problem will be discussed in the next section.

---

[3]Note that precipitation rate values are 6-hour average values; therefore, times are approximate, cover a 6-hour period, and only give a general sense of the diurnal cycle.
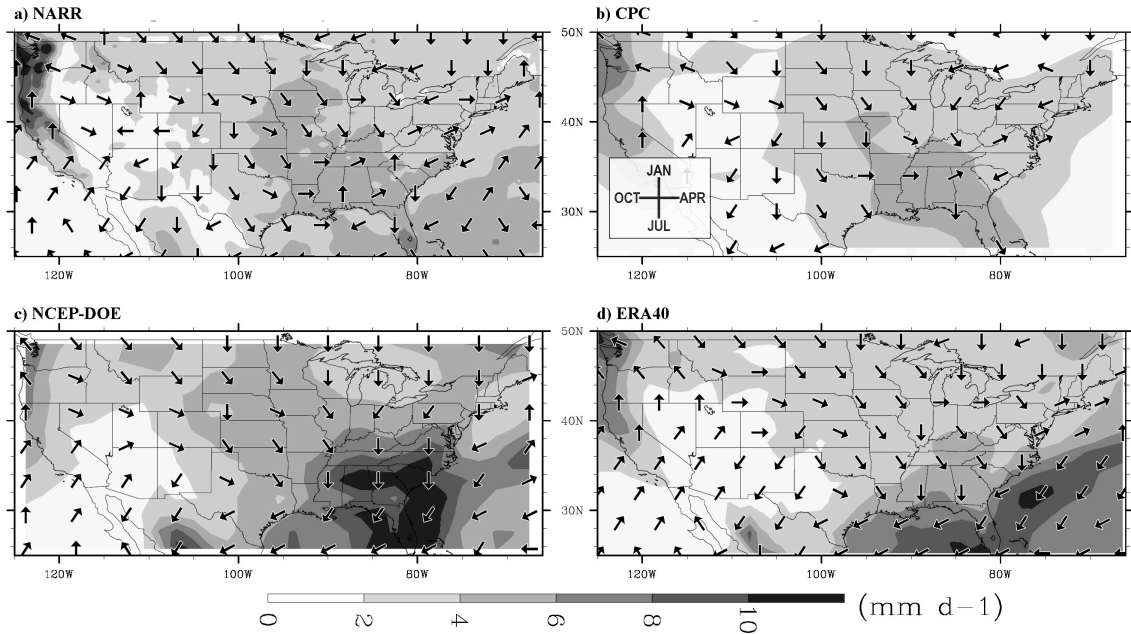
FIG. 2. 1991-2000 maximum monthly average precipitation rate (mm/day, contours) and month of maximum (vectors) from a) NARR, b) CPC, c) NCEP-DOE, d) ERA-40. Vector key inset in b). Vectors placed at the horizontal resolution of the data in all panels except panel a), where they have been "thinned". Ocean vectors in b) have been masked since the CPC data is only valid over land. Note: NARR data horizontal resolution decreased as in Fig. 1.

Over the western half of the U.S., the NARR and ERA-40 correctly place maximums in the annual cycle in the winter and an early evening peak in the summer, while the NCEP-DOE places the maximum in the spring (note that the winter maximum would be stronger if the coastal data were not removed by the ocean mask, not shown). The magnitude of the average wintertime precipitation is also well handled. The diurnal cycle of precipitation in the winter is problematic, but, again, it is not as amplified as the warm-season diurnal cycle and, therefore, is not as obvious. Discrepancies here are largely due to differences in the timing of precipitation over Washington and Oregon. The enhanced summertime diurnal cycle in the west is well captured by the NARR and ERA-40, which both correctly place the peak time of precipitation around 0000 UTC and minimum around 1200 UTC. The NCEP-DOE, for all seasons places the peak of the diurnal cycle around 1800 UTC.

18

More details on the spatial distribution of the annual cycle of precipitation rate over the U.S. are given in Fig. 2. As with the annual average precipitation rate, this figure shows that the reanalyses and the CPC dataset are in general agreement in terms of the distribution and timing of the maximum monthly average precipitation rate. The eastern half of the U.S. is dominated by warm-season precipitation, while cool season months receive the most precipitation along the west coast. However, some disagreements are evident; especially near the transition zones between two dominant seasons of precipitation (this is especially true in the western half of the U.S.).

A closer look will now be taken at the JJA convective season. Figure 3 shows the maximum average 6-hour seasonal precipitation and its time of occurrence for JJA. For ease of interpretation, the time of the maximum precipitation in this figure is presented in LST instead of UTC. Also, note that the distribution of the maximum 6-hourly precipitation in this figure is similar to the distribution of the average JJA precipitation (not shown). As in the annual distribution, it is obvious here that the NCEP-DOE produces a surfeit of precipitation in the Southeast. The ERA-40 and NARR, however, well represent the maximum and timing of the maximum precipitation over the Southeast that is associated with the afternoon peak in surface heating and atmospheric instability, as measured against the CPC dataset.

The other important region of precipitation during JJA occurs over the Great Plains. Precipitation that produces the nocturnal maximum over this region in JJA is primarily produced by MCSs that organize from convection initiated on the east slope of the Continental Divide typically in the late afternoon. These systems usually propagate into the Midwest during the late evening and early morning (Carbone et al. 2002). Figure 3 illustrates that the NARR captures this process, while the ERA-40 and NCEP-DOE generally do not[4]. The location of the Plains maximum is displaced eastward in the ERA-40, and because the time of the maximum precipitation does not change much from west to east to

---

[4]To capture some detail in the NCEP-DOE southeastern U.S. precipitation, a gray scale was used in Fig. 3 that does not emphasize this important secondary maximum.
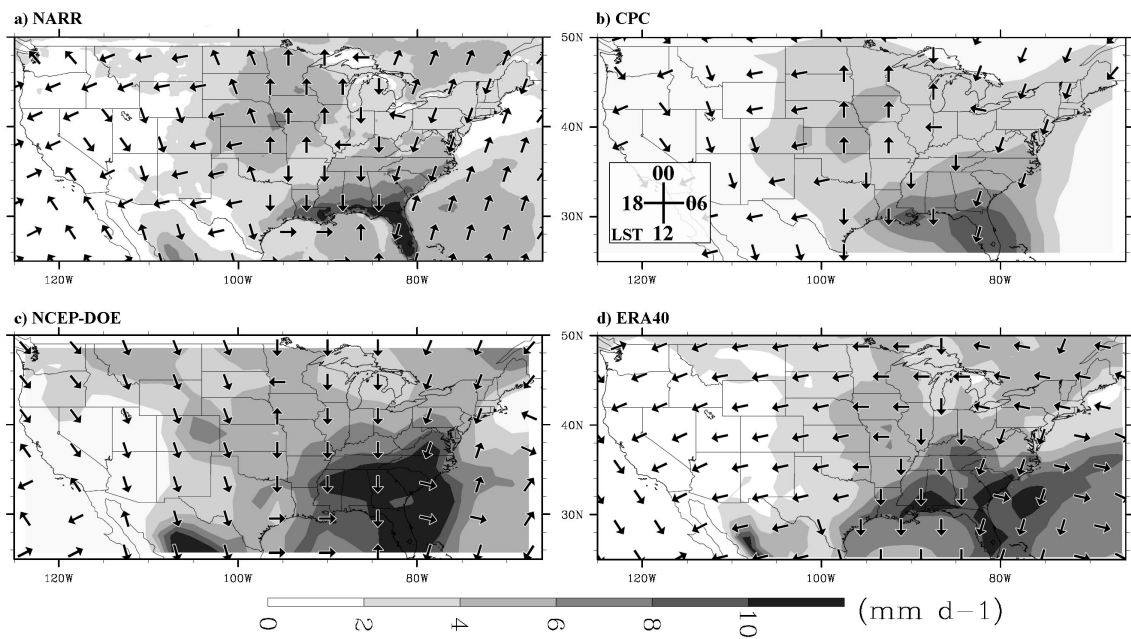
FIG. 3. 1991-2000 JJA maximum 6h seasonal average precipitation rate (mm/day, contours) and time of maximum (vectors, LST) from a) NARR, b) CPC, c) NCEP-DOE, d) ERA-40. Vector time clock key inset in b). Vectors placed at the horizontal resolution of the data in all panels except panel a), where they have been "thinned". Ocean vectors in b) have been masked since the CPC data is only valid over land. Note: the NARR data has been used at its full 32-km resolution and not 64-km as it was in Fig. 1.

indicate propagating convection, it is doubtful that the maximum encompasses the correct convective process. The NCEP-DOE does have a secondary maximum centered in eastern Colorado and a grid cell in northeast Kansas where the maximum occurs around 0000 UTC, but the overall pattern of maximum precipitation in the central portion of the U.S. is not captured well, and the timing of the maximum precipitation in the Midwest is off by around 12h everywhere except for the aforementioned location in Kansas and an area in south-central Minnesota . Pattern correlations for the maximum amplitude and the timing of the maximum were computed for this region (87°W to 108°W and 34°N to 47°N) to quantitatively compare the amplitude and phase. The CPC, NCEP-DOE, and the ERA-40 were measured against the NARR after regridding the NARR to match the horizontal resolution of each individual dataset. Comparisons were completed using the NARR instead of the CPC dataset since the goal of this study is to examine the usefulness of the NARR relative to the other datasets. Computing correlations against the NARR also allows for a greater resolution to be used in the comparisons, as the CPC has the lowest spatial resolution of all the datasets. The correlations for the maximum amplitude in the CPC, ERA-40, and the NCEP-DOE are 0.925, 0.671, and 0.268, respectively, and for the time of the maximum, 0.686, 0.385, and 0.287. The correlation for the timing of the maximum is lower between the NARR and CPC than for the amplitude. This is likely because the transition from afternoon to evening precipitation occurs further west in the NARR than in the CPC. Otherwise, the correlation values reinforce the qualitative statements made above.

2) A CLOSER LOOK AT NARR PRECIPITATION

As shown above, NARR precipitation is superior to the other reanalyses examined over a domain encompassing the U.S., as it was designed to be. The previous results are consistent with the statement made by Mesinger et al. (2006, pg. 344) that "the assimilation of precipitation during the reanalysis was found to be very successful, obtaining model precipitation quite similar to the analyzed precipitation input." To further illustrate the

usefulness of the NARR, an example of an extreme event will be given to show that the NARR captures such events, even over western topography. But first, some quirks possibly caused by the model ingestion of the precipitation observations and other issues in the precipitation reanalysis are presented as a warning to potential users of this reanalysis. Since precipitation over the contiguous U.S. in all seasons at all times appears to be very good[5] overall, but other users may draw on the data outside of the contiguous U.S., the information presented below is seen as completely relevant.

To start, the different precipitation observations used in creating the NARR are revealed through minimums in precipitation along the U.S.-Canada and U.S.-Mexico borders (see Fig. 3a, but note that these are observed more readily with finer contour intervals). More details on this discontinuity can be found in Mo et al. (2005). Other interesting features are also apparent. For instance, as shown in the rightmost panel in Fig. 1a, when averaged over a domain encompassing the eastern half of the U.S., the peak in the diurnal cycle does not match observations in all months. With the precipitation in a 6-hour monthly averaged form, the peak occurs at 0600 UTC, but in its original 3-hourly form, this shows up as an even stronger peak at 0900 UTC in all seasons, and is caused by exceptionally heavy precipitation at 0900 UTC in Ontario and Quebec. This is due to large precipitation systems that show up at 0900 UTC and unrealistically disappear by 1200 UTC. An example of a day where one of these systems occurs is shown in Fig. 4. Observations for the nearest stations that archived observations on that day are shown in Table 1. As the locations of the stations and the observations indicate, the system that occurred around 0900 UTC on this day may or may not have existed; however, it is much like others that often occur at 0900 UTC and its evolution does not seem realistic. This problem is greatest in the fall, but it is also quite obvious in summer and spring. Systems like these show up often enough and are intense enough to also impact the frequency distribution of precipitation in individual seasons and over the whole year when a domain is used that includes part of southeast Canada (not

---

[5]One exception, however, was made by West et al. (2006) in the occasional occurrence of spurious grid-scale convection. This is not obvious in any of the climatological fields presented here though.
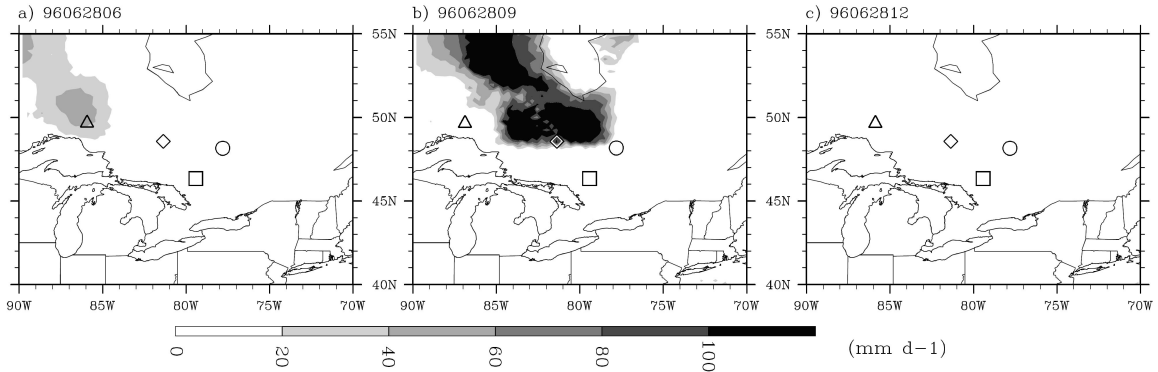
FIG. 4. 3h average precipitation rate from the NARR for June 28, 1996. a) 0600 UTC, b) 0900 UTC, c) 1200 UTC. Symbols indicate locations of stations listed in Table 1: Geraldton, Ontario (triangle); Timmons, Ontario (diamond); North Bay, Ontario (square); Val-d'or, Quebec (circle).

TABLE 1. Observations from 28 June 1996 for the four stations shown in Fig. 4. Times where observations are not available are indicated as n/a.

Time (UTC)	Geraldton (triangle)	Timmons (diamond)	North Bay (square)	Val-D'or (circle)
0300	Mostly Cloudy	Cloudy	Mostly Cloudy	n/a
0400	Cloudy	Cloudy	Mostly Cloudy	n/a
0500	Cloudy	Cloudy	Mainly Clear	n/a
0600	Cloudy	Cloudy	Mainly Clear	n/a
0700	Thunderstorms	Cloudy	Mostly Cloudy	n/a
0800	Thunderstorms	Cloudy	Mostly Cloudy	n/a
0900	Thunderstorms	Cloudy	Mostly Cloudy	Mostly Cloudy
1000	Thunderstorms	Cloudy	Cloudy	Mostly Cloudy
1100	Thunderstorms	Mostly Cloudy	Cloudy	Mostly Cloudy
1200	Thunderstorms	Mostly Cloudy	n/a	Mostly Cloudy
1300	Rain Showers	Cloudy	n/a	Cloudy
1400	Cloudy	Cloudy	Mostly Cloudy	Cloudy
1500	Thunderstorms	Cloudy	Cloudy	Cloudy
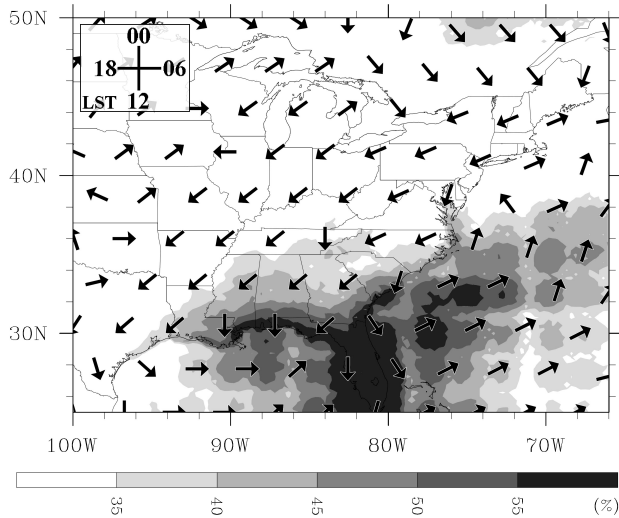
FIG. 5. NARR 1991-2000 JJA maximum frequency of 3h precipitation rate greater than 1 mm/day (percent, contours) and time of maximum frequency (vectors, LST). Vector time clock key inset in figure.

shown). Mesinger et al.(2006, p. 357) do note that the precipitation field over Canada is "not as good as we had hoped for" due to a small number of rain gauge observations, but this is likely not a complete explanation for these events. Finding the exact cause, however, is beyond the scope of this study.

Mesinger et al. (2006) also warn that the NARR is meant to be chiefly used over land and not to be fully trusted over the oceans (especially the northern oceans) due to the lack of observations; however, one ocean oddity was noticed that is worth pointing out. Figure 5 shows the time and magnitude of the maximum frequency of 3-hour precipitation greater than 1 mm/day (which is also representative of the spatial distribution of the average frequency of precipitation) for JJA. It shows peculiar bull's-eyes of greater frequency in the waters surrounding the southeast U.S. coast that seem to be gridded at approximately a 2.5° interval, the same spacing as the ingested precipitation observations. It is likely, therefore, that some part of the assimilation of the CMAP data is responsible for the bull's-eyes of precipitation that show up sporadically over these waters (e.g. see Fig. 6). These abnormally round areas of precipitation do fit to and are likely responsible for the apparently 2.5° gridded bull's-eyes on the frequency plot.
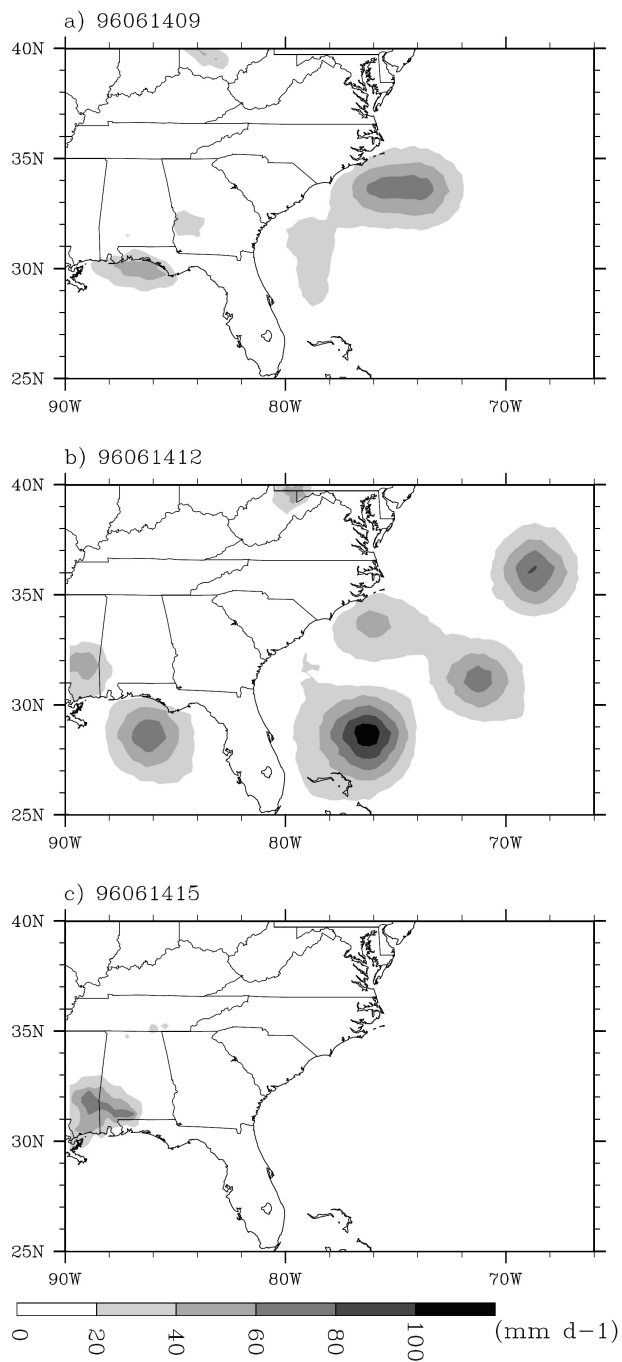
FIG. 6. 3h average precipitation rate from the NARR for June 14, 1996. a) 0900 UTC, b) 1200 UTC, c) 1500 UTC.

As another way to assess its utility, an example of an extreme event was chosen to see if the NARR could capture such an event. Other useful examples showing months with extreme precipitation can be found in Mesinger et al. (2006). Since it is also valuable to see how well individual precipitation episodes are portrayed, a day when flash flooding occurred in Las Vegas, Nevada was chosen for illustration. This event took place on July 8, 1999 and is described fully by Li et al. (2003). For brevity, only one period around the time of the flash flooding is considered, but as shown in Fig. 7, the 3-hour average precipitation rate from the NARR captures this event reasonably well. It portrays the intense precipitation (which is not necessarily expected from other reanalyses that do not assimilate precipitation), and the spatial pattern of the precipitation is close to what is seen in the radar imagery. As it is compared against instantaneous composite radar in this figure, an exact match is not expected (for the full evolution of the event, see Li et al. 2003). The hourly precipitation from the CPC also captures this event, but with little detail at its coarse resolution (a contour plot shows a large diamond shaped bull's-eye over most of southern Nevada, not shown). Six-hourly precipitation from the NCEP-DOE, on the other hand, does not clearly portray this event. The precipitation it produces in southern Nevada is too light by nearly an order of magnitude and is exceptionally underdone in terms of spatial coverage as well (not shown). Finally, it is also useful to mention that a few Midwestern MCS events were examined in addition to this one and the NARR precipitation was found to compare well spatially and temporally with the actual events (not shown).

d. Discussion

The main purpose of this chapter was to document several aspects of the precipitation climatology available from reanalysis datasets over the continental U.S. The examination of the reanalyses in section 2.c.1 demonstrates the superiority of the NARR in the representation of precipitation over the continental U.S. compared with two other widely used reanalyses. As precipitation is assimilated during the reanalysis process in the NARR,

26
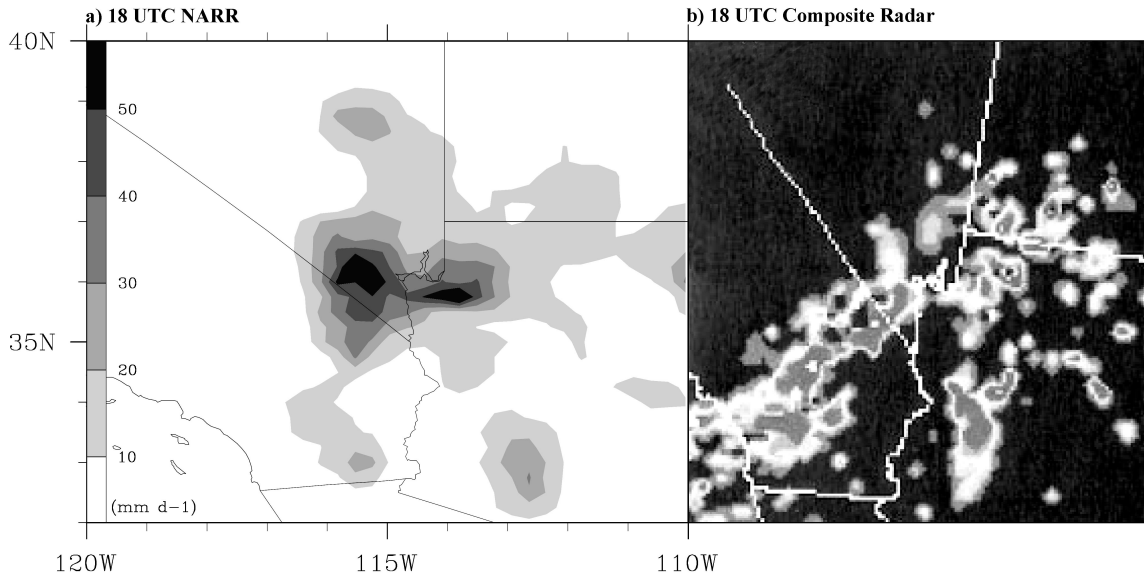
FIG. 7. 8 July 1999 a) NARR 1800 UTC 3h average precipitation rate (mm/day), b) 1800 UTC composite radar from Fig. 7 of Li et al. (2003). Darkest grey radar echoes indicate reflectivities over 50 dBz.

whereas it is completely parameterized in the ERA-40 and NCEP-DOE, this result was anticipated. Summertime precipitation is most improved as the Plains nocturnal maximum is difficult to reproduce in models using convective parameterizations only, since parameterizations typically do not allow convection to undergo the upscale growth necessary for organization into an MCS (the primary cause of this maximum). Even if organized MCSs could be parameterized, propagation then provides another challenge (Davis et al. 2003, Bukovsky et al. 2006). For this reason, the NARR likely captures this maximum because it assimilates precipitation and not because it uses any particular parameterization.

It was also shown in section 2.c.2 that while the NARR replicates continental U.S. precipitation well, care should be taken when using the precipitation analysis over the rest of the North American domain as interesting, but not necessarily valid features in other areas are found as a strong signal in some climatological fields. This note serves not only as a warning to users of the data, but also as general guidance on which aspects of the precipitation reanalyses are most useful. Overall, as the precipitation information required

becomes more detailed, the NARR becomes more useful compared to the other reanalyses, with, of course, the previously mentioned exceptions.

3. Climate Model Precipitation Intercomparison

a. Introduction

Climate models, like weather forecasting models, are based on the fundamental physical laws that govern atmospheric and oceanic motion. Mathematical equations for fluid dynamical, chemical, and biological processes based on these laws and on observations are estimated for computational purposes and integrated in time to understand and predict global climate. Due to increases in computational capabilities, global climate models (GCMs) now often contain coupled ocean models and sea ice and land surface (soil, plants, and river routing) components.

Output from select GCMs run for the IPCC AR4 are examined in this chapter and one is used later for downscaling purposes. A suite of twenty-three models was run in support of the AR4 effort. They have horizontal resolutions ranging from 1°-3°, approximately, and most of them no longer use flux adjustment (artificial adjustments to heat, water, and momentum fluxes) to maintain a stable control climate. As stated in the AR4, "[t]here is considerable confidence that climate models provide credible quantitative estimates of future climate change, particularly at continental scales and above" (Randall et al. 2007, pg. 600). This is because models have a physical foundation and the ability to represent current and past climate with reasonable accuracy (Fig. 8). Simulation for certain variables and processes is still better for some than for others though. For example, temperature is handled better than precipitation, and in some models the El Niño-Southern Oscillation (ENSO) is represented satisfactorily in some aspects while the Madden-Julian Oscillation (MJO) is not (Randall et al. 2007).

This chapter will explore the simulation of precipitation in five of the models used in the AR4 over the U.S., focusing on summertime precipitation. As all aspects of this review are problematic for the AR4 suite of models in terms of the size of the region, the variable chosen, and the season of interest in the chosen region, this effort mainly aims to identify
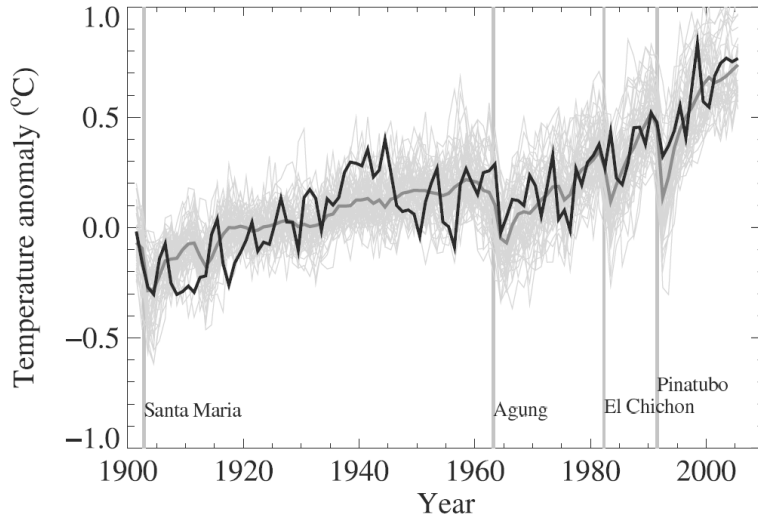
FIG. 8. "Global mean near-surface temperatures over the 20th century from observations (black) and as obtained from 58 simulations produced by 14 different climate models driven by both natural and human-caused factors that influence climate ([light grey]). The mean of all these runs is also shown (thick [medium grey] line). Temperature anomalies are shown relative to the 1901 to 1950 mean. Vertical grey lines indicate the timing of major volcanic eruptions." (Figure 8.1 from Randall et al. (2007). Refer to corresponding caption for further details.)

the specific inaccuracies over the U.S. and discuss potential reasons for their existence as a backdrop for and as motivation for the later downscaling of the output. Therefore, this chapter will focus on precipitation from simulations of the 20th century, but we will take a brief look at some aspects from simulations of future climate.

b. Models and Methods

Precipitation from the following coupled global climate models will be used in this intercomparison: NCAR's Community Climate System Model version 3.0 (CCSM 3.0, Collins et al. 2006); the Geophysical Fluid Dynamics Laboratory (GFDL) climate model version 2.0 (GFDL 2.0, Delworth et al. 2006); the National Aeronautics and Space Administration (NASA) Goddard Institute for Space Studies (GISS) Model EH (Model E with the HYCOM ocean model) (GISS EH, Schmidt et al. 2006); and the Center for Climate System Research (The University of Tokyo), the National Institute for Environmental Studies, and

the Frontier Research Center for Global Change's medium and high resolution Model for Interdisciplinary Research on Climate (MIROC-MED and MIROC-HI, Hasumi and Emori 2004). An overview of selected components from these models is given in Table 2, while more details pertaining to the production of precipitation follows. Output from all models is available from the Program for Climate Model Diagnosis and Intercomparison (PCMDI) in support of the IPCC AR4. In part, these models were chosen because three or six hourly precipitation data are available from each for overlapping 20th century time periods. Simulations in section c use the IPCC 20C3M (20th century) scenario, while those in section d where run using the A2 and A1B (future) emission scenarios. Three-hourly values from the GCMs are only available from 1991-2000 (except for the CCSM 3.0 which is only available every 6 hours from 1991-1999); therefore, the 1990s are the chosen decade for the 20th century part of this study. For each emission scenario, multiple runs may be available. However, output with a higher time frequency (3-6h) is usually only offered for one of them. Here, all data are for run one, except for the CCSM 3.0 and GISS EH for which run 5 is used (3h data are not available from the other runs). For the brief examination of future precipitation in section d, daily climate model output will be used, as 3-6 hourly output is either not obtainable or not available for more than at least a 5 year period for most of the chosen models.

As in the reanalysis intercomparison, all models will be used at their original horizontal resolution. This gives the greatest impression of how much information can be gleaned from the data, and, furthermore, scaling them to matching grids does not change the overall results presented in this chapter. For the 20th century intercomparison presented in section c, model precipitation will be compared to precipitation from the NARR, as the NARR was found to be the most reliable, highest-resolution, gridded, observation based dataset in terms of precipitation in the last chapter. Also, for all percentile calculations, precipitation rates of a trace or less were excluded from the calculation. Here, and in other chapters,

31

Model	Atmosphere Top Resolution	Ocean Resolution Z Coord., Top BC	Sea Ice Dynamics, Leads	Coupling Flux Adjustments
CCSM 3.0	top = 2.2 hPa T85 (1.4° x 1.4°) L26	0.3°-1° x 1° L40 depth, free surface	rheology, leads	no adjustments
GFDL 2.0	top = 3 hPa 2.0° x 2.5° L24	0.3°-1° x 1° depth, free surface	rheology, leads	no adjustments
GISS-EH	top = 0.1 hPa 4° x 5° L20	2° x 2° L16 density, free surface	rheology, leads	no adjustments
MIROC-MED	top = 30 km T42 (~2.8° x 2.8°) L20	0.5° - 1.4° x 1.4° L43 sigma/depth, free surface	rheology, leads	no adjustments
MIROC-HI	top = 40 km T106 (~1.1° x 1.1°) L56	0.2° x 0.3° L47 sigma/depth, free surface	rheology, leads	no adjustments

TABLE 2. Select model features. Also listed: pressure at atmospheric model top, horizontal and vertical resolution, oceanic vertical coordinate type, upper boundary condition (BC: free surface or rigid lid), sea ice dynamic/structure (e.g., rheology vs 'free drift' assumption and inclusion of ice leads), whether adjustments of surface momentum, heat, or freshwater fluxes are applied in coupling the atmosphere, ocean, and sea ice components, land features, presence of canopy or river routing. From Randall et al. (2007) Table 8.1.

a trace is defined as a precipitation rate of 0.25 mm/day or less (approx. 0.01 in/day, as defined by AMS (2000)).

1) CCSM 3.0

The CCSM 3.0 is a fully coupled global climate model containing atmosphere, ocean, sea ice, and land surface components. It contains a Eulerian spectral dynamical core with a triangular spectral truncation at T85 (approximately 1.4°) and 26 sigma-pressure hybrid vertical layers in the atmosphere with no flux correction (Collins et al. 2006). The resolution of the ocean model is set at 1°. This model utilizes the Zhang and McFarlane (1995) CPS for deep convection only. This CPS is a simplified version of the AS scheme. Convective available potential energy (CAPE) is required for deep convection, and a low-level unstable parcel will convect if it can penetrate any stable layer. A parameterization for shallow and upper-level convection developed by Hack (1994) is included, and large-scale condensation is treated prognostically, as described in Rasch and Kristjànsson (1998) (with modifications by Zhang et al. 2003) (Boville et al. 2006).

2) GFDL 2.0

The GFDL 2.0 is also a fully coupled global climate model containing atmosphere, ocean, sea ice, and land components. It contains a B-grid dynamic core with 2° latitude by 2.5° longitude resolution and 24 vertical levels in the atmospheric component and no flux adjustments (Delworth et al. 2006). Ocean resolution is 1° with increasing resolution equatorward of 30° to a 1/3° grid spacing. The dynamic core in this version of the GFDL CM is responsible for the equatorward drift of the mid-latitude westerlies over time seen in its simulations. This is eliminated in version 2.1 with the use of a finite volume dynamical core. Precipitation is, however, simulated better in version 2.0 than version 2.1 (Delworth et al. 2006). Convection in GFDL 2.0 is parameterized using the relaxed AS scheme pro-

posed by Moorthi and Suarez (1992). Closure in this version of AS is still based on quasi-equilibrium, except that quasi-equilibrium is not required with the large-scale forcing; it is obtained, approximately, on shorter time scales depending on cloud type. That is, the CPS relaxes the cloud work function[6] for each cloud type to a specified value. Convective downdrafts are not included in this version of the CPS. Large-scale condensation is computed in a prognostic sense using Rotstayn (1997) and Tiedtke (1993).

3) GISS EH

The GISS EH model is the coarsest resolution global coupled climate model used in this study at 4° latitude by 5° longitude on an Arakawa B grid with 20 mixed sigma-pressure layers. Convection is based on the mass flux type scheme by DelGenio and Yao (1993) and DelGenio et al. (1996). In this scheme, convection triggers when an air parcel lifted one level saturates and becomes buoyant. Convection transports enough mass for parcels lifted from cloud base to obtain neutral buoyancy. Downdrafts are allowed for parcels that rise more than one level. Large scale condensation is prognostic and based on moisture convergence (Sundqvist 1978, Sundqvist et al. 1989).

4) MIROC-HI AND MIROC-MED

The two MIROC models examined here differ only in resolution. They are both global coupled models with five components: atmosphere, land, river, sea ice, and ocean. MIROC is a spectral model and uses a sigma coordinate system in the vertical. MIROC-HI has a spectral truncation of T106 (~1.125°) and 56 vertical layers while MIROC-MED has a truncation of T42 (~2.8125°) and 20 vertical layers. The convective parameterization is a simplified version of AS where the closure has been changed from a diagnostic quasi-equilibrium closure to a prognostic cumulus kinetic energy closure based on Pan and Ran-

---

[6]When entrainment is zero for a given cloud type in AS, the cloud work function is equal to CAPE.
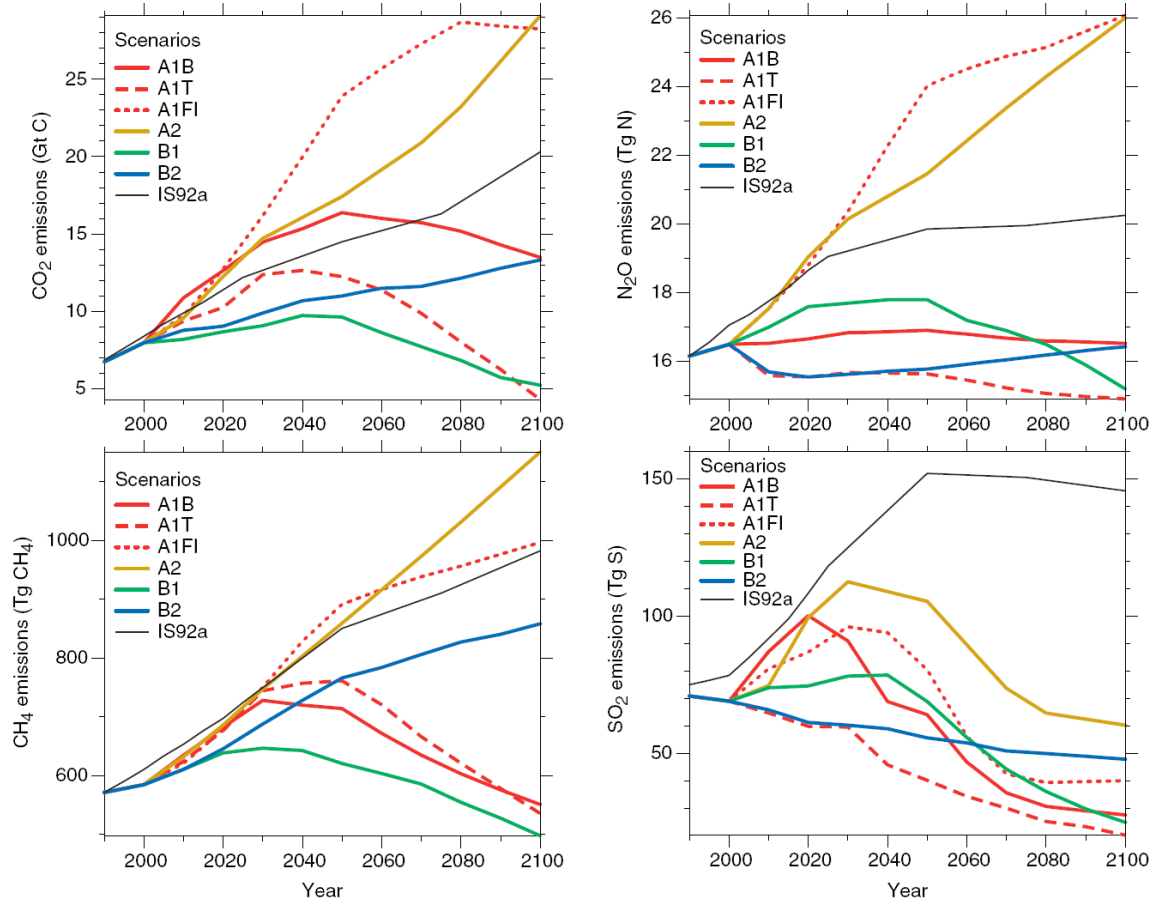
FIG. 9. Anthropogenic emissions of CO2, CH4, N2O and SO2 for the six SRES scenarios, A1B, A2, B1, B2, A1FI, and A1T. (From Albritton et al. 2001)

dall (1998). In addition, cumulus convection is not allowed when the cloud-mean ambient relative humidity is less than 80%. Downdrafts are included in this CPS. Large-scale condensation is based on Le Treut and Li (1991).

5) FUTURE SCENARIOS

Future climate change results are based on emission scenarios developed by the IPCC. Predicting concentrations of greenhouse gasses is obviously subject to considerable uncertainty given the many difficult to predict factors that control them. Therefore, a number of possible scenarios were developed for use by the IPCC (IPCC 2000). They outline emissions of carbon dioxide, methane, nitrous oxide and sulfur dioxide. The IPCC SRES
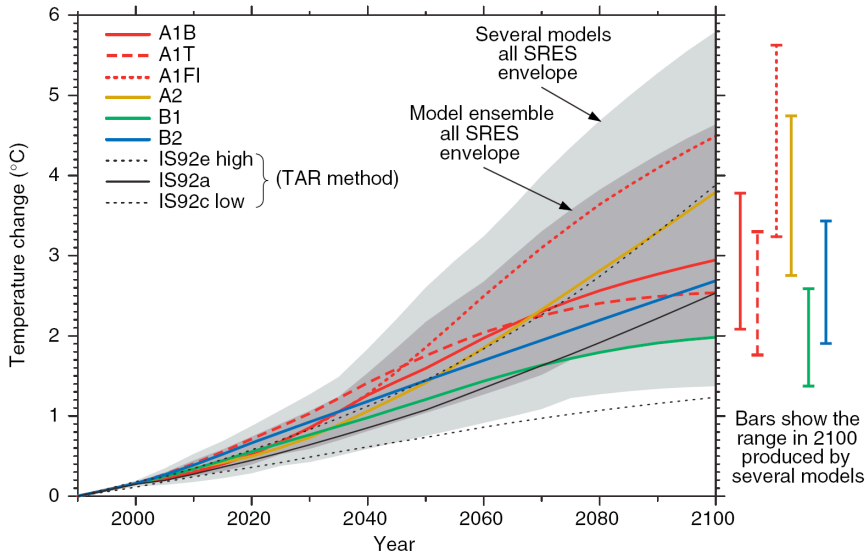
FIG. 10. Simple model results. Global mean temperature projections for the six SRES scenarios using a simple climate model tuned to a number of complex models with a range of climate sensitivities. The darker shading represents the envelope of the full set of 35 SRES scenarios using the average of the model results (mean climate sensitivity is 2.8°C). The lighter shading is the envelope based on all seven model projections (with climate sensitivity in the range 1.7 to 4.2°C). The bars show, for each of the six scenarios, the range of simple model results in 2100 for the seven climate model tunings. (From Albritton et al. 2001)

(Special Report on Emissions Scenarios, IPCC 2000) A2 and A1B scenarios were chosen for the future simulations used in section d because they represent high and mid-range emissions and because model output is available. The A2 scenario is based on a very heterogeneous world, where the population is continuously increasing, economic development is regionally oriented, and technological change and economic per capita growth is fragmented and relatively slow. The A1B scenario describes a more homogeneous world with a population that peaks in mid-century and then declines. New, more efficient technologies evolve more rapidly, and the use of fossil fuels and alternative energy sources is balanced (IPCC 2000). Prescribed greenhouse gas emissions for these simulations and the corresponding predicted temperature changes are shown in Figs. 9 and 10.

c. Results: Present Climate

As illustrated in Figs. 11 and 12, the only feature in the distribution of the annual average precipitation over the U.S. that is captured throughout the suite of models examined here is the maximum in precipitation over the Pacific Northwest. The maximum in the Southeast is not consistently represented. For instance, GFDL 2.0 is generally too wet over the eastern half of the U.S., except over Florida where it is too dry. The CCSM 3.0 does not have a Southeast maximum and produces a plethora of precipitation over the Gulf Stream like some of the other models. MIROC-MED and MIROC-HI highlight most of the east coast with the exception of the MS, AL, GA, and FL region. The best distribution of the annual average precipitation seems to be produced by the lowest resolution model, GISS EH, but the intensity of the precipitation is so light that the values plotted in Fig. 11c had to be multiplied by a factor of four so that some detail could be seen using the chosen contour values.

The annual cycle of precipitation over the U.S. is roughly captured by most of the climate models (right half of Figs. 11 and 12). Over the eastern half of the country, the peak in precipitation rate occurs in the summer, except in MIROC-MED and MIROC-HI, which produce an extraordinary amount of precipitation over the Gulf Stream around October. The general seasonal and diurnal distribution of precipitation over the western half of the U.S. is superior to that over the eastern half. The diurnal spread is greatest in the summer with dominant afternoon/evening precipitation, and cool season precipitation is greater than warm-season precipitation due to the NW maximum. The greatest problem over the western half of the nation is in the magnitude of the precipitation rate.

The simulation of the predominantly convective JJA precipitation is not highly improved over the annual average, as expected. Figure 13 shows the time and magnitude of the maximum precipitation for the various models. All but MIROC-MED capture the summertime maximum over the southeast U.S. The distribution seems to be best in the GISS-EH, except over FL, where important land-sea interactions are likely not well re-
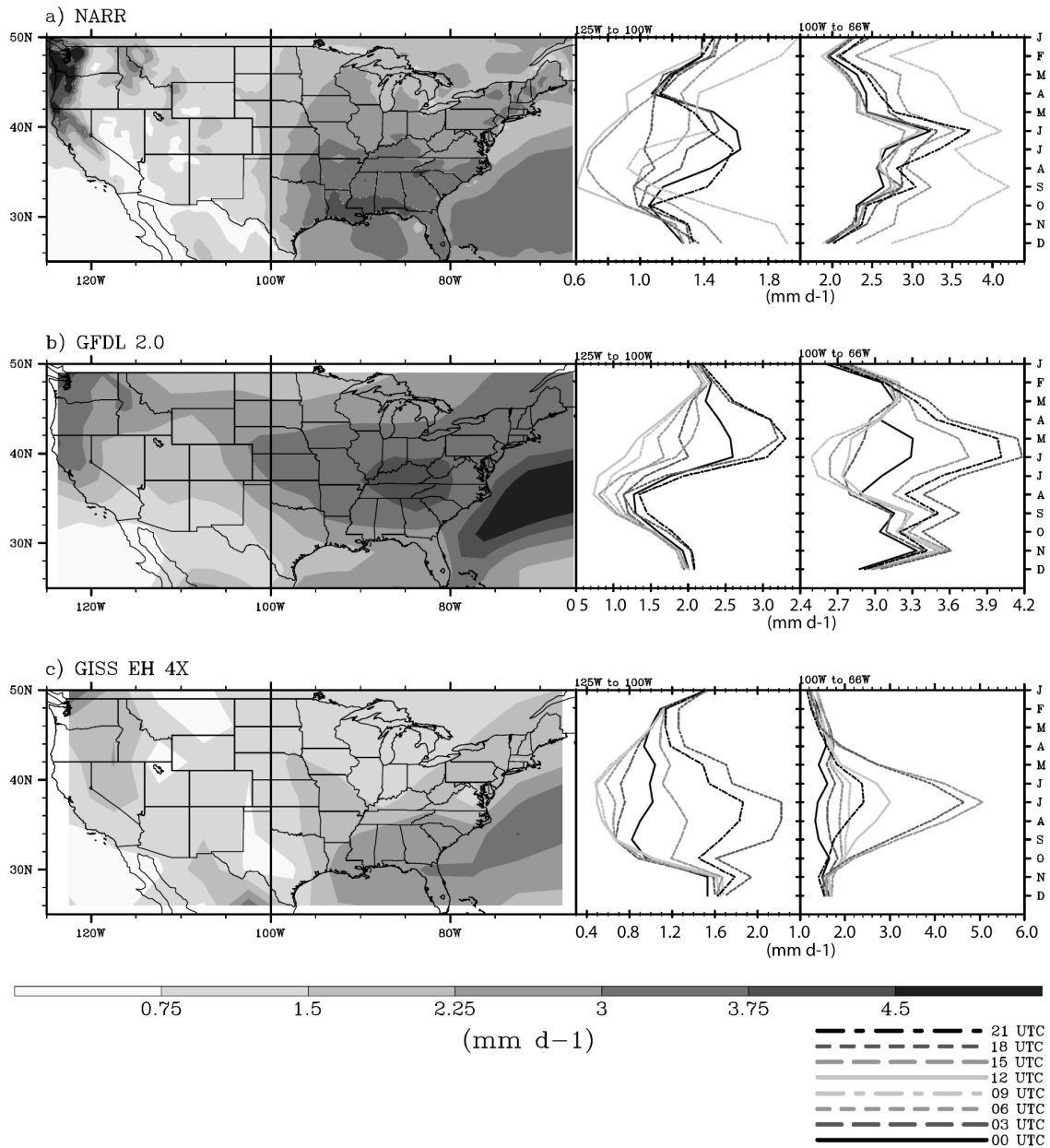
FIG. 11. Part 1 of 2. 1991-2000 annual average precipitation rate (left column, mm/day, contours) and 3h monthly average precipitation rate for the domain shown in the left column from 125°W to 100°W (center column, mm/day) and from 100°W to 76°W (right column, mm/day) for: a) NARR, b) GFDL 2.0, c) GISS EH. The month of the year is noted on the right-most y-axis by the first letter of each month. The U.S. divide at 100°W is indicated on the images in the left column by the heavy black line. Note: GISS EH precipitation was multiplied by a factor of four to facilitate comparison with the other models.
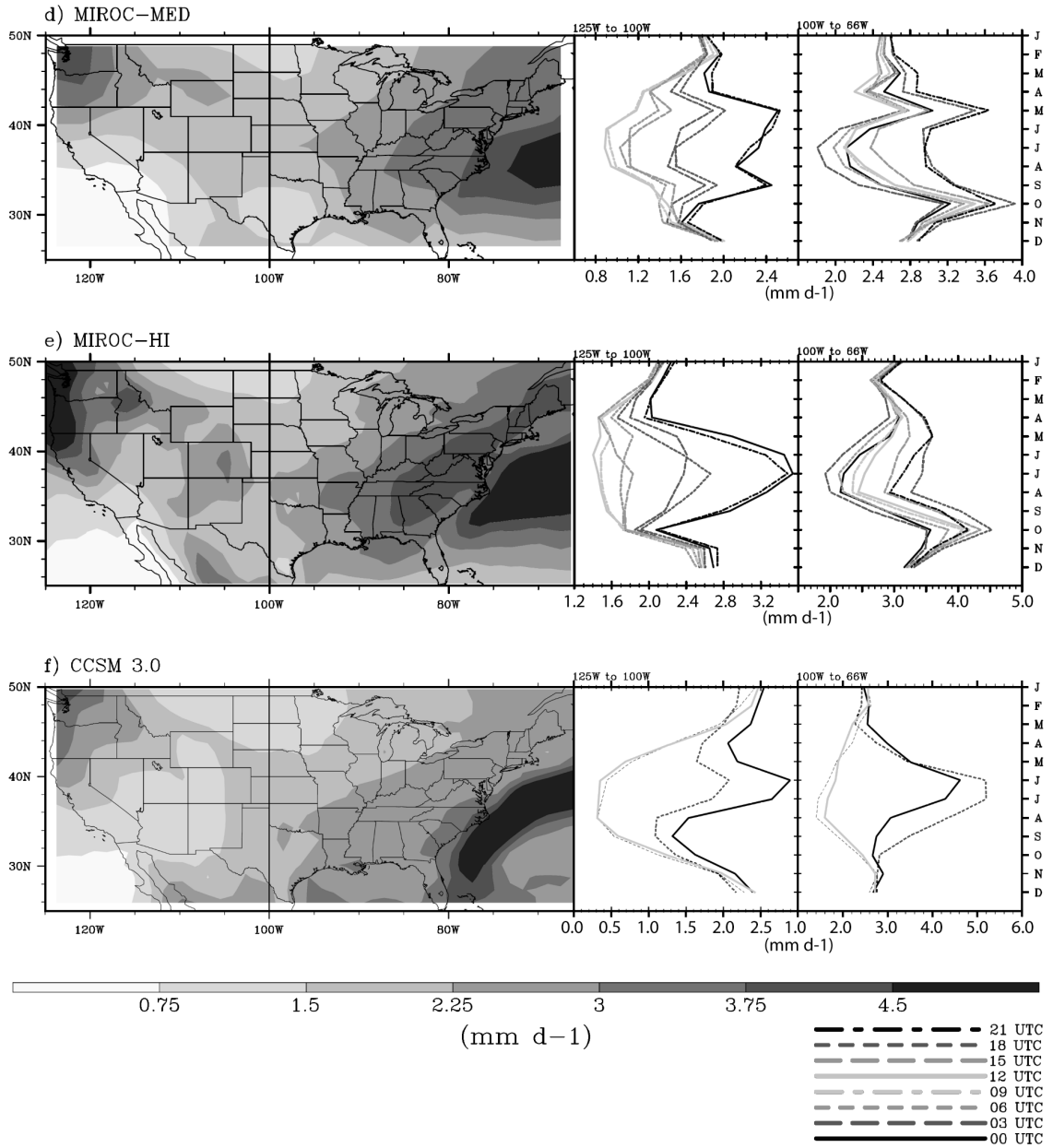
FIG. 12. Fig. 11 Part 2. For d) MIROC-MED, e) MIROC-HI. Panel f): same, but for 1991-1999 and 6h monthly average precipitation rate from CCSM 3.0.
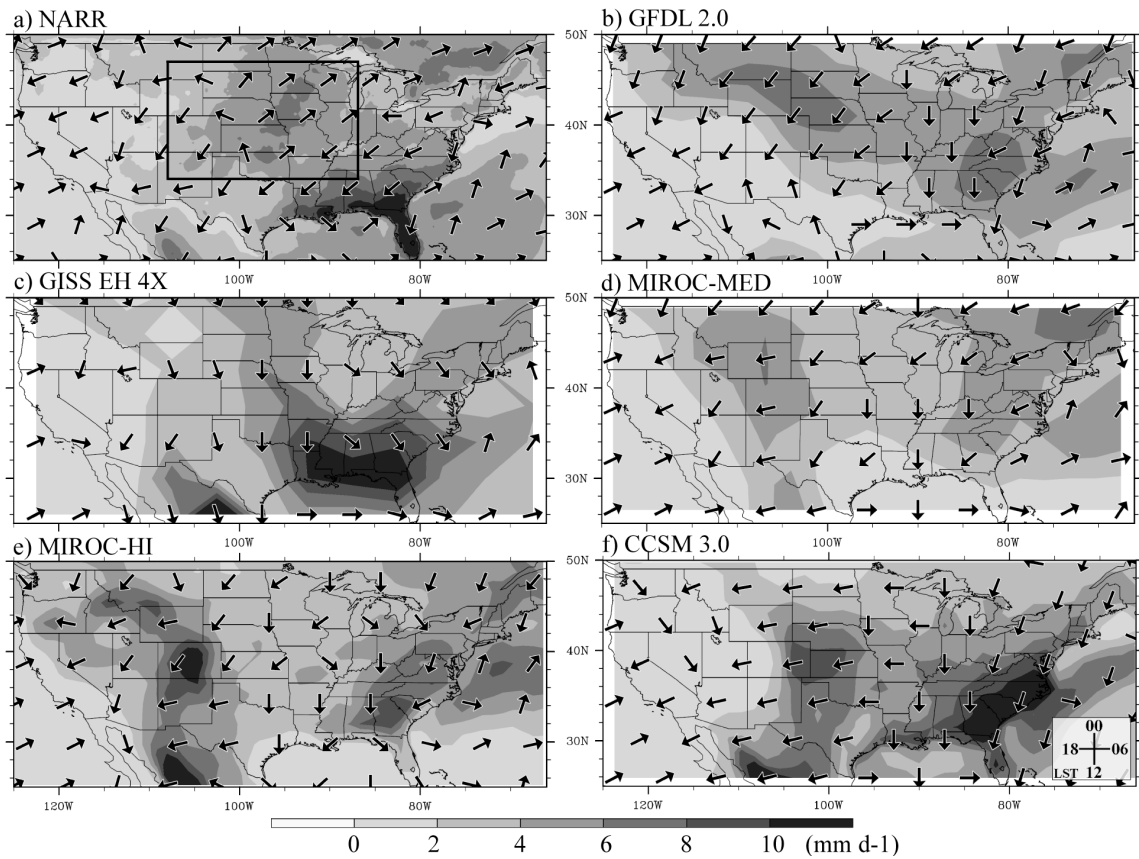
FIG. 13. 1991-2000 JJA maximum 3h average precipitation rate (mm/day, contours) and time of maximum (vectors, LST) from a) NARR, b) GFDL 2.0, c) GISS-EH (precipitation multiplied by a factor of 4), d) MIROC-MED, e) MIROC-HI. Panel f): same, but for 1991-1999 6h average precipitation rate from CCSM 3.0. Vector time clock key inset in panel f.

solved. The CCSM 3.0 and MIROC-HI have the most accurate timing for the maximum precipitation in the Southeast.

The summertime Great Plains nocturnal maximum is not particularly well captured in any model. The GFDL 2.0 and MIROC-MED do simulate an early afternoon maximum that appears to be orographically forced, and MIROC-HI produces a late afternoon maximum in Colorado, but no model seems to propagate this precipitation into the Plains. The GISS-EH produces a decent distribution, considering its resolution, but the maximum occurs around noon local solar time (LST), approximately twelve hours early. The Great Plains maximum and timing is best represented by the CCSM 3.0. Precipitation is not intense enough into IA, MN, and WI, but the timing of the maximum on the CO front range is only off by about 3h and there is some extension of that precipitation into the central Plains; although, given the time vectors (and Hovmöller diagrams, not shown), this does not appear to be precipitation propagating off the front range.

The frequency distribution of precipitation rates greater than 0.25 mm/day for the central U.S. is shown in Fig. 14 (the region in question is outlined in Fig. 13a). Frequency is defined as the percentage of 3h (or 6h) periods at all points in the region with a given range of precipitation rates out of all possible 3h periods and points with data. Examining precipitation above the 0.25 mm/day value excludes trace values of very light precipitation, though light rates , including those above a trace are generally too frequent in the climate models, even in this newest generation of models (Sun et al. 2006). Figure 14d shows that the GISS-EH produces precipitation that is too light too frequently (although at this resolution it is expected to be lighter, here the original precipitation rates have been multiplied by a factor of 4). The GFDL 2.0 also precipitates too frequently in the 4-44 mm/day category, while the two MIROC models produce values that are much closer to what is observed. The most frequent precipitation in the 4-44 mm/day category occurs roughly between 2100 and 0000 UTC in all of the models, which is close to observed values. Precipitation rates greater than 44 mm/day do not occur frequently enough in any
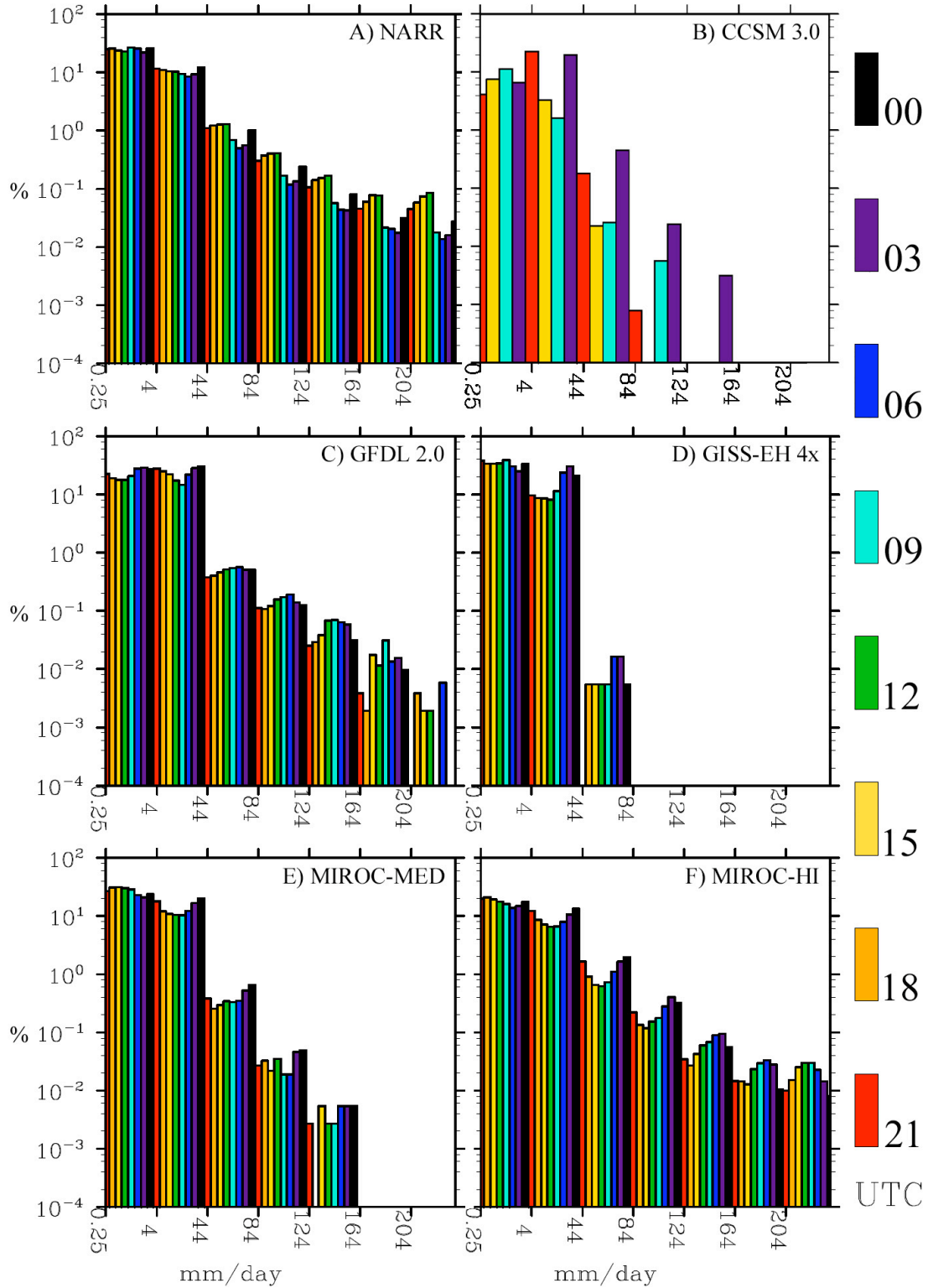
FIG. 14. 1991-2000 JJA 3h precipitation rate frequency distribution for the domain outlined in Fig. 13a from: a) NARR, c) GFDL 2.0, d) GISS-EH, e) MIROC-MED, f) MIROC-HI. Panel b): same, but for 1991-1999 6h precipitation rate from CCSM 3.0. Values used to calculate the distribution in d) were multiplied by a factor of 4.

model except MIROC-HI, which has the most representative frequency distribution, even though the diurnal cycle is off. The CCSM 3.0, although one of the higher resolution models, does not produce enough intense precipitation in this portion of the country (that this is from 6h and not 3h average precipitation does not make a difference, not shown), it produces a distribution close to that of the MIROC-MED only with a much-amplified diurnal cycle. As far as being able to produce precipitation rates greater 164 mm/day, the GFDL 2.0, is probably the second best in that it does produce precipitation in this range with any frequency greater than zero, although the greatest frequency occurs about 3-6 hours late.

The percentage of very heavy precipitation from the total precipitation in any given model in JJA is not much better than the magnitude of the heavy precipitation shown in the frequency distribution (Fig. 15). Over 20% of the total JJA precipitation in the central U.S. is generally from daily precipitation events heavier than the 99th percentile, and this is not captured well by the models. However, all show a maximum of some sort in the Great Plains (even the GISS EH, though not visible on this color scale), and the GFDL 2.0, MIROC-MED, and MIROC-HI do contain areas with values greater than 20% for this part of the country.

d. Results: Future Climate

Results from future simulations of precipitation are subject to the same distribution problems shown above and, thus, must be used with caution over any given region in the U.S. General trends and variation between models, however, may provide useful insight into the future of precipitation over the U.S. Two statistics will be briefly examined here for two climate change scenarios. The models from the previous section that have data available will be used.

The percent change in annual mean precipitation rate between the 1990's and 2081-2100 are given in Fig. 16. Three of the four models agree that there will be a decrease in annual mean precipitation over the central U.S. by the end of the 21st century of about 10-
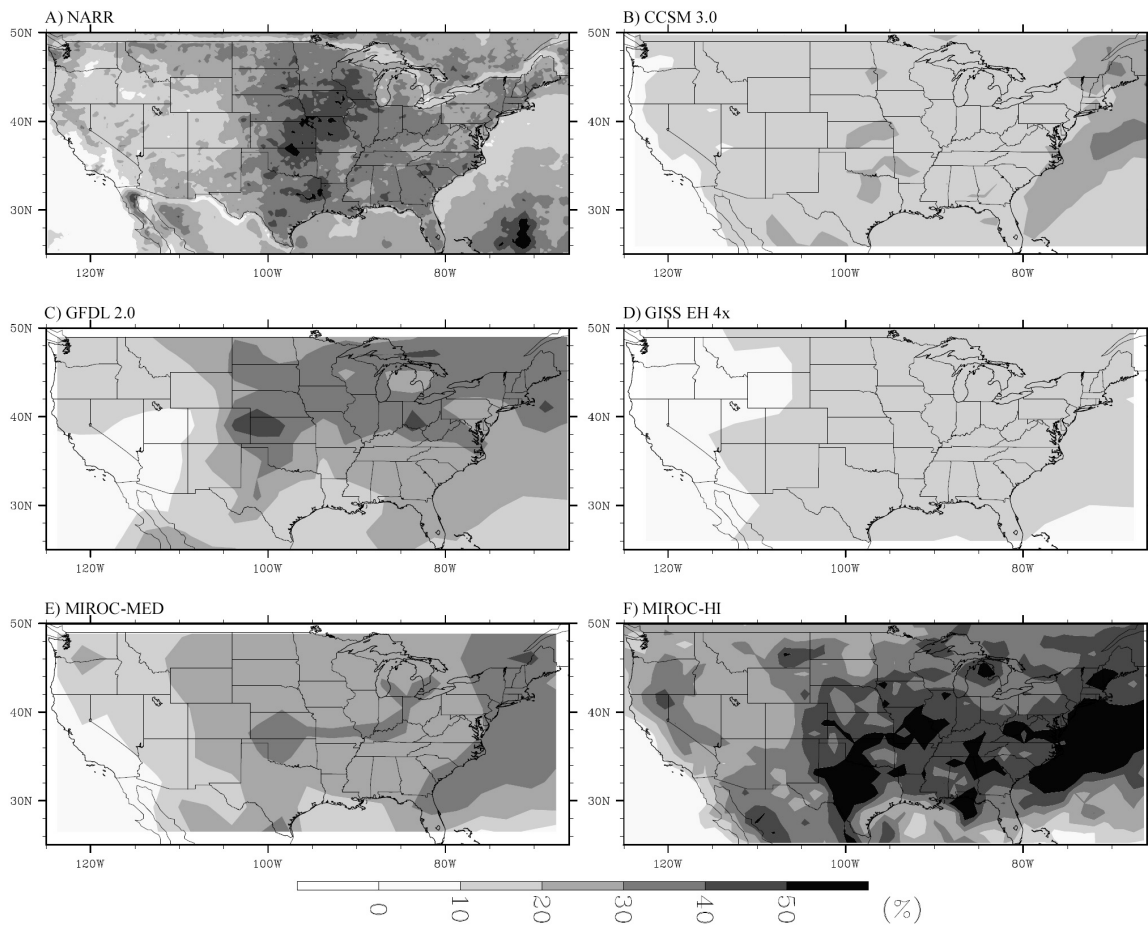
FIG. 15. 1991-2000 percent of the total daily precipitation in JJA greater than the 99th percentile from: a) NARR, c) GFDL 2.0, d) GISS-EH, e) MIROC-MED, f) MIROC-HI. Panel b): same, but for 1991-1999 precipitation rate from CCSM 3.0. Daily rates used in d) were multiplied by a factor of 4.
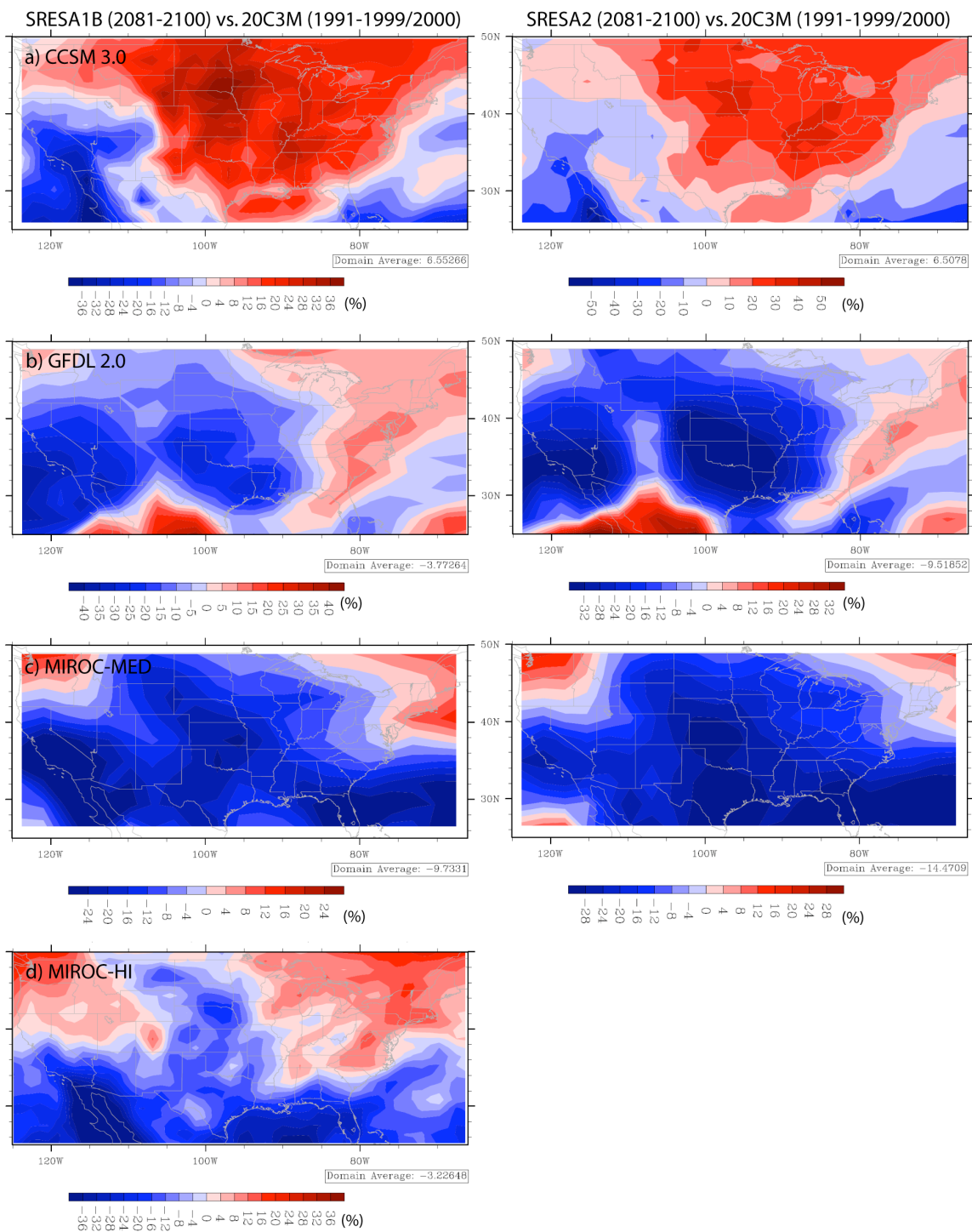
FIG. 16. Percent change in the annual mean between 1991-1999 and 2081-2100 for the SRESA1B scenario (left column) and the SRESA2 scenario (right column) for a) CCSM 3.0. Panels b) GFDL 2.0, c) MIROC-MED, and d) MIROC-HI same, but for the percent change between 1991-2000 and 2081-2100.

20% depending on the model, scenario, and location. The outlier, the CCSM 3.0, predicts an increase in annual mean precipitation for this region. A decrease is predicted throughout all simulations for the southwest U.S.. These trends are echoed in JJA precipitation (not shown), but to a greater extent. The only regions predicted in all models and scenarios to see an increase in annual mean precipitation is the far Northeast and Washington state.

While a decrease in mean annual and JJA (not shown) precipitation in the central U.S. is predicted by three of the models, an increase in very heavy JJA precipitation is expected in the same three models (Fig. 17). Once again, the CCSM 3.0 is in opposition; over the central U.S. it projects a decrease. In most cases, the magnitude of any change here and in average precipitation is greater in the SRESA2 scenario than in the SRESA1B scenario, as anticipated given the greenhouse gas concentration increase over time in each scenario.

e. Discussion

The results presented in section 3c agree with results presented in other studies. For instance, Sun et al. (2006) show that frequency of light precipitation is overestimated and the frequency of heavy precipitation is under estimated by current GCMs, as is seen here in most cases. The higher resolution models examined above tend to exhibit better spatial patterns of precipitation, with the exception of the GISS-EH which is the coarsest resolution model, yet still does fairly well with distribution (not intensity). The MIROC-HI also shows an improved solution for the intensity and frequency of heavy precipitation. These agree with the results presented by Duffy et al. (2003) using the Community Climate Model 3 (CCM3); wherein, the increase in resolution from T42 to T170 to T239 led to an improved spatial distribution and intensity of extreme precipitation over the U.S.. The same study also showed that the JJA nocturnal precipitation maximum in the center of the country did not improve with resolution changes only and stated that the same misplaced maximum occurs in most CMIP (Coupled Model Intercomparison Project) models.
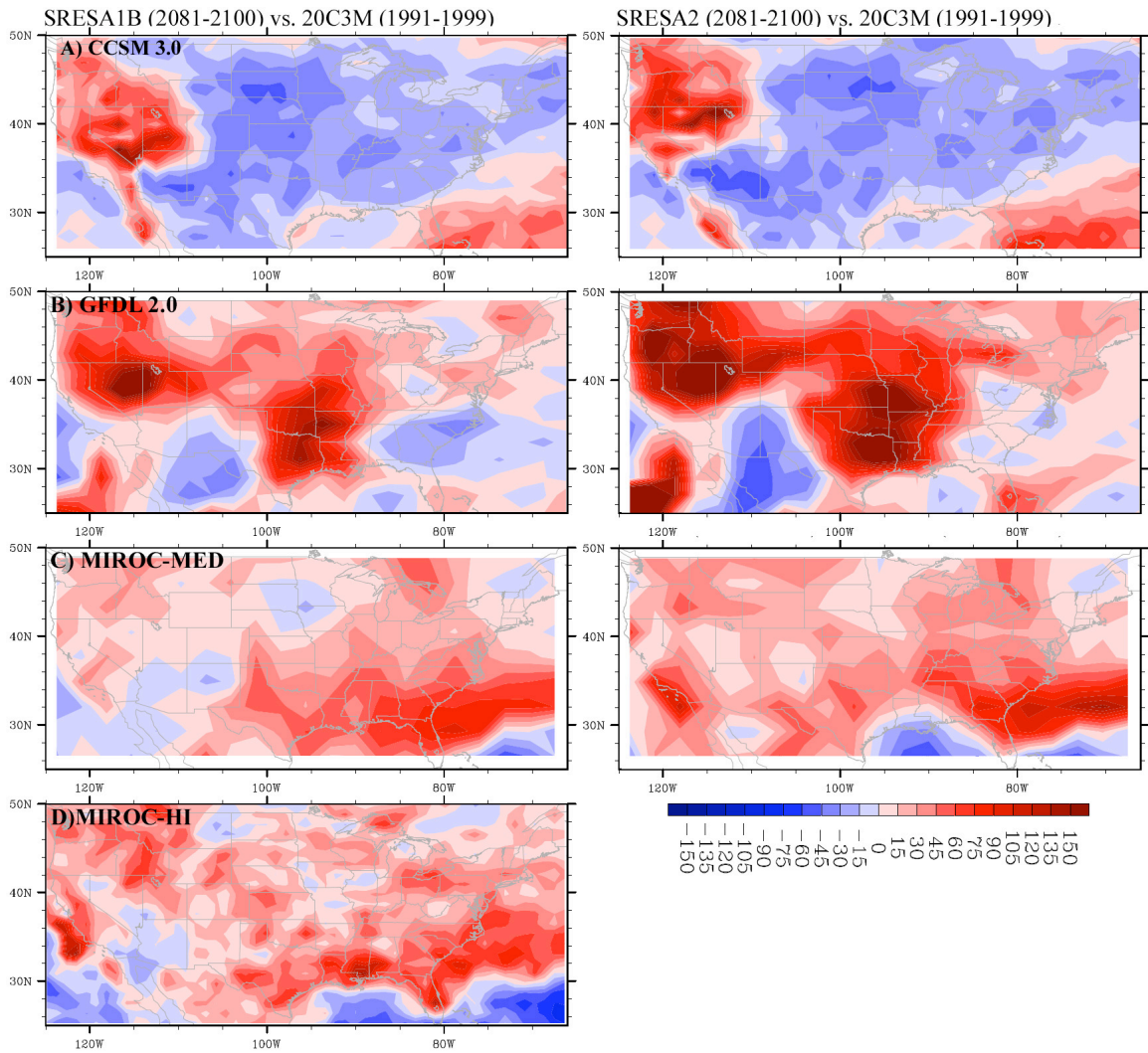
FIG. 17. Percent change in the percent of the total daily JJA precipitation greater than the 99th percentile (excluding trace amounts) between 1991-1999 and 2081-2100 for the SRESA1B scenario (left column) and the SRESA2 scenario (right column) for a) CCSM 3.0. Panels b) GFDL 2.0, c) MIROC-MED, and d) MIROC-HI same, but for the percent change between 1991-2000 and 2081-2100.

47

The diurnal cycle and frequency of precipitation is also highly related to convective parameterization; the CPS used, therefore, is of great importance in the warm-season when most continental U.S. convection occurs (Heideman and Fritsch 1988). Triggering and closure methods dictate when and where convection will occur. As mentioned, JJA convection in the Southeast is related to surface heating and atmospheric instability. It is not surprising, therefore, that most of the models discussed above captured the maximum in precipitation and its timing in this part of the country fairly well as all but the GISS-EH use CAPE-based triggers (i.e. CAPE greater than zero with possibly one other constraint triggers convection). The maximum over FL may not be captured well, but this may be a resolution issue and less related to physical parameterizations (i.e. FL may not be a well resolved land mass).

Problems in the representation of precipitation in the central U.S. were expected in all of the climate models as the propagation of convective systems and, specifically, the nocturnal precipitation maximum are major modeling problems (Davis et al. 2003). Convective inhibition usually allows instability to build up before intense convection triggers. Triggering is also linked to large-scale and mesoscale forcing in this region. Furthermore, all but the GISS-EH use triggers that do not use parcel theory and instead rely on the existence of CAPE. Therefore, the frequent triggering of weaker convection is expected (Xie et al. 2002). Some of the models appear to initiate convection just east of the Rockies, but all except one are too early (they peak more with the daytime heating cycle). The CCSM 3.0 maximizes convection at a more realistic time, but fails to propagate it. For convection to propagate its effects must be felt on the grid-scale through upscale growth which is problematic in mesoscale models and probably not possible in climate models at their current resolution. The more realistic initiation time may be a result of the added constraint in the CCSM 3.0 CPS trigger that a parcel must be able to rise through a stable layer to convect; thus, accounting for the presence of convective inhibition (CIN) to some extent.

Increased resolution holds some promise for improving the representation of precipitation, but physical parameterizations do not always perform as expected as resolution is increased, which complicates the issue (Duffy et al. 2003). Choice of convective parameterization can have a large impact on precipitation simulation, but most of the models examined here used a similar type of convective scheme and, thus, gave similar results. The next several chapters present the results from the work that has been done to downscale global climate model output in an effort to overcome some of the problems documented above and produce simulations that have the potential to be more useful for regional climate change impact work.

4. Nested Regional Climate Modeling Using the WRF

As mentioned in section 1d, nested regional climate modeling is becoming more popular as a way to diagnose the regional impacts of climate change as global climate modeling is currently inadequate for regional assessments. Global climate modeling can only capture broad scales of atmospheric processes and interactions. This is a particular problem when it comes to predicting precipitation on regional scales, as illustrated in the previous chapter. Nested regional modeling allows for higher resolution orography, land-sea contrasts, land surface characteristics, and for the regional model to develop local and mesoscale flows (depending on its resolution) that can then interact with the large-scale circulation induced by the initial and boundary condition source. It is the same concept that has been used in short-term forecast modeling, but applied to climate.

Dynamic downscaling allows regional climate features and extreme events to be more realistically simulated and has been shown to produce results that are more accurate than those from the driving GCM or reanalysis (Takle et al. 1999, Pan et al. 2001, Liang et al. 2001, Anderson et al. 2003, Liang et al. 2004a, Fowler et al. 2005, Frei et al. 2006, Liang et al. 2006, Salathé et al. 2008, Leung and Qian 2009). As reviewed by Christensen et al. (2007), RCMs generally have more skill simulating average cold-season temperature and precipitation than they do warm-season precipitation. This is because warm-season climate is not fully controlled by large-scale forcing. Issues have also been noted regarding the sensitivity of regional climate simulations to domain size (Pan et al. 2001), lateral boundary condition source (Plummer et al. 2006), and the location and season of the climate to be simulated (Caya and Binder 2004). Much of the latter is also apparent in the IPCC AR4 chapter "Regional Climate Projection" (Christensen et al. 2007). There are also ongoing projects using ensembles of dynamically downscaled GCM output from different RCMs; e.g., the Prediction of Regional Scenarios and Uncertainties for Defining European Climate Change Risks and Effects (PRUDENCE, Fowler and Ekström 2009) and the North American Regional Climate Change Assessment Program (NARCCAP, Mearns et al.

2005). These should allow a better estimate of the sources of uncertainty in projections of regional climate change.

Many regional climate studies that employ dynamic downscaling over the U.S. have focused on the western U.S., where the availability of water is an ongoing issue. Furthermore, a number of these studies use a version of the Pennsylvania State University/NCAR Mesoscale Model version 4 or 5 (MM4 or MM5) adapted for regional climate modeling. The use of the WRF as a nested regional climate model is, relatively speaking, very new. To the author's knowledge, it has been developed for use as an RCM by the Illinois State Water Survey (Liang et al. 2005a, Liang et al. 2005b, Liu et al. 2006), run for the NARCCAP project (e.g. Correia and Leung 2008), proved useful for downscaling over the western U.S. (Leung and Qian 2009), and has been tested in terms of its initialization methods as an RCM (Lo et al. 2008). Thus, there is much that still needs to be explored with regards to the use of the WRF as a nested regional climate model and its abilities to produce realistic simulations of current climate and regional projections of climate change. .

This chapter covers the setup and testing of the WRF model as used as a nested regional climate model for simulating current climate. Once again, the focus is on warm-season precipitation; however, as temperature is always of interest in discussions of climate change, it will be included as well.

a. The Model and the Sensitivity of Precipitation to Variations in its Setup

To start, the WRF model was run using a global reanalysis for initial and boundary conditions instead of global climate model output so the simulations could be verified against observations and reanalyses. Initially, the WRF was developed and tested for regional simulation and forecasting of weather. Little has been reported, to the author's knowledge, on the testing of longer-term (e.g. seasonal) simulations from the WRF. Some responses of the model to specific setup options may not be apparent in shorter simulations and may only become evident over longer periods of time. This section explores some of the sensitivities

of simulated precipitation in the WRF that were identified in 4-month long simulations. This sort of examination is necessary for insight into the performance of the WRF as used as a nested regional climate model, but also to fully understand the behaviors in the model as used for forecasting and event-based research.

To this end, numerous warm-season runs of the WRF model have been made with an assortment of options in search of a setup that would give reasonable results in a feasible amount of computational time. Parameterization, dynamics, domain, boundary, and nesting options have been explored along the way, and a switch from version 2.2 to version 3.0.1 of the WRF was also made. The goal of this section is to document the more interesting and, in some cases, unanticipated parts of this journey. In doing such, it serves more than one purpose. Obviously, it will document some of the sensitivities found while using the WRF as a regional climate model and hopefully verify that it is of use for regional climate prediction. In addition, as some of the issues presented are not apparent in simulations on a day-to-day basis, it is hoped that this analysis will also be of interest to people who use the WRF in its more traditional roles in research and forecasting, whether or not they have moved on to higher resolutions. While there are a number of sensitivity studies using the WRF, there are a few publications where the WRF is used as a regional climate model. Likewise, most sensitivity studies using the WRF focus on single to multiple weather events, as in Gallus and Bresch (2006) where 15 cases are utilized. As mentioned above, little has been done examining longer-term WRF runs.

The following sub-sections will provide a subjective evaluation of varying WRF simulations and a discussion of their differences. Section 1 will also provide a description of the WRF and a few of the options that will be tested.

1) THE WRF MODEL AND ITS CONFIGURATION

Two versions of the Advance Research version of the WRF (ARW) were used in this sensitivity analysis, version 2.2 and version 3.0.1. Both are fully compressible and non-

hydrostatic, with a terrain-following hydrostatic pressure vertical coordinate (Wang et al. 2007). The Arakawa C-grid is used for grid staggering. For the most part, the default (and recommended) dynamics solver options for real data cases are used. The latter includes 3rd order Runge-Kutta split-explicit time integration, 5th order horizontal advection, and 3rd order vertical advection. Positive-definite advection of moisture is on. Using flux form prognostic equations, the WRF dynamics solver conserves mass, momentum, entropy, and scalars. The time step of the 90-km parent domain is 540s.

Initially, runs were completed using a 30-km resolution domain with 28 vertical levels. All of the simulations presented here, however, were produced with a 30-km horizontal resolution domain nested inside of a larger 90-km resolution domain. Nesting was required to remove large-scale flow problems that were resulting from the placement of the eastern boundary through the general region of the Bermuda high. Instead of increasing the size of the 30-km domain to move this boundary further east and, therefore, significantly increase the computational time, nesting was used instead[7]. Feedback between the nest and its parent domain is either on or off (i.e. 2-way or 1-way, respectively), depending on the simulation.

Initial and boundary conditions for the first part of this study are derived from the first version of the NCEP/NCAR global reanalysis project (NNRP, Kalnay et al.1996). The NNRP has a horizontal resolution of 2.5° with 17 pressure levels (excluding the surface) and is available in 6h increments. Later on, initial and boundary conditions will also be derived from the CCSM 3.0. For all simulations, the WRF is initialized on April 23rd of each simulated year and run through August 31st.

There are many parameterization options available in the WRF, and numerous options were tested, but only a few variations will be covered here.

---

[7]It was also noted, before the 90-km parent domain was added, that placement of the southern boundary impacted moisture flow into the Great Plains. This was greatly overshadowed by the eastern boundary problem, but later mitigated by placing the southern parent domain boundary through the Caribbean.

All simulations shown use the Community Atmosphere Model 3.0 (CAM) radiation package for longwave and shortwave radiation. The CAM is more expensive to use than other radiation options, but it was ultimately deemed more appropriate for the 30-km/90-km resolution simulations. CAM was designed for coarser grids. Specifically, it includes a relative humidity (RH) based cloud fraction function, so a grid cell is not just defined as having cloud cover or not (Kiehl et al. 1998, Collins 2001, Collins et al. 2002).

Surface layer processes are handled by the Monin-Obukov scheme in all simulations, and all but one employs the Noah land-surface model to provide sensible and latent heat fluxes to the planetary boundary layer (PBL). The other uses a less complex 5-layer diffusion model (Wang et al. 2007). The 5-layer land-surface model (LSM) predicts ground and soil temperature only. Soil moisture and snow-cover are not included, and surface moisture is based on land-use only. The Noah LSM is a more detailed 4-layer soil temperature and moisture model. It includes canopy moisture, snow cover prediction, a root zone, evapotranspiration, soil drainage, runoff, vegetation categories, monthly vegetation fraction, and soil texture (Ek et al. 2003).

Boundary layer fluxes and vertical diffusion are calculated by the Yonsei University (YSU) PBL scheme (Hong et al. 2006) in all simulations. This is an updated version of the Medium Range Forecast (MRF) model treatment of the PBL. It is a non-local-K scheme that uses a parabolic K profile in the dry convective mixed layer and treats entrainment explicitly[8].

The WRF Single-Moment 5-class[9] microphysics parameterization is also used in all simulations (Hong et al. 2004). It is suitable for mesoscale grid sizes and allows for ice, snow, mixed-phase, and super-cooled water processes as well as ice sedimentation.

Two different convective parameterization schemes were used: the Kain-Fritsch (KF; Kain and Fritsch 1992, Kain 2004), and the Betts-Miller-Janjić (BMJ; Betts 1986, Janjić 1994). In the following sensitivity analysis, the KF scheme is utilized in all but one sim-

---

[8]As opposed to implicitly as part of the non-local-K mixed layer.
[9]Water vapor, ice, snow, cloud water, and rain.

ulation. As this study focuses on precipitation simulation, a more detailed description of these parameterizations follows:

The BMJ scheme is a convective adjustment type scheme. It applies a lagged adjustment towards predetermined reference profiles of temperature and dewpoint, approximating convective equilibrium. To start, the scheme finds the most unstable parcel within roughly 200-hPa of the surface. The lifting condensation level (LCL) for this level is calculated and marked as cloud base. This parcel is then lifted moist-adiabatically to find cloud top. If the cloud depth is less than about 200-hPa (20% of the surface pressure value), deep convection is not allowed and the scheme checks for shallow, non-precipitating convection. Reference profiles for temperature and water vapor are calculated in the next step of the deep convective process and adjusted to conserve total enthalpy. That is, the reference profiles are adjusted until the latent heat release due to convection is balanced by the removal of water vapor through the depth of the convective layer. If enthalpy conservation cannot be achieved without cooling and moistening occurring after adjustment, deep convection is not allowed. Because net heating and drying must occur (the generation of precipitation requires the net removal of moisture and latent heat release), layers that are warm and/or dry initially tend to inhibit convection since this condition becomes more difficult to satisfy. Implicit controls on convection from deep-layer moisture convergence and convective inhibition are thus imposed with the enthalpy conservation restraint (Baldwin et al. 2002). Once final reference profiles are found, precipitation is calculated as a residual to the convective drying.

The KF CPS is a mass flux type scheme. It uses a cloud model to determine when and where convection will occur and what effect it will have on the environment. Parcel theory is used to decide if conditions are suitable for deep convection. Starting at the surface, layers that are at least 60-hPa deep are mixed and lifted to their LCL for a buoyancy check. There they are given a perturbation and, if warmer than the environment at the LCL, allowed to rise. The lowest parcel that can continue to ascend past a minimum cloud depth

TABLE 3. Notation and WRF options used in each simulation shown. Note, 'Simulation ID' corresponds to the panels in Figs. 18 and 19.

Simulation ID	Version	30-km SST update	Nest feedback	LSM	CPS
B	2.2	off	on	5-layer	KF
C	2.2	off	on	Noah	KF
D	2.2	off	off	Noah	KF
E	3.0.1	off	off	Noah	KF
F	3.0.1	on	off	Noah	KF
G	2.2	on	off	Noah	KF
H	3.0.1	on	on	Noah	KF
I	3.0.1	on	off	Noah	BMJ

(2-4 km, depending in direct proportionality to the temperature at the LCL) while experiencing the effects of entrainment, detrainment, and condensation loading, will be used for deep convection. If deep convection is an option, three vertical transport mechanisms are used to eliminate CAPE within a grid column. Specifically, updraft, downdraft, and compensating environmental mass fluxes are calculated and adjusted incrementally until at least 90% of the CAPE in the column is removed.

Finally, other variations that will be shown include changes in the feedback between the parent domain and nest, and sea-surface temperature (SST) update modifications. Table 3 lists the notation used for each run in the following section, as well as any varying options.

2) A COMPARISON OF WRF PRECIPITATION SIMULATIONS

Figures 18 and 19 show 1991 May-August (MJJA) average precipitation for simulations forced by the NNRP for the 90-km parent domain and the 30-km nest, respectively. The domains have not been clipped to remove the relaxation halo, as evident in the pattern of precipitation framing each map. Panels 18A and 19A display the average precipitation from the NARR for the corresponding time period, regridded to match the given WRF domain resolution. Recall that the NARR does have some problems over oceans, islands, and at country boundaries.

56
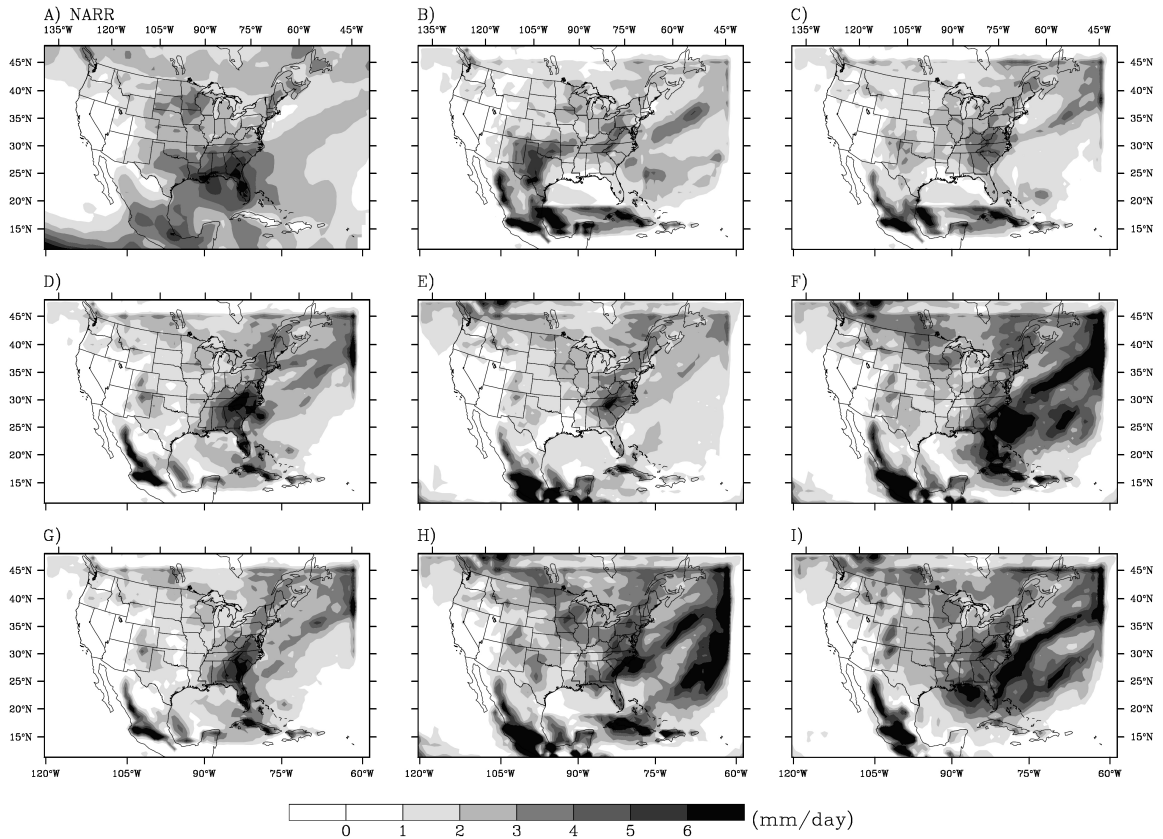
FIG. 18. 1991 MJJA average precipitation rate (mm/day; contours) from A) NARR and B) - I) 90-km WRF domain simulations. NARR data have been re-projected to match WRF domain size and resolution. Specification of the different WRF options in B) - I) are given in Table 3.
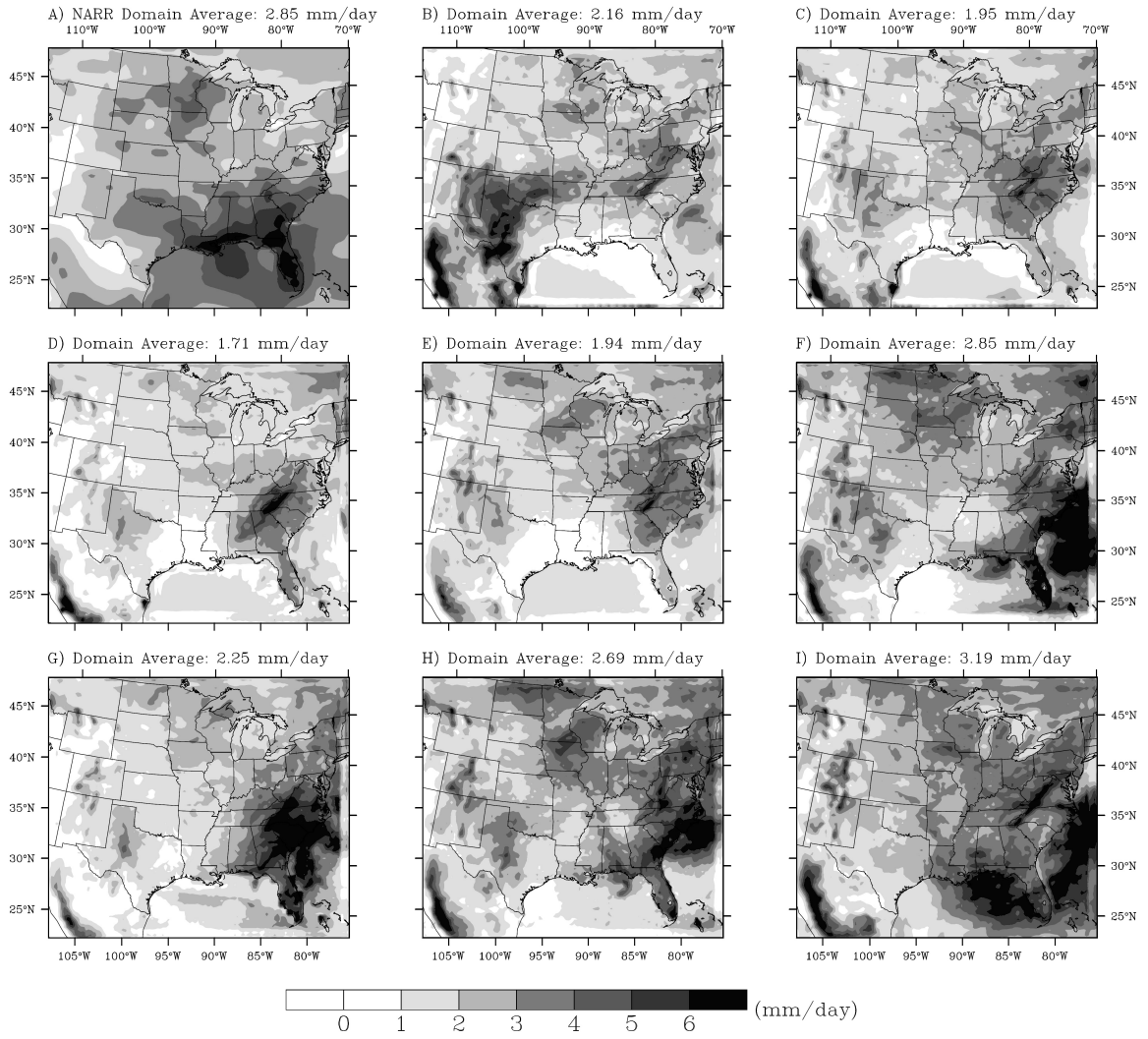
FIG. 19. As in Fig. 18, except for B) - I) from 30-km inner WRF nest. NARR data have been re-projected to match WRF inner nest size and resolution.

The pattern of average precipitation exhibited in Figs. 18 and 19 is moderately variable. This is also reflected to some extent in the domain average values shown in Fig. 19[10]. Simulation B (Figs. 18B and 19B[11]), unlike the others, uses the 5-layer LSM. It is identical to C in every other aspect of its configuration. Changing from the simple LSM in B to the more complex Noah LSM had an obvious impact on the amount of precipitation in TX and OK and along the East Coast, especially east of the Appalachian Mountains. The only other example of the impact of a physical parameterization change is conveyed in panel I. This simulation used the BMJ CPS instead of the KF. It is otherwise identical to the simulation shown in panel F. This change caused minor differences in average precipitation between I and F in most regions of the domain, but a more obvious change in the character of precipitation over Florida. Instead of producing a relative maximum, there is a minimum of precipitation over Florida relative to the surrounding waters in panel I, using the BMJ CPS. The exact reason for this has yet to be diagnosed.

The simulations shown in Figs. 18 and 19 panels B, C, and H all exhibit a very distinct edge in the pattern of precipitation in the Gulf of Mexico and off the East Coast, which marks the location of the inner nest. These particular simulations all used 2-way feedback; i.e., the feedback from the nest to the parent domain was turned on. Similar discontinuities are also obvious in the specific humidity fields from these simulations at levels below the tropopause (not shown). This problem is evident in WRF versions 2.2 and 3.0.1 (B and C vs. H, respectively). However, turning the feedback off had a much greater impact in version 2.2 than in version 3.0.1. Both versions, when feedback is turned off, exhibit an increase in precipitation over the Southeast, especially over FL, but this is more marked in version 2.2. Panels H and F illustrate the impacts of this change for otherwise identical setups of WRF version 3.0.1 (no equivalent illustration with version 2.2 shown). This

___

[10]Domain average values are not shown for the 90-km domain because less of the domain is land-based and the values from the NARR over the oceans are questionable.

[11]Panel labels in Figs. 18 and 19 correspond to the simulation ID given in Table 3.

problem is not evident while examining the 3-hourly output, as it is only upon averaging over a longer time period that it becomes evident.

It was not noticed through many runs that SST was not updating in the inner nest in WRF version 2.2, although the SST in the parent domain was updating properly. The fix for this required a slight change in the WRF model initialization program code for real data cases, and it is not a problem in version 3.0.1. The influence of time-varying SSTs on the precipitation in the parent domain was much stronger in version 3.0.1 (cf. Figs. 18E and 18F) than in version 2.2 (cf. Figs. 18D and 18G), particularly over the Gulf Stream. This difference in version 3 is intriguing since the SST in the parent domain was always set to update and the feedback between the domains is off in the simulations shown in Figs. 18E and 18F. Both versions show marked differences in precipitation in the 30-km nest (cf. corresponding panels in Fig. 19). Updating SSTs in the nest increases the average precipitation in the Southeast as well as in the secondary maximum in the Great Plains and North Central U.S., possibly due to greater moisture flux as the SSTs are then warmer as the season evolves.

Certain panels in Figs. 18 and 19 also illustrate the effect that switching WRF versions had on average precipitation. The best example of this impact can be seen by comparing simulations F and G. Both have SST updating in the inner nest and feedback off - they are, subjectively speaking, the best and most problem-free simulations produced for this particular season from each version of the WRF. Except for the model version, the setups are identical. Average precipitation in the parent domain is noticeably higher in the version 3.0.1 simulation than version 2.2 (domain average of 2.62 mm/day vs. 1.47 mm/day, respectively). The same effect materializes in the 30-km nest, although not to the same extent (nest average of 2.85 mm/day vs. 2.25 mm/day, respectively). Average precipitation in the version 3.0.1 simulation (F) is favorably higher in the Great Plains and North Central U.S.. The exact cause of these differences is unknown and outside the scope of this study. Only one parameterization used between these runs had any changes made to it in the new

version (the YSU PBL scheme); it may be that changes made outside of the model physics are having the greatest impact.

In the end, the WRF setup used in simulation F was chosen for continued study. As mentioned above, it is one of the best and most problem-free configurations tested, subjectively speaking, including those not shown here. Thus far, all of the simulations have been assessed over one 4-month period in 1991. Simulation F, however, has been run for five consecutive warm-seasons. The average precipitation for this simulation of MJJA of 1991-1995 is shown in Fig. 20. For comparison, average precipitation from the NARR and the NNRP for the corresponding period are also shown. While not without problems, the dynamically-downscaled NNRP/WRF simulations for this longer period were considered to be acceptable. Overall, the 5-year nested WRF precipitation agrees better with the NARR than does the NNRP precipitation. Average precipitation along the Texas and Louisiana Gulf coast up into Oklahoma and Arkansas may be too light, and there may be too much precipitation in the Northeast, but in contrast to the plethora of precipitation over the Southeast in the NNRP, for example, the nested WRF simulations are a definite improvement.

b. A Brief Discussion of the Sensitivity Tests

The various simulations in section 2 brought to light some issues that may not otherwise be as apparent in shorter-term weather forecast model runs. Specifically, there is a clear issue with feedback between the inner nest and parent domain that greatly impacts average precipitation when turned on - this is present in both WRF versions examined. Furthermore, while changing physical parameterizations, especially the convective parameterization, was expected to have an influence on average precipitation, it was not anticipated that switching WRF versions would have as great an impact on average precipitation as it did. Despite the variety of issues discussed, a reasonable setup of the WRF was found (i.e., it is seemingly problem-free) that produced simulations that improved upon the precipi-
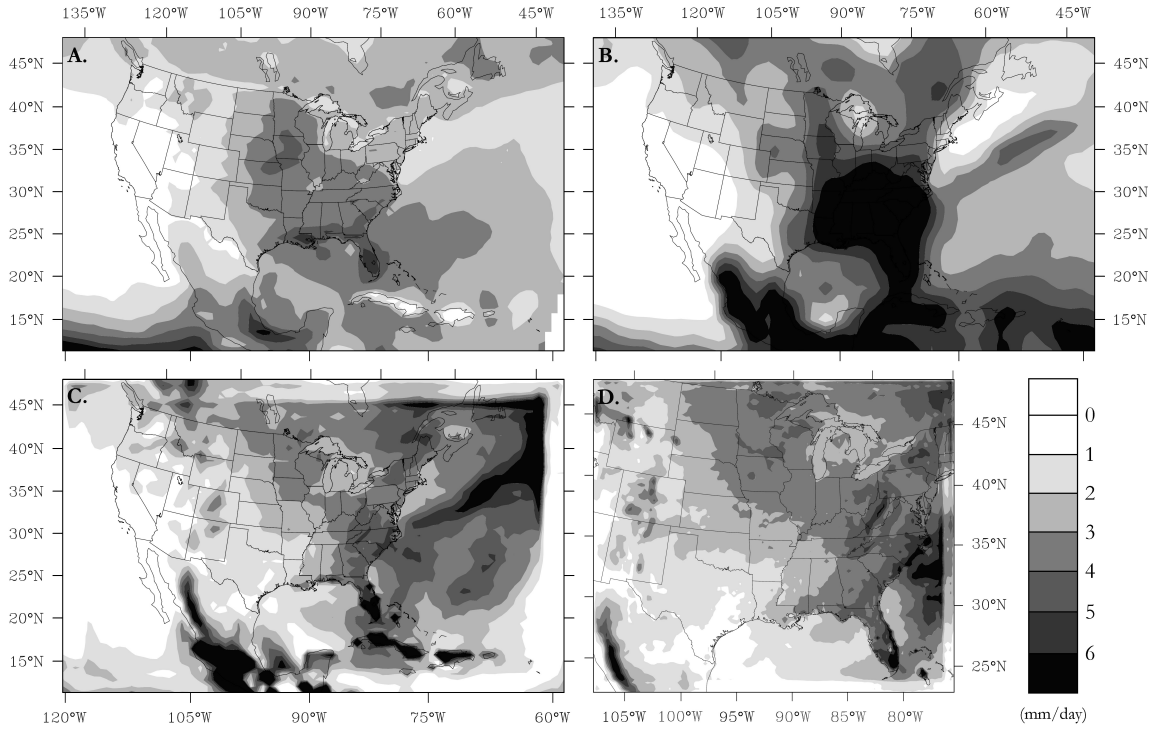
FIG. 20. 1991-1995 MJJA average precipitation rate (mm/day) from A) NARR, B) NNRP, C) WRF 90-km parent domain, D) WRF 30-km inner nest. NARR data have been re-projected to match 90-km WRF parent domain size and resolution.

tation fields found in the NNRP, the source of the initial and boundary conditions for the these simulations. This setup (from simulation F, hereafter referred to as WRF-NNRP) will be the only one used in subsequent sections and chapters for regional climate simulation, although the source of the initial and boundary conditions will change.

5. The Simulation of Present Climate using the WRF

For the projection of future climate, relative to the present, the WRF was also run using initial and boundary conditions from the CCSM 3.0 (this combination hereafter referred to as the WRF-CCSM). This section will investigate the usefulness of the WRF in dynamically downscaling CCSM 3.0 output for the present and compare it to the WRF-NNRP simulations and the NARR before moving on to the late 21st century in the next chapter.

a. WRF-CCSM Methods

Running the WRF using global climate model simulations for forcing is not a standard practice yet, relative to its other uses; thus, it is practical to include a few brief comments here on what was required to do so. Of note is the current inability of the WRF pre-processing system (WPS) to handle input data in netCDF format and/or regional data on a Gaussian grid (the latter is a bug that has not been fixed as of the writing of this dissertation). The majority of the data from the models run for the IPCC AR4, including the CCSM 3.0, incorporate both obstacles. Thus, running the WRF as a nested regional climate model starts out in a less than straightforward manner.

The CCSM 3.0 was chosen for this exercise because it is one of few global climate models to have all of the necessary output data available with a time and spatial resolution suitable for use with the WRF. Variables from the CCSM 3.0 at a 6h time interval used for WRF initial and boundary conditions include: geopotential height, temperature, specific humidity, east-west and north-south wind components, soil moisture, and soil temperature. Surface pressure, sea level pressure, surface geopotential height, land-sea fraction, surface skin temperature, SST, and water equivalent snow depth are also necessary. Furthermore, one monthly average field is used to avoid a problem that occurs in the WRF preproces-
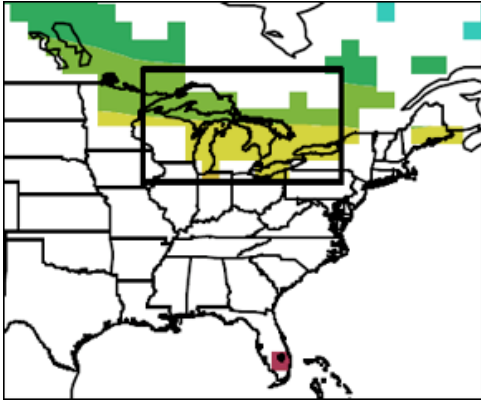
FIG. 21. 1990-1999 20C3M average lake temperature from the CCSM 3.0 (turquoise-yellow: 264°-280°K, red: 288°-292°K). White area filled with missing values. Monthly average values within the black box masked into 6h skin temperature field.

sor[12]: lake temperature. This field is not available at a greater time frequency, but lake temperature is not highly variable, and this is a more realistic option than setting the lake temperature to a constant value (for all months). Lake temperature is masked in over the input skin temperature field before it is used in WPS. Because the CCSM has a relatively low resolution, this field is coarse (e.g. Fig. 21), but that does not have a great impact on land surface temperatures once it is preprocessed.

Note also that in some of the comparisons presented between the WRF-CCSM and the WRF-NNRP, the number of years used in the comparison is not always equal. For late 20th century, only 5 years of simulation were completed from the WRF-NNRP (1991-1995), and 10 years were completed for the WRF-CCSM (1990-1999). It was possible to compare the WRF-NNRP simulations to reality with only 5 years of output data, as the initial and boundary conditions from those 5 years correspond directly to the same five years in reality. This is not the case with the simulations from the WRF-CCSM. WRF-CCSM simulations from the 20th century were forced using CCSM 3.0 simulations from the 20C3M emissions scenario. This scenario includes known historical variations in nat-

---

[12]For an unknown reason, the WRF preprocessor sets the surface skin temperature over the Great Lakes, Salt Lake, and other lakes and East Coast bays to an unrealistically high temperature, even though this is not what is input. This causes a large amount of lake-effect convection. Using monthly average lake temperature combined with two other modifications to the default preprocessing settings has significantly restrained this problem.

ural and anthropogenic forcing (e.g. solar, volcanoes, green house gasses, ozone, aerosols, etc.); however, the particular CCSM run for the 20th century used here was initialized in 1870. Thus, the internal variability in the WRF-CCSM and CCSM 3.0 of weather, and seasonal and interannual climate variability, will not exactly match that found in reality. That is, any given year from the CCSM 3.0 does not necessarily correspond directly to that given year in reality, though the external forcing may match observations. Thus, the WRF-CCSM and CCSM 3.0 simulations of the 1990s are an approximation of the climate from that decade. To minimize the impact of potential differences in seasonal and interannual climate variability between reality and the WRF-CCSM, a full decade of simulations was completed and used in this analysis. It is still an approximation, as are the comparisons between the WRF-NNRP and WRF-CCSM. An identical match is not expected, but a reasonable comparison between warm-season climate characteristics for that decade is possible. A direct comparison of the WRF-CCSM and WRF-NNRP for the 1991-1995 period is made only in instances where the statistical significance of the difference between a given variable from the two WRF versions was desired. In the two instances where this occurs, the average variable quantity from the WRF-CCSM would not have differed much if the full 1990-1999 period was used in the average in any case.

1) SIGNIFICANCE TESTING

Some of the differences presented in this chapter and the next will be tested for statistical significance. Due to the limited number of years simulated in each century and the unknown distribution of some of the variables to be tested, bootstrapping was used to estimate confidence intervals following von Storch and Zwiers (1999). In every application of this method, the same number of seasons from the present and the future were pooled as if drawn from the same distribution (usually 5 or 10 MJJA seasons from both the 1990s and the 2090s). From this pool, two lots of x number of cases were randomly selected (where x is the number of seasons used from a given decade in the pooling), with replacement,

and the difference between the two randomly sampled lots was estimated. Monte Carlo simulation was used to generate 1000 bootstrap samples of each difference between the present and the future in this manner, giving a distribution from which the lower and upper tail critical values were estimated (0.05 and 0.95, respectively).

b. Precipitation Simulation

The complement to Fig. 20 for the WRF-CCSM appears in Fig. 22. Given the difference in initial and boundary conditions, the average precipitation from the WRF-CCSM for the 1990s was not expected to exactly match that from the WRF-NNRP, but as shown, it does exhibit some of the same basic characteristics that mark average warm-season precipitation in the U.S., though not as realistically as the WRF-NNRP. It too is not perfect, but the dynamically downscaled precipitation appears to be an improvement on the original from the CCSM 3.0. There is less precipitation in the Midwest and Northern and Central Great Plains in the WRF-CCSM compared to the WRF-NNRP (though not particularly obvious with the color scale in Fig. 22), but there is still the suggestion of the secondary warm-season precipitation maximum. This is an improvement from the CCSM 3.0. As illustrated in Fig. 22a, the CCSM 3.0 instead produces too much precipitation in the central and high Plains that is possibly orographic in nature. However, like the WRF-NNRP, the WRF-CCSM is too dry in the South, but to a greater extent - here the WRF-CCSM average precipitation is not an improvement on the average precipitation from the CCSM 3.0.

As discussed previously in chapters 2 and 3, reanalyses and climate models have difficulties capturing the diurnal cycle of precipitation, especially in the Great Plains during the warm-season. Figure 23 depicts the time and magnitude of the maximum precipitation rate for MJJA for the WRF-NNRP, WRF-CCSM, and the relevant reanalysis and climate model. Once again, the NARR is also shown in this figure as an approximation for reality over land only. As shown in Fig. 23e and f, the WRF-CCSM has greater difficulty capturing the magnitude of the maximum compared to the WRF-NNRP, especially over the South-
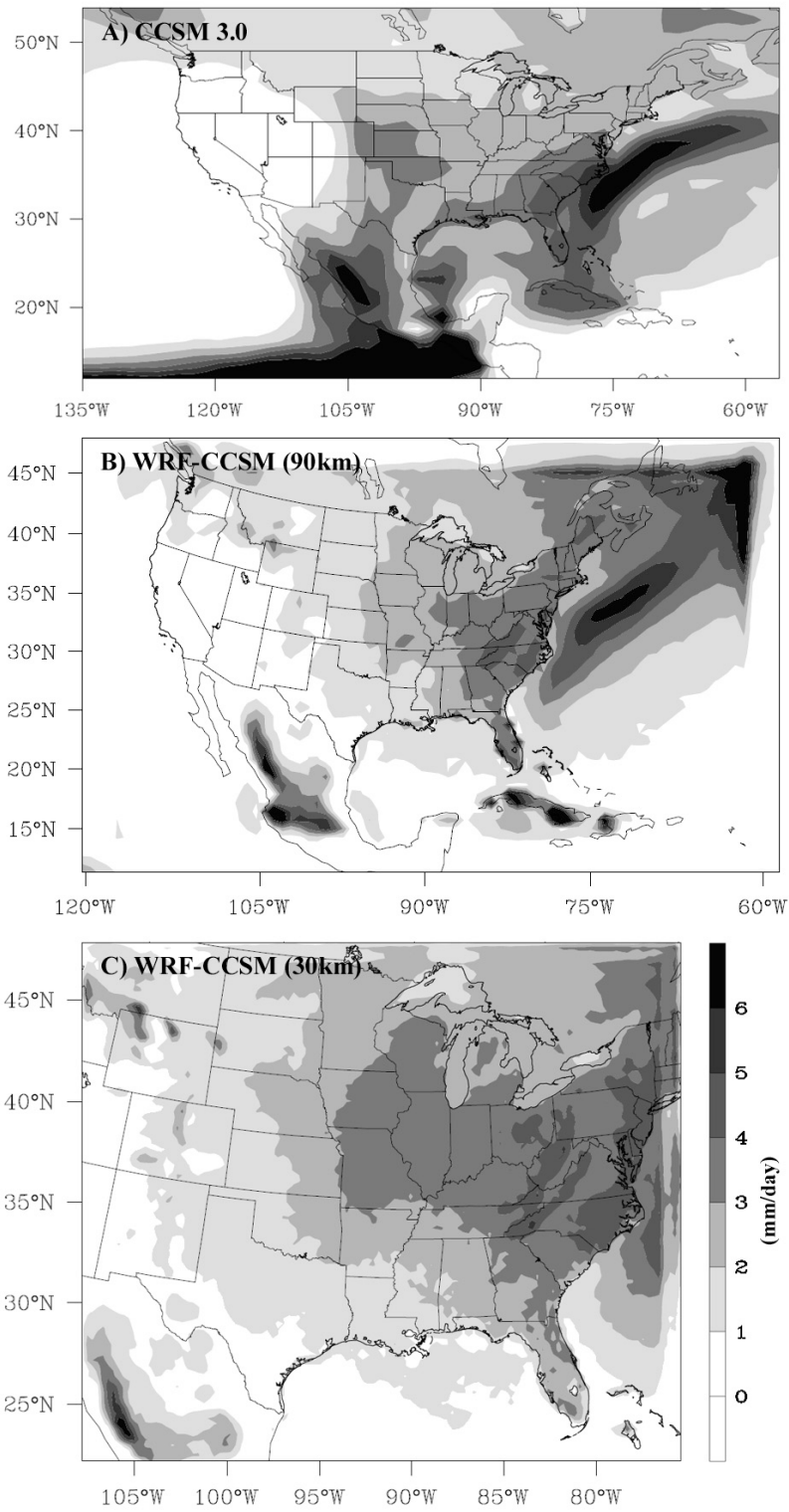
FIG. 22. 1990-1999 MJJA average precipitation (mm/day) from A) CCSM 3.0, B) WRF-CCSM (90-km parent domain), and C) WRF-CCSM (30-km nest).

east, and more so than its forcing climate model. What both WRF simulations improve on, however, is the timing of the precipitation over certain areas of the country; specifically, the Midwest and Upper Great Plains. Both the WRF-NNRP and the WRF-CCSM hint at a nocturnal maximum where there should be one in this region. At the horizontal resolution of either domain, it is not expected that this occurs for the "right" reason[13]. However, it does indicate that heavier precipitation is occurring and not primarily at the time of maximum solar heating for the day; thus, there must be other mechanisms in play that the WRF and its CPS are picking up on to produce precipitation in the late afternoon and evening.

While precipitation in both the WRF-NNRP and WRF-CCSM is not without error, it is still an improvement over the precipitation simulated by the relevant climate model or reanalysis system. The greatest benefit to using the WRF as a nested regional climate model, in terms of the simulated precipitation, emerges in the frequency distribution of precipitation rate. Figure 14 clearly illustrated that climate models generally produce too much light precipitation and too little heavy precipitation. As shown in Fig. 24, dynamically downscaling the CCSM 3.0 greatly improves the distribution of precipitation. The distribution shown in Fig. 24 is restricted to the central U.S. (for the region shown in Fig. 25c or d). There is now a more realistic tail of heavy precipitation rates and fewer light precipitation events. The WRF-CCSM domains for this region (Figs. 24c and d) may contain more extreme precipitation rates than the NARR (Fig. 24a), but the NARR may not contain a good representation of these more extreme events either since they may also be constrained by the modeling system used to produce the NARR. Unfortunately, there is no better way to verify this distribution. However, it is still clear that the precipitation from the WRF-CCSM simulations is more realistic than that from the CCSM 3.0. The same can also be said for the WRF-NNRP (not shown).

---

[13]The convective systems are not realistically structured MCSs at this resolution, after all. In this case, they more closely resemble the convective "blobs" of forecasting models that were previously run near this resolution (not shown).
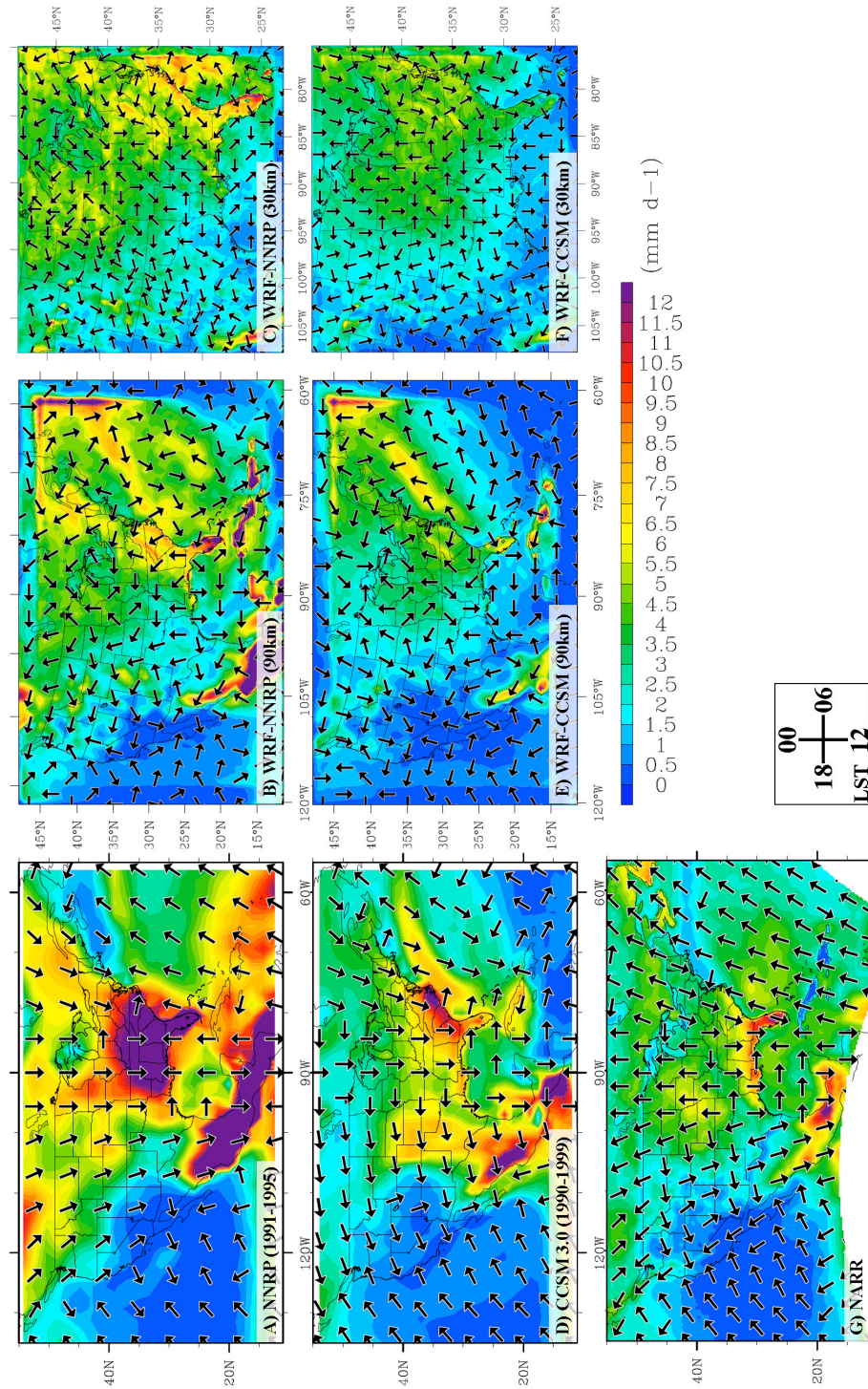
FIG. 23. A)–C) 1991-1995 MJJA maximum 3h or 6h average precipitation rate (mm/day, contours) and time of maximum (vectors, LST) from A) NNRP (6h), B) WRF-NNRP (90-km domain, 3h), and C) WRF-NNRP (30km nest, 3h). D)–G) same as A)–C) but for 1990-1999 and D) CCSM 3.0 (6h), E) WRF-CCSM (90-km domain, 3h), F) WRF-CCSM (30-km nest, 3h), and G) NARR (6h). Vector time clock key inset at bottom center.

Also of note in Fig. 24 is the difference between the two WRF-CCSM domains. As one might expect, given the difference in resolution, there are more occurrences of heavier precipitation rates in the 30-km nest than in the 90-km parent domain. It is also interesting that the 90-km domain's distribution is closer to that from the 30-km domain's than it is to the CCSM 3.0's even though it is not that dissimilar in resolution from the CCSM 3.0 (which has a horizontal resolution of approximately 1.4° or approximately 155-km north-south by 120-km east-west at 40°N). Thus, resolution may not entirely explain the lack of heavy precipitation events in the CCSM 3.0.

Similarly, the simulations from the WRF-CCSM also improve upon the magnitude of some of the heaviest precipitation rates in the Central U.S., though not necessarily the spatial distribution, as illustrated in Fig. 25. This can also be said for other extreme percentile values (e.g. the 95th percentile, not shown). Given that the values calculated in Fig. 25 used only precipitation rates above a trace, the 99th percentile is equivalent to a return period of approximately one 6 hourly event at the rate shown per year per grid point. As expected given the frequency distribution shown in Fig. 24, the 99th percentile values of precipitation in the CCSM 3.0 are approximately half those from the NARR and the WRF-CCSM (note the difference in color scale between Fig. 25, panel b and panels a, c, and d). However, the axis of greatest magnitude between the NARR and the WRF-CCSM is different, and may be suggestive of cold-frontal forcing or a shift in the region of favorable conditions for most of the events that produce these values in the WRF-CCSM.

c. Near-Surface Temperature Simulation

Improvements after downscaling are not limited to precipitation. This is illustrated for average MJJA 2m temperature from 1991-1995 in Fig. 26. Using the WRF as a nested regional climate model allows for much more detail in the spatial distribution of near-surface temperature in both the 90km domain and especially the 30km domain. Regions of cooler average temperature at higher elevation are much more distinct and of a more appropriate

70
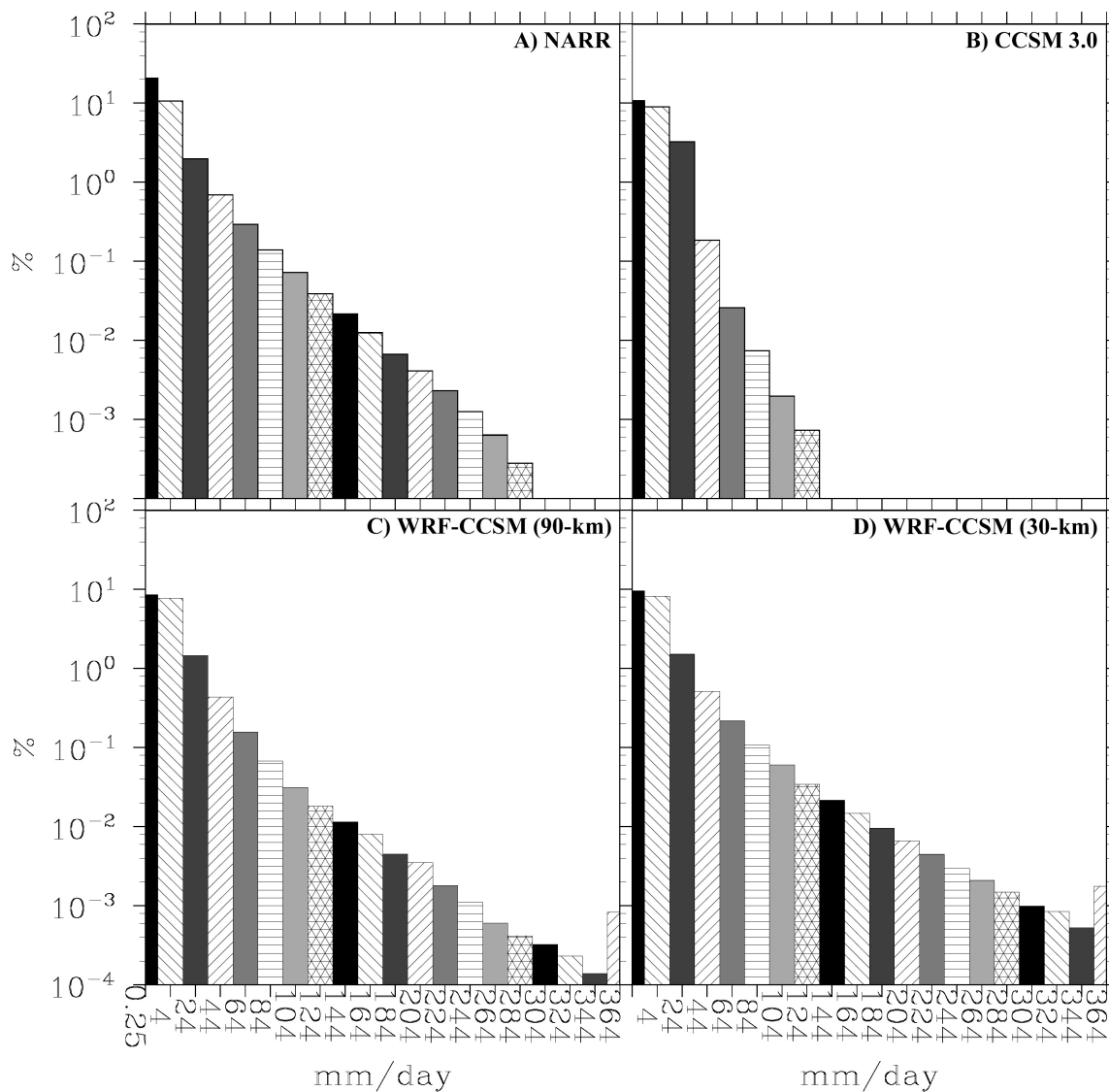
FIG. 24. 1990-1999 MJJA frequency distribution for 6h average precipitation rates (mm/day) from A) NARR, B) CCSM 3.0, C) WRF-CCSM (90-km domain), D) WRF-CCSM (30-km nest) for the region central U.S. region used in Fig. 25. The number under a given bar is the starting point for values in that bin. Frequency is shown as the percent of 6h periods with an average rate that falls into a given bin from all possible 6h periods and grid points in the given region.
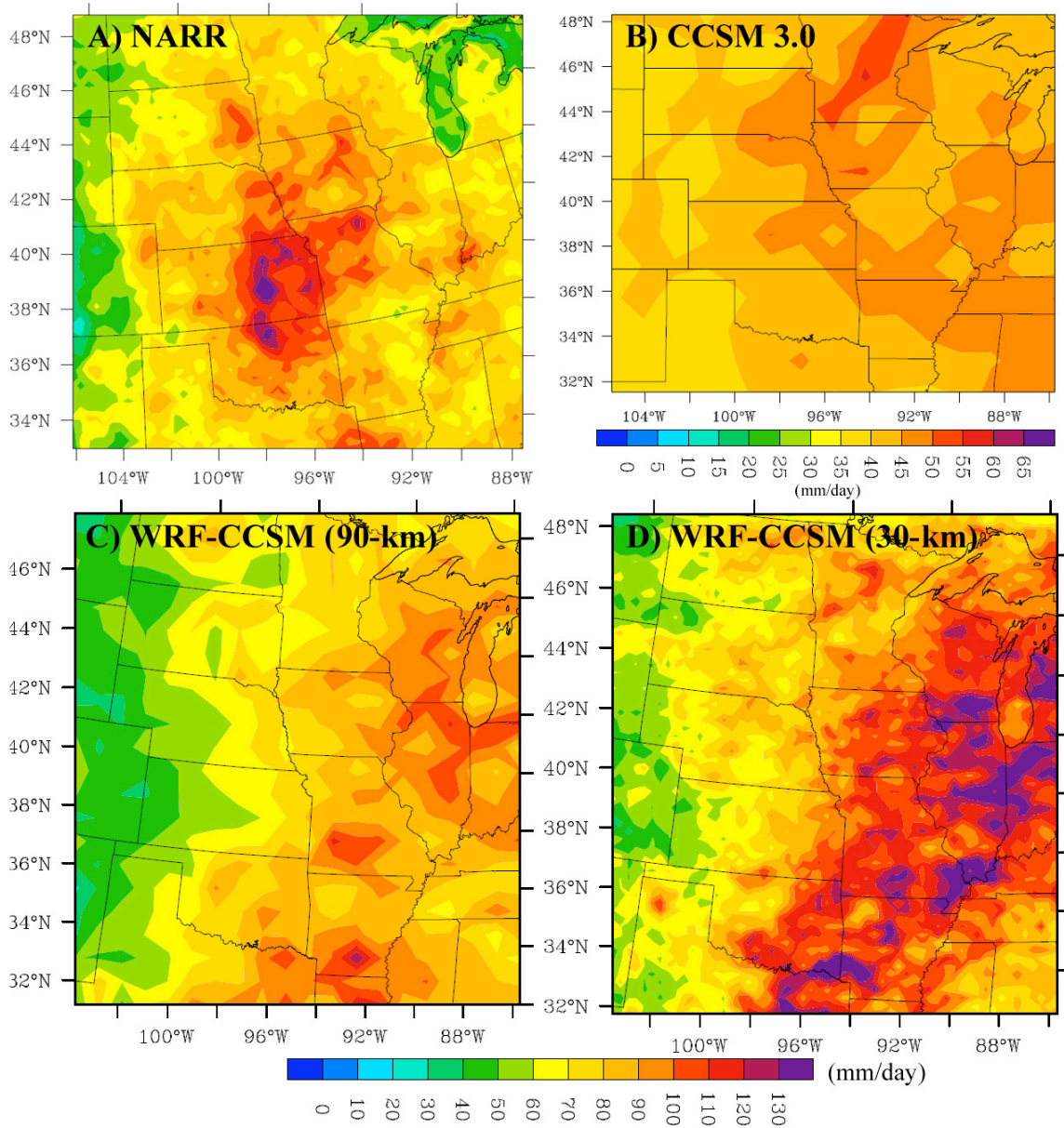
FIG. 25. 1990-1999 MJJA 99th percentile 6h average precipitation rate (mm/day) from all values greater than a trace (as previously defined at 0.25 mm/day) from A) NARR, B) CCSM 3.0, C) WRF-CCSM (90-km domain), D) WRF-CCSM (30-km nest). Color contour scale for B is half of that used in the other panels and is included below panel B.

magnitude in both the WRF-NNRP and WRF-CCSM simulations. The region of maximum temperature in the Southern Plains in the WRF simulations is too widespread, but in the CCSM and NNRP it is generally too cool throughout the Plains, relative to the NARR. The temperature in the WRF-NNRP and the WRF-CCSM is cooler in the Southeast, especially over FL, compared to the NARR, but not to the same extent as the NNRP and, particularly, the CCSM.

Again, the WRF-NNRP and WRF-CCSM are similar over the continental U.S. This is illustrated in panels h and i of Fig. 26. However, the near-surface temperature in the WRF-CCSM is significantly different than that in the WRF_NNRP over most bodies of water. For the most part, the average temperature in the WRF-CCSM over water is too cool; however, there are areas off the Pacific coast and the NE coast that are about 2°-6° warmer than those in the WRF-NNRP. These cooler and warmer temperatures in the WRF-CCSM over large bodies of water are the result of biases in the CCSM 3.0 SSTs.

d. Discussion

Overall, the WRF-CCSM does improve upon precipitation characteristics compared to those from the CCSM 3.0. It also adds useful regional detail to the near-surface temperature field. As discussed in the introduction to chapter 4, this is not an uncommon result when a regional model is used to dynamically downscale GCM simulation output. The downscaled CCSM 3.0 and NNRP precipitation is not perfect, but both the WRF-NNRP and the WRF-CCSM indicate that there should be a maximum of precipitation in the northern Great Plains and western Midwest in the warm-season, something their forcing systems do not do. This is similar to the basic result obtained byAnderson et al. (2003) for the June-July 1993 season of unusually heavy precipitation using 13 RCMs and the NNRP for initial and boundary conditions. The WRF-CCSM is also able to better simulate the frequency distribution of 6h precipitation for the central U.S. In general, the results from this chapter

have indicated that the WRF is able to add realistic detail to GCM output and not just that from reanalyses where the forcing conditions are likely to be more accurate.
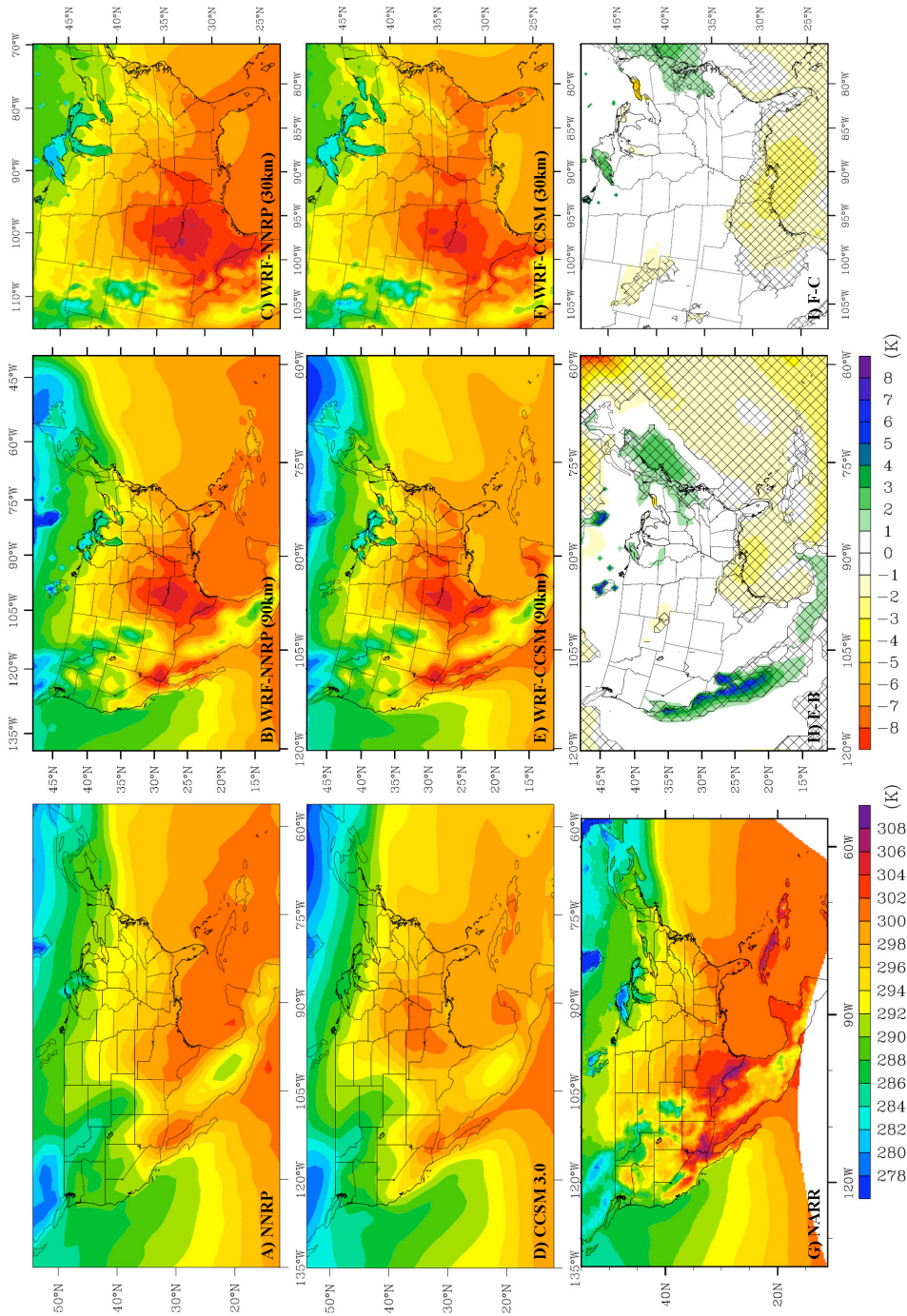
FIG. 26. A)-G) 1991-1995 MJJA average 2m temperature for from A) NNRP, B) WRF-NNRP (90-km parent domain), C) WRF-NNRP (30-km nest), D) CCSM 3.0, E) WRF-CCSM (30-km nest), F) WRF-CCSM (90-km parent domain), G) NARR (K, contours). H) 90-km WRF-CCSM, WRF-NNRP difference. I) 30-km WRF-CCSM, WRF-NNRP difference. Hatching in H) and I) indicates that the difference is significant at the 10% level.

75

6. Regional Climate Projections

Since it was demonstrated in the previous chapter that the WRF is an effective tool for dynamically downscaling CCSM 3.0 output from the 20th century, it was used to produce regional simulations of the later part of the 21st century. This chapter presents differences between the 1990s and the 2090s in near-surface temperature and various aspects of precipitation. The CCSM 3.0 simulations used to force the WRF for the 2090s utilized the SRESA2 emissions scenario (IPCC 2000). As discussed briefly in section 5, and as illustrated in Figs. 9 and 10, this is a high-end emissions scenario. It was chosen for use here as it is likely to produce a stronger signal for climate change, increasing the ability to diagnose the direction of change in the fields to be analyzed and whether or not those changes are outside of random variability.

a. Near-Surface Temperature

Figure 27 illustrates the difference in 2m temperature between the 1990s and the 2090s. At no point in this region do either the CCSM 3.0 or WRF-CCSM simulations show average cooling for the warm-season. In a broad sense, the difference from the WRF-CCSM is consistent with that from the CCSM 3.0. Both indicate an increase in average near-surface temperature of over $4°K$ for nearly all of the continental U.S. The spatial distribution of this change is slightly different between the two - the WRF-CCSM simulates greater warming in the northern Great Plains and Midwest than its forcing model, and a lesser warming in some of the land based areas in southern North America. The difference from the 30-km nest is not shown here because it is comparable to the 90-km domain; specifically, no further detail is gained despite the increased horizontal resolution with the given contour scale in Fig. 27. The hatching in Fig. 27 indicates that the increase in temperature is statistically significant at the 10% level; here, for every grid point in both WRF-CCSM domains (30-km nest not shown) and and the CCSM 3.0.

76
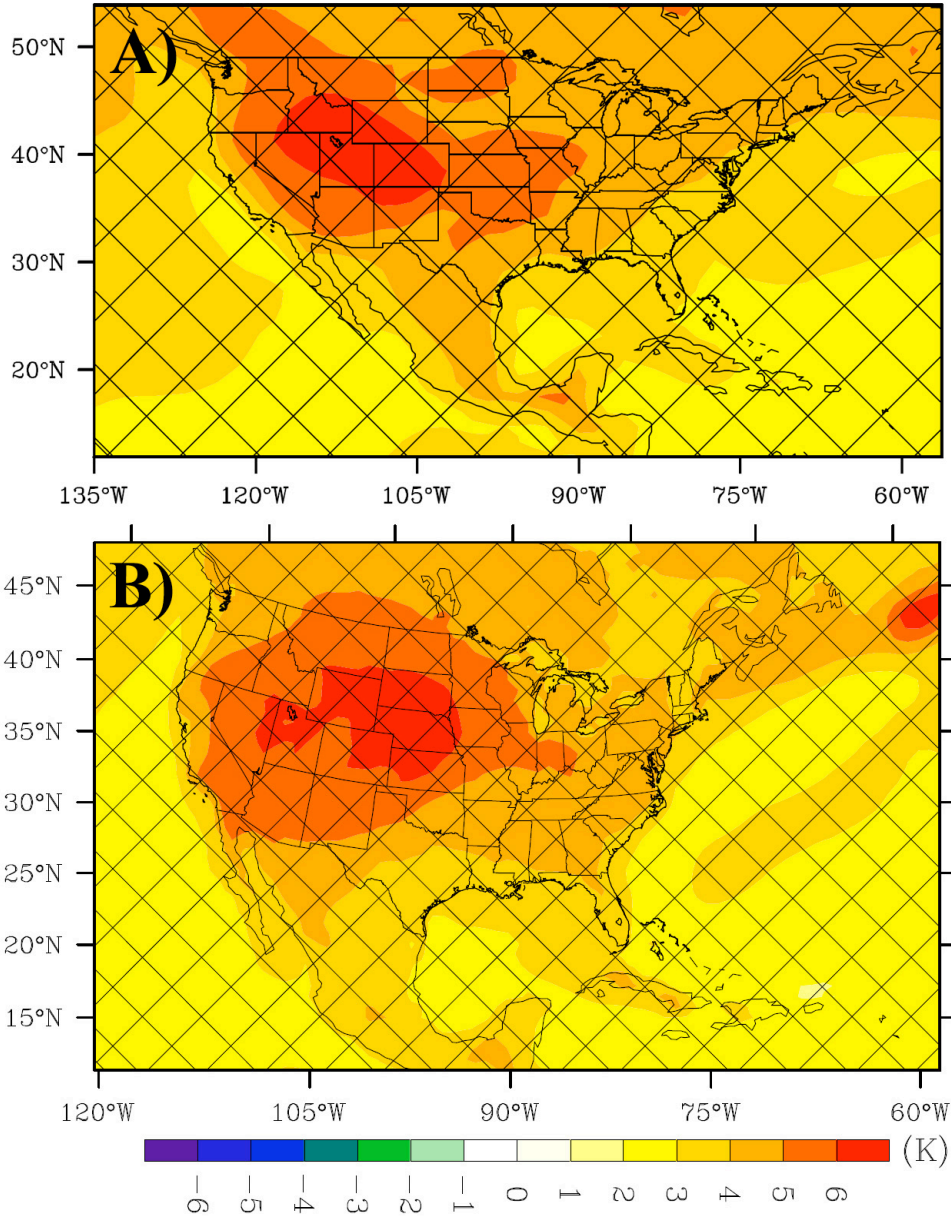
FIG. 27. Difference between 2090-2099 and 1990-1999 MJJA average 2m temperature (K) from A) the CCSM 3.0 and B) the WRF-CCSM 90-km domain. Hatching indicates that the difference is significant at the 10% level; here, at every grid point.

b. Precipitation

The WRF-CCSM also projects a decrease in mean MJJA precipitation between the 1990s and the 2090s, as indicated in Fig. 28. While there is a decrease of 10% or greater over most of the continental U.S., this difference is only statistically significant (at the 10% level) in certain regions; specifically, in the Southeast, along the Gulf Coast into eastern TX, and in parts of the central Plains, certain Rocky Mountain States, and the West Coast. There is also a significant decrease in average precipitation shown in the 90-km domain over most of the Atlantic and Caribbean waters included in the simulations. This decrease in average precipitation over most of the continental U.S. for the summertime is consistent with projections from most climate models run in support of the IPCC AR4 (Christensen et al. 2007); however, it is not consistent with the change in average MJJA precipitation in the CCSM 3.0 between these two decades (Fig. 29). The CCSM 3.0 projects an increase of over 10% in mean MJJA precipitation in almost all continental regions of the U.S. except the Northwest and Gulf Coast. Where the CCSM 3.0 projects increases in average precipitation through the Southwest and Great Plains, the WRF-CCSM does produce less of a decrease or a very slight increase (in regions where the increase in the CCSM 3.0 are strongest). It is still interesting, however, that given the initial and boundary conditions from the CCSM 3.0, the WRF indicates a much drier summertime climate than its parent model for the future.

The decrease in mean MJJA precipitation in both domains is not accompanied by a decrease in the entire distribution of precipitation. It is mainly caused by a decrease in the occurrence of the light to moderate, but most frequent rainfall events. This is illustrated for the central U.S. in Fig. 30. Here, the shift in the distribution is more pronounced, but does follow the same general shift evident in either the full 30-km or 90-km domain. The change in the distribution of precipitation rates in Fig. 30 also indicates an increase in the much less frequent, but most intense precipitation events. For example, in Fig. 30, we see that increases in frequency are statistically significant at the 10% level starting in the
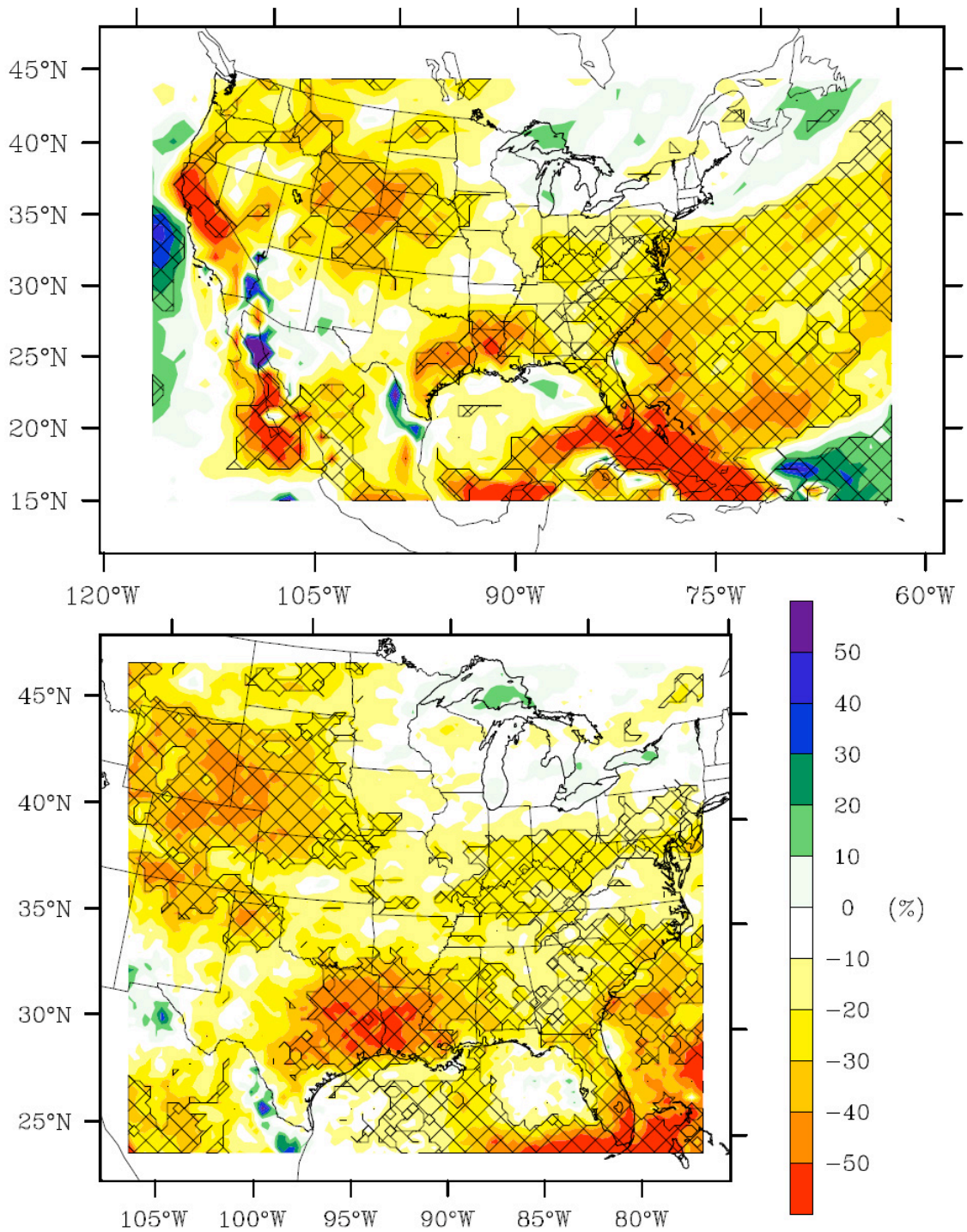
FIG. 28. Percent difference between 2090-2099 and 1990-1999 MJJA average precipitation from the WRF-CCSM. Top) 90km domain difference. Bottom) 30-km domain difference. Hatching indicates that the difference is significant at the 10% level.
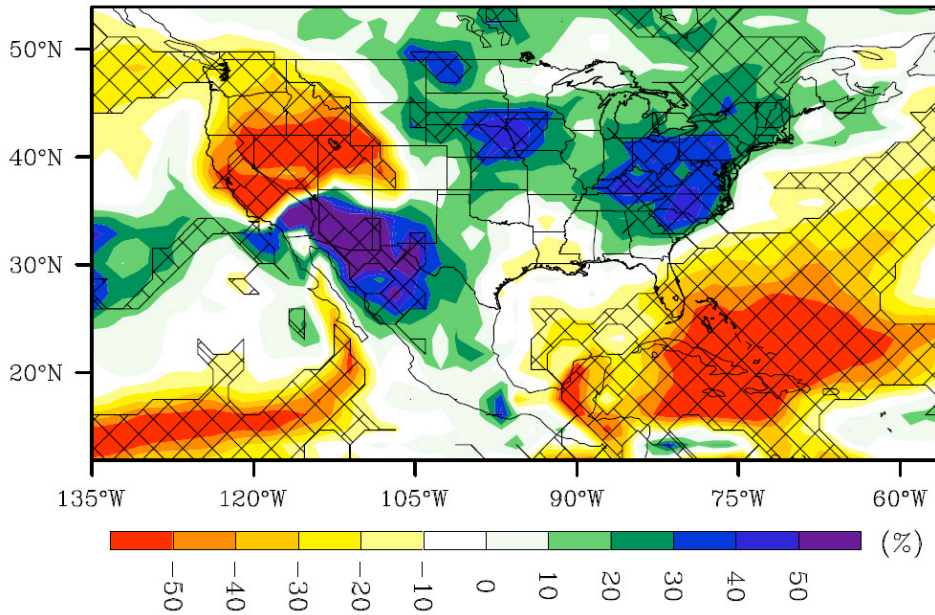
FIG. 29. Percent difference between 2090-2099 and 1990-1999 MJJA average 6h precipitation rate from the CCSM 3.0. Hatching as in Fig. 28.

264-284 mm/day bin. Occurrences of 6h average precipitation rates in this bin anywhere in the central U.S. increase by about 55% between the 1990s and the 2090s. However, in this region, the shift to more frequent extreme precipitation rates is obviously not enough to compensate for the decrease in lighter rates, resulting in the overall decrease in average precipitation.

Although the WRF simulates an increase in the frequency of intense precipitation events over the central U.S., for the most part, there is not an increase in the magnitude of these events over the entire central U.S. region, as shown in Fig. 31 for the 99th percentile. However, the average 99th percentile value for the 30-km domain in the region shown in Fig. 31 increases from 88.06 mm/day in the 1990s to 94.41 mm/day in the 2090s, an increase of 7.21%. For more common, yet still heavy precipitation events, the WRF-CCSM also shows slight increases in magnitude in the central U.S. The regional average increase in the 90th percentile 6h average precipitation rate is 1.11% in the central U.S. using the 30-km nest simulations. For more rare events, the increase in magnitude is greater. The upper 0.3th percentile is projected to increase by 14.27% and the upper 0.1 percentile by
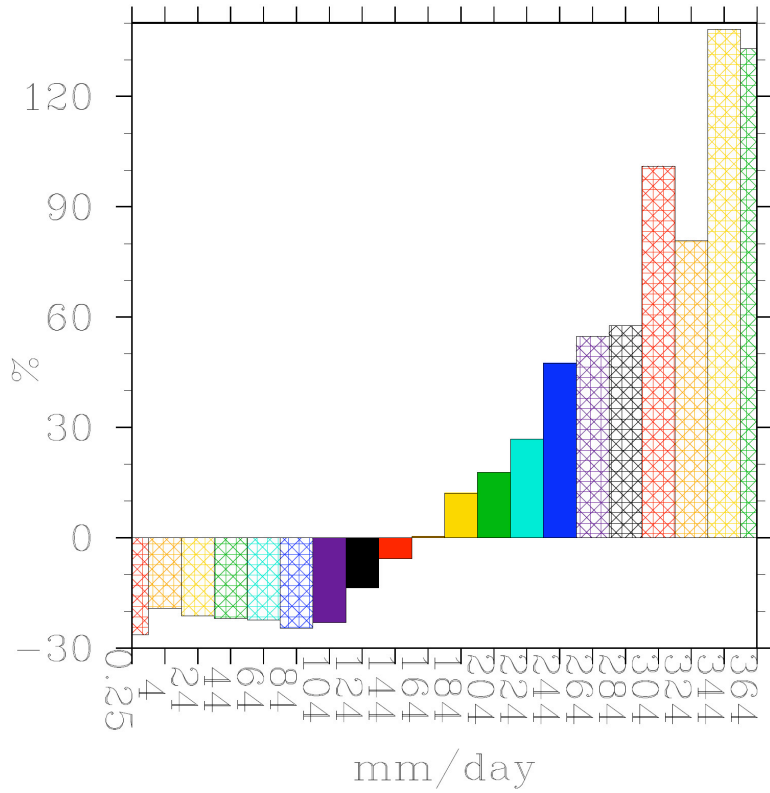
FIG. 30. Percent difference between 2090-2099 and 1990-1999 MJJA 6h average precipitation rate frequency distribution from the WRF-CCSM 30-km nest for the region shown in Fig. 25c (central U.S. only). Hatching indicates that the difference is significant at the 10% level.

20.78% (defined as "very heavy" and "extreme", respectively, by Groisman et al. (2005), who also defined the upper 10th percentile as "heavy").

Using the entire distribution of 6 hourly average rates from every point in the central U.S., i.e. those used in Fig. 30 and excluding trace values and those equal to zero, we can more easily illustrate that although the magnitude of "heavy" to "very heavy" events might increase, the frequency of those events may still decrease. This is the case for the 90th percentile value. For the rates in Fig. 30, the magnitude of the 90th percentile value increases just slightly from 28.13 mm/day to 28.70 mm/day.However, rates of this value occur in a category that shows a significant decrease in frequency of around 20% (again, this is just for this particular value, not for all of the values in the upper 10th percentile, as they exhibit a small increase). The same is true of the 99th percentile value, but to a greater extent. It increases from 94.84 mm/day to 103.01 mm/day, but these values are also contained in a bin that exhibits a decrease in frequency in Fig. 30, this time of around 25%. It is the very heavy to extreme events that show an increase in both magnitude and frequency. The 99.7th percentile value increases in magnitude from 149.34 mm/day to 177.97 mm/day, this is the point in the distribution where values begin to show an increase in frequency. The 99.9th percentile value increases in magnitude from 207.99 mm/day to 258.03 mm/day, or 24.1%, and spans bins that exhibit clear increases in frequency.

Thus, even though there are increases in the magnitude of heavy precipitation rates, there is no increase in the frequency of those events until they reach a rate that might be defined as very heavy. These are, either way, events that are more likely to be disruptive and have a greater impact.

Another, more simplistic way to look at what happens to precipitation in the future is to examine the change in the number of wet and dry periods (or the number of periods contributing to the total precipitation for a given time span, or not), and the average intensity of precipitation when it does rain (Frich et al. 2002, Sun et al. 2006). Both are usually calculated from daily precipitation data, and the latter is known as the Simple Daily Intensity

Index (SDII): the total precipitation from wet days over a period of time divided by the number of wet days in that period (where wet days are are defined as having precipitation greater than 1 mm/day, Frich et al. 2002). Here, these metrics are applied to 6 hour average precipitation rate to better understand changes in the frequency and intensity of precipitation seen above. Wet periods are defined at every grid-point as 6h rates greater than a trace (previously defined at 0.25 mm/day); all others are defined as dry periods.

In the 30-km WRF-CCSM simulation over the central U.S. region, there is a decrease in MJJA average precipitation, as illustrated in Fig. 28. The total percent decrease in this region is approximately 18.2%. Between the 1990s and 2090s, the number of wet periods decrease by 22.7% while the number dry periods increase by 5.8%. The simple intensity index for 6h periods (S6II) increases by approximately 6.2%. This indicates that periods of rain are fewer and farther between, but that when it does rain, it is more intense. The slight increase in intensity when it does precipitate is not enough to compensate for the decrease in rain periods, leading to an overall decrease in average precipitation for the region. The increase in the number of dry periods and decrease in the number of wet periods also suggests an increase in the number of consecutive dry periods and/or dry days. Therefore, the overall results from the WRF-CCSM suggest an increase in the frequency of droughts and floods for the central U.S.

A similar analysis can be completed for the CCSM 3.0. In the central U.S., the CCSM 3.0 shows an increase in average precipitation of about 15%. The direction of change in the number of wet and dry periods is the same as in the WRF-CCSM, but lesser in magnitude, at -2.3% and +0.7%, respectively. However, combined with an increase in S6II of about 17.9%, it may be raining slightly less often, but the increase in the intensity of precipitation when it does rain is enough to compensate for this, leading to an overall increase in precipitation between the 1990s and the 2090s in MJJA.
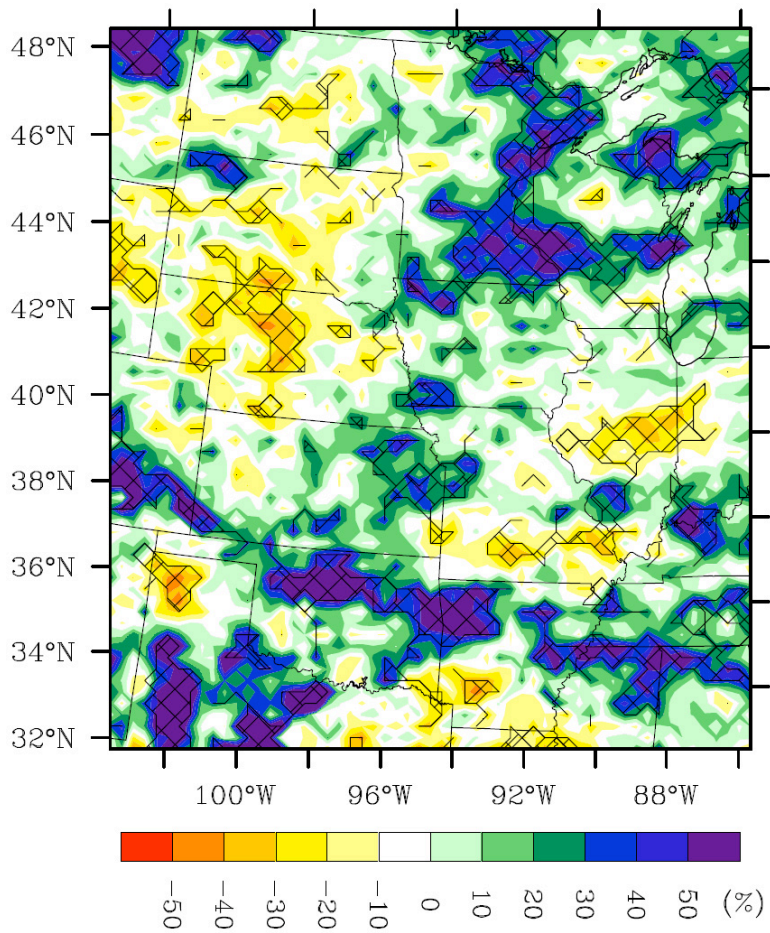
FIG. 31. Percent difference between 2090-2099 and 1990-1999 MJJA 99th percentile 6h average precipitation rate from the WRF-CCSM 30-km domain for the Central US only (for values above a trace only, as in Fig. 25). Hatching indicates statistical significance at the 10% level.

c. Discussion

There is a consistent increase in MJJA temperature over the U.S. between the 1990s and the 2090s in the WRF-CCSM and the CCSM 3.0 that is also consistent with the summertime increase projected by the suite of GCMs run in support of the IPCC AR4 (Christensen et al. 2007). Overall, little extra information is provided here on changes in average summertime temperature versus that provided by global models. More detailed and/or improved information on changes in other characteristics of warm-season temperature may be available using the WRF, but as this is outside the focus of this study, only the change in average temperature was provided as a reference.

As with temperature, the results from the WRF-CCSM for MJJA average precipitation are consistent with those from the IPCC AR4 (Christensen et al. 2007, section 11.5.3.2, Fig. 11.12), in that there is an average decrease over most of the country. As mentioned, however, this result is not consistent with that from the CCSM 3.0. This is not the first study to show a change in an average quantity from a regional model that is in a direction opposite to that from the parent GCM. Han and Roads (2004) and Pan et al. (2004) both encountered this in simulations over the U.S. using different RCMs (and forcing GCMs) in precipitation or temperature, respectively, and both also show increased skill in the regional model over that from the driving global model or reanalysis.

Similarly, many studies have indicated an increase in the intensity of daily precipitation globally and in numerous regions, as the S6II did here for 6h average precipitation (Meehl et al. 2005). That there is an increase in intensity projected along with a decrease in mean precipitation over the central U.S. is not wholly unexpected given similar results from GCMs for other subtropical and mid-latitude regions (Meehl et al. 2007). Though not discussed, results for the number of wet and dry periods and the S6II for the central U.S. are quite similar to those for the entire 30-km WRF-CCSM domain in direction and magnitude. Overall, the total average change is due more to a change in the number of wet/dry periods than to the change in intensity.

However, the intensity does increase, and as discussed above, the frequency of extreme precipitation is also projected by the WRF-CCSM to increase, though lighter but still heavy precipitation events are projected to decrease in frequency in the central U.S. in this analysis. In a broad sense, this is consistent with studies that have shown a shift toward an increased number of intense precipitation events in models as well as observations (e.g. Karl and Knight 1998, Frich et al. 2002, Diffenbaugh et al. 2005, Kharin and Zwiers 2005, IPCC 2008).

7. Understanding the WRF Simulation Differences

Some of the differences presented in the previous two chapters have brought to fore a couple of questions that will be addressed in this chapter. The specific irregularities to be explored in more detail include the difference in precipitation between the WRF-NNRP and the WRF-CCSM in the 20th Century and the difference of the projected changes in average precipitation from the late 20th century to the late 21st century between the WRF-CCSM regional model and the CCSM 3.0 global model simulations.

a. Late 20th Century Precipitation Simulation Differences

As expected, the precipitation simulated using the WRF with initial and boundary conditions from the NNRP is different from that using the CCSM 3.0 for initial and boundary conditions. Although warm-season precipitation simulated by the WRF-CCSM is more realistic than that from the CCSM 3.0 in many ways, the spatial distribution and magnitude of average MJJA precipitation does not match observations/reanalysis nearly as well as that from the WRF-NNRP. This difference is significant in the majority of the 90-km domain, as shown in Fig. 32. The WRF-CCSM is much drier than the WRF-NNRP over most large bodies of water and the western U.S (though the latter is not particularly apparent in Figs. 20 and 22 since the West does not receive much warm-season rainfall). Over land east of the Continental Divide, differences are generally smaller and less significant. The region that is particularly noteworthy in this domain is the northern Plains, where the WRF-CCSM is significantly drier than the WRF-NNRP. This is reflected in the weak magnitude of the secondary maximum in Fig. 22.

Given that the setup of the WRF is identical between these two simulations, these differences are clearly due to differences in initial and boundary conditions. Much of this is illustrated in Figs. 33 and 34. As shown, it is clear that the CCSM and the WRF-CCSM are deficient in low-level moisture in many areas of the domain. In the Great Plains, it is
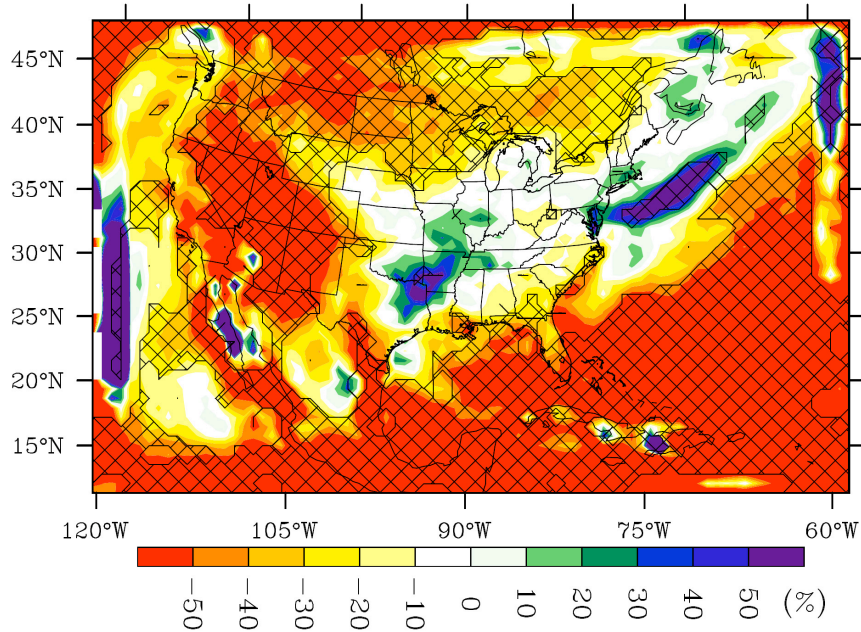
FIG. 32. 1991-1995 MJJA percent difference in average precipitation between the WRF-NNRP and the WRF-CCSM 90-km domains.

evident that poleward flow out of the Gulf of Mexico is much weaker in the CCSM and the WRF-CCSM than it is in the NNRP and WRF-NNRP. It does not reach the northern Plains. This is coincident with a weaker dominant surface low-pressure region in the central Plains that is located further south, on average, than compared with that in the WRF-NNRP. The lack of low-level moisture and the necessary circulation to increase it is likely responsible for the lower-than-average precipitation simulated in the Plains and Midwest by the WRF-CCSM. Inadequate low-level moisture implies lower CAPE, which in turn would suggest less convective activity - the main producer of warm-season precipitation in this region.

Similarly, average precipitation over the Southeast and, specifically, Florida, is also insufficient in the WRF-CCSM. Once again, the lack of low-level moisture in the CCSM and, consequently, the WRF-CCSM, likely plays a strong role in this deficiency. While also influencing the moisture transport into the Great Plains, here, the cool SSTs mentioned previously in respect to Fig. 26, are apt to have an influence as well. This may also be true with regard to the deficiency in average precipitation over the Gulf of Mexico, Caribbean, and the part of the Atlantic ocean included in the 90-km WRF-CCSM domain. Collins
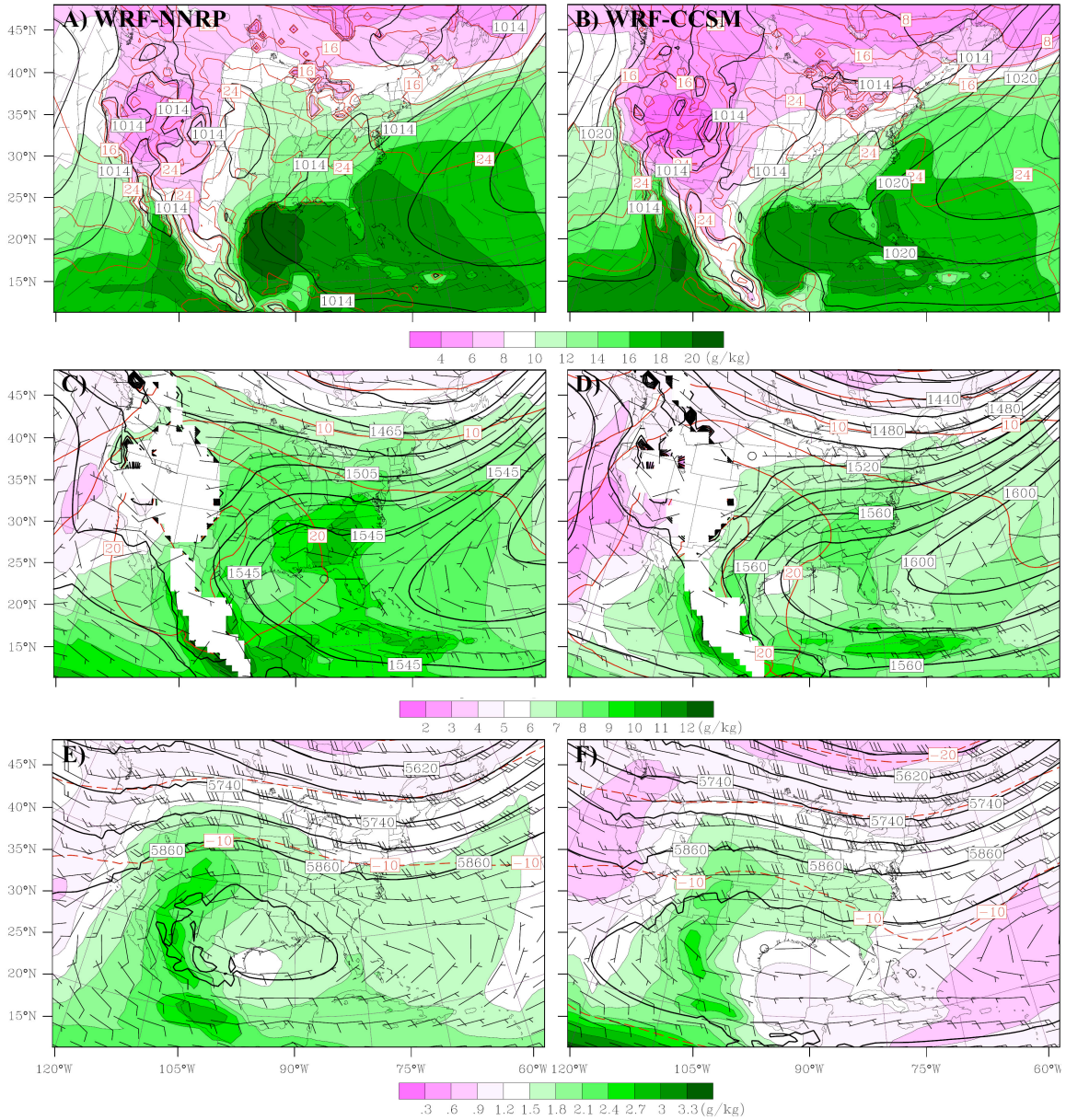
FIG. 33. 1991-1995 WRF-NNRP (left column) and 1990-1999 WRF-CCSM (right column) MJJA average: A and B) 2m water vapor mixing ratio (g/kg, filled contours), 2m temperature (ºC, red contours, by 4º), 10m wind velocity (full barb = 10kts, half barb = 5kts, open circle = calm), and mean sea-level pressure (hPa, black contours, by 3-hPa). C and D) As above, but for 850-hPa water vapor mixing ratio, temperature (by 5º), and geopotential height (by 20m). E and F) As above, but for 500-hPa (geopotential height by 60m).
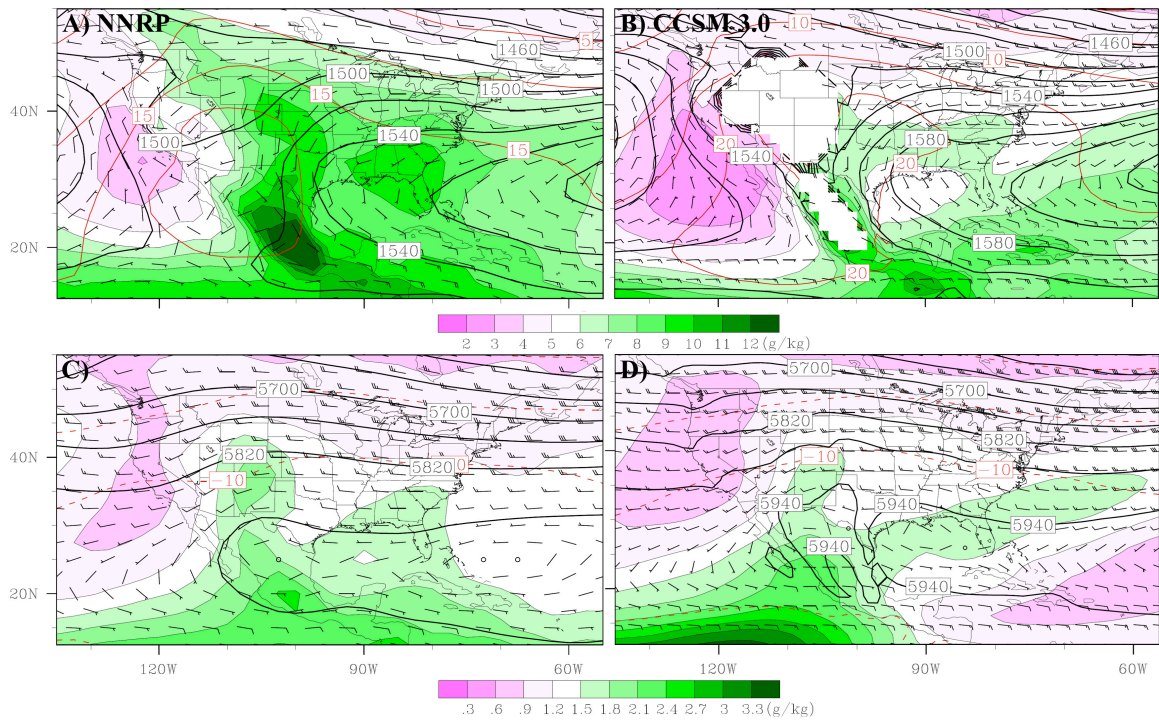
FIG. 34. 1991-1995 NNRP (left column) and 1990-1999 CCSM 3.0 (right column) MJJA average: A and B) 850-hPa water vapor mixing ratio (g/kg, filled contours), temperature (ºC, red contours, by 5º), wind velocity (kts, barbs as in Fig. 33), and geopotential height (m, black contours, by 20m). C and D) As above, but for 500-hPa water vapor mixing ratio, temperature, and geopotential height (by 60m).
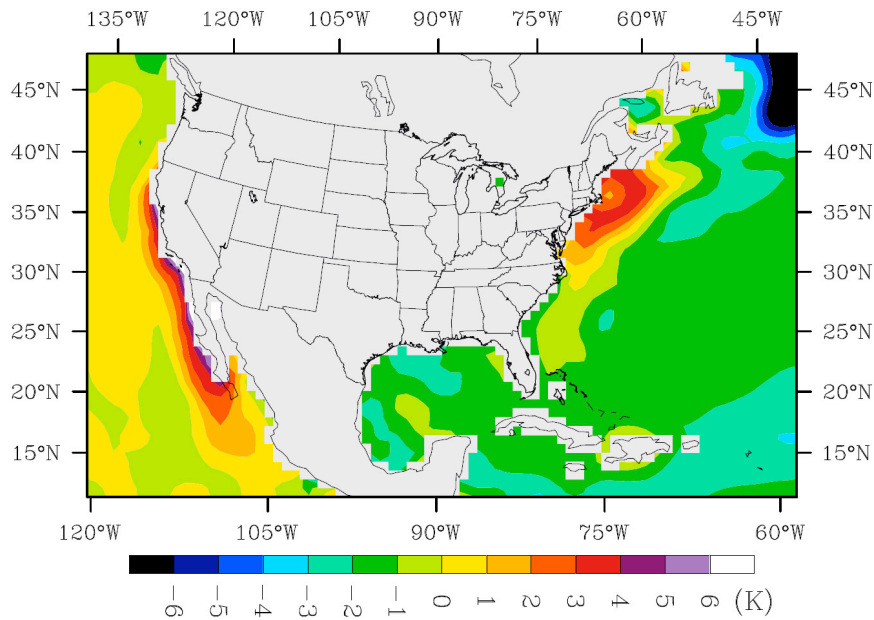
FIG. 35. 1991-1995 MJJA average SST difference between the WRF-CCSM and WRF-NNRP 90-km simulations.

et al. (2006) show that on an annual average basis, CCSM 3.0 SSTs in the Gulf are 0.5°-2°K too cold, and up to 3°K too cold in the Caribbean, compared to observations. For the southern half of the eastern seaboard, the difference is smaller, but in the same direction. SST differences between the WRF-NNRP and WRF-CCSM for MJJA are similar (see Fig. 35), and are also reflected in near-surface temperature (Fig. 26)[14]. As the NNRP system does take into account observed SSTs (Kalnay et al. 1996), the WRF-NNRP SSTs are likely to be a reasonable representation of actual SSTs, as they are updated every 6h in the WRF from the NNRP.

Related to this discussion is the contrast between the CCSM 3.0 and the WRF-CCSM in Fig. 33d and f and Fig. 34b and d. Most obvious are the differences in mixing ratio. While still lacking, the WRF-CCSM does contain greater and more realistic values of mixing ratio. In brief, this improvement implies that the domains used in this study are large enough to allow the WRF to generate an independent solution.

[14]The positive SST bias along western coastal regions, as also seen here in the WRF-CCSM, is well documented and also discussed in Collins et al. (2006), as well as its related atmospheric issues.

Clues that explain some of the variation between the WRF-NNRP, WRF-CCSM, and observed precipitation over the U.S. can also be gained from Figs. 33 and 34. For instance, the summer wet bias in the Northeast is present in both the WRF-NNRP and the WRF-CCSM, but not in the NNRP or the CCSM 3.0. This implies that it is introduced by WRF physical processes.

Both WRFs also contain a dry bias in the southern Plains that extends to the Texas/Louisiana Gulf Coast. This bias is similar to one seen in Diffenbaugh et al. (2006), using the RegCM3 driven by the NNRP or CAM3, though not necessarily caused by the same processes. While the WRF-CCSM is lacking in low-level moisture, the WRF-NNRP is not; thus, this does not explain the lack of precipitation in this case. However, both WRFs are warmer in the south-central Plains at 850-hPa in this region than the NNRP suggests that they should be (this is also the case at the surface - note the location of the maximum in the WRFs relative to the NARR in Fig. 26). The WRF-NNRP also generates a stronger anticyclonic circulation aloft over the southern Plains than the NNRP, which indicates that it should be over north-central Mexico at 500-hPa. The same is true in the WRF-CCSM, though not to the same extent (the CCSM places this feature over the Gulf). The increased subsidence in this region, combined with the warmer low-level temperatures would act to inhibit convection in this region, explaining the deficiency in precipitation here.

b. Late 21st Century Precipitation Simulation Differences

As shown in the previous chapter, the WRF-CCSM projects decreases in average precipitation rate in the late 21st century relative to the 20th century in several regions where the CCSM 3.0 does the opposite. This occurs despite an increase in average mixing ratio (and vertically integrated moisture content, not shown) in both the CCSM 3.0 and the WRF-CCSM. This increase is evident by comparing Figs. 33 (right column) and 36. It is consistent with the increase in saturation vapor pressure that would occur with the increase in temperature also illustrated in Fig. 36. Similar discrepancies occur in evaporation rate

and precipitation minus evaporation (P-E). Differences in these fields are shown in Fig. 37. To demonstrate why this could occur, the central U.S. was examined in more detail.

For the region shown in Fig. 38 (the "central U.S."), the CCSM 3.0 contains an approximately 14.3% increase in average precipitation rate, a 13.9% increase in average evaporation rate, and an increase in P-E from -0.090 to -0.071 mm/day[15]. The WRF-CCSM, on the other hand, shows a decrease in average precipitation rate of about 19.5%, a decrease in evaporation rate of 10.0% and a decrease in P-E from -0.211 to -0.388 mm/day[16]. The area of significant decrease (increase) in the central Plains in precipitation and evaporation in the WRF-CCSM (CCSM 3.0) is located near the northern terminus of the southerly LLJ in the 850-hPa maps. Given an increase in SSTs in the Gulf of Mexico in the 2090s, it would make sense for precipitation to increase in this region. An increase in Gulf of Mexico SSTs would likely lead to an increase in precipitable water over the Gulf, promoting low-level moisture convergence in the Central U.S., which, in turn, is favorable for convection. The increase in moisture convergence in this region is where the CCSM 3.0 and the WRF-CCSM differ, however.

---

[15]P-E in the CCSM 3.0 is slightly positive over almost all of the central U.S. region. It is slightly negative in the quoted regional average because P-E over the Great Lakes is strongly negative relative to the rest of the region (not shown), this is because the CCSM 3.0 simulations produce a large amount of surface latent heat flux over the Great Lakes and, therefore, a large amount of evaporation since evaporation is calculated from the surface latent heat flux in all simulations used in this study. The WRF-CCSM, on the other hand simulates a relative minimum in evaporation over the Great Lakes, and while P-E is positive over the Lakes, it is overcome by negative values in P-E of relatively the same magnitude over the majority of the central U.S. in the regional average. This does not impact the increase in P-E projected by the CCSM3.0, the change is positive over most of the region, as shown.

[16]WRF-CCSM values given were calculated using the 30-km simulations.
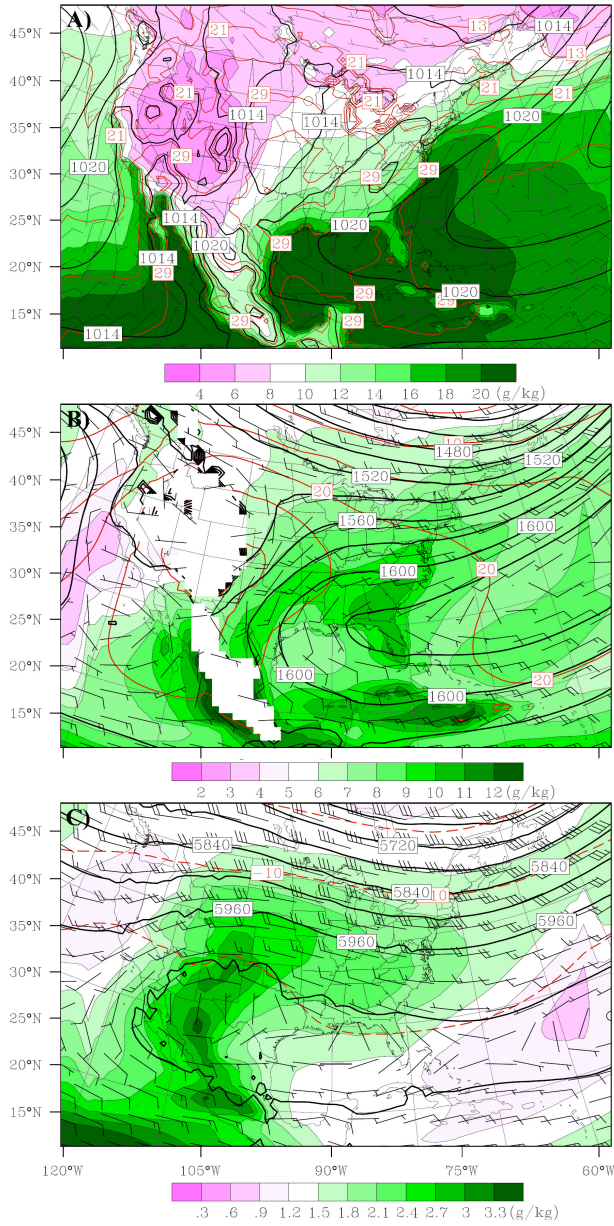
FIG. 36. As in Fig. 33, except for 2090-2099 WRF-CCSM MJJA averages.
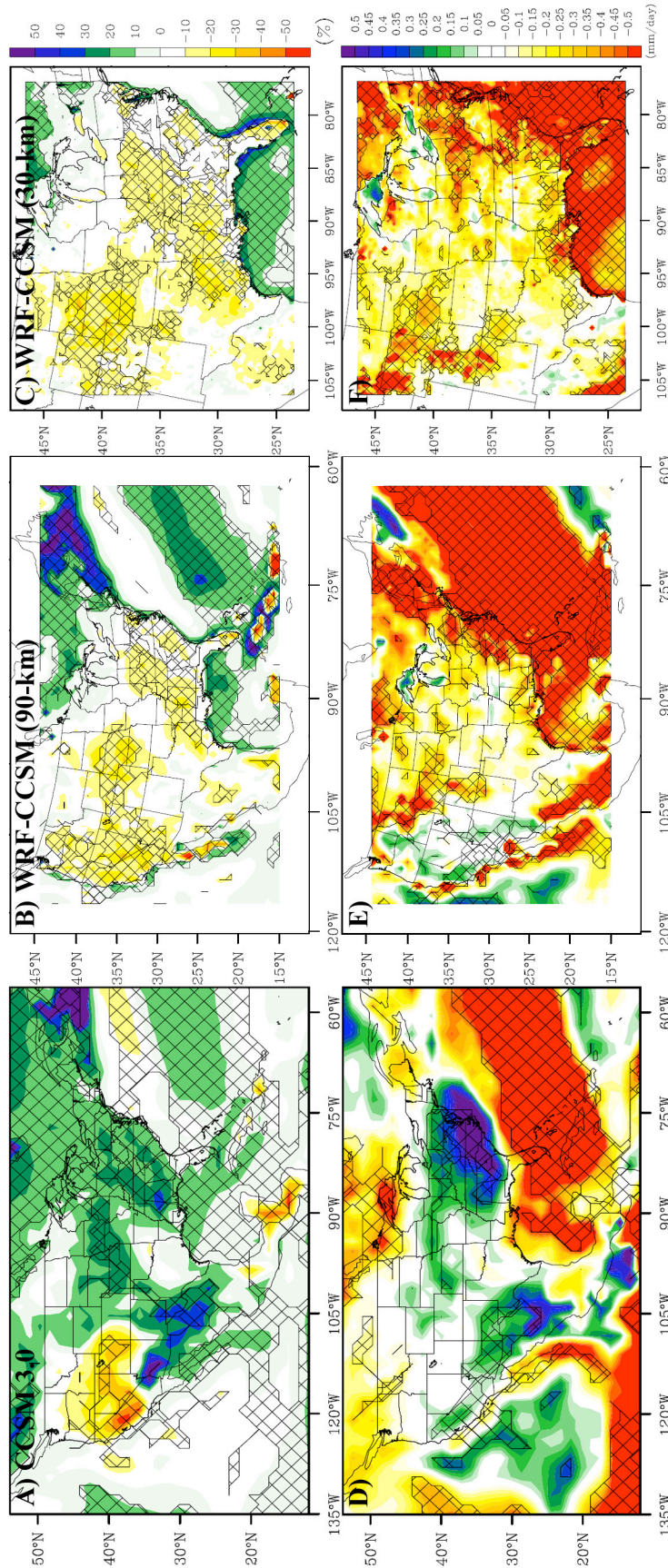
FIG. 37. A-C) Percent difference between 1990-1999 and 2090-2099 MJJA average 6h evaporation and D-F) Difference (mm/day) between 1990-1999 and 2090-2099 MJJA average 6h precipitation rate and average 6h evaporation rate difference from A and D) CCSM 3.0, B and E) WRF-CCSM 90-km domain, C and F) WRF-CCSM 30-km nest.

The vertically integrated transport of moisture from the CCSM 3.0 and the WRF-CCSM is shown in Fig. 38. Both exhibit an increase in moisture transport. What is not particularly obvious from this figure is net moisture convergence/divergence for this region. According to observations and several reanalyses, including the NNRP, the central U.S. should exhibit summertime moisture flux convergence (Roads et al. 1994, Ruiz-Barradas and Nigam 2005, Ruiz-Barradas and Nigam 2006). The CCSM 3.0 does, and, as is necessary considering the positive change in P-E, it also projects an increase in moisture convergence for this region of approximately 47%. The WRF-CCSM, on the other hand, simulates net moisture divergence for the central U.S. and an increase in moisture divergence of about 152%[17], consistent with it's decrease in P-E. The WRF-NNRP also simulates net moisture divergence for the central U.S., despite the NNRP containing the opposite (not shown). The net transport of moisture out of the eastern boundary of the central U.S. region is larger in the WRF-CCSM than in the CCSM 3.0 relative to the net transport into the region at the southern boundary. This difference increases in the future in the WRF-CCSM. Furthermore, the net transport from the south increases in both, but that increase is greater in the CCSM 3.0, leading to the differences between the two.

c. Discussion

While the WRF-NNRP and the WRF-CCSM both improve upon the representation of precipitation from their forcing datasets such that the simulated precipitation better matches observed precipitation, especially in the WRF-NNRP, both contain inconsistencies that cannot be explained given their initial and boundary conditions. Specifically, some of the biases in precipitation explored in section a and the differences in moisture convergence in the central U.S. discussed in section b. Both may be due to more than just errors in the representation of various physical processes in the WRF. As shown in Fig. 39, there

---

[17]Values of divergence were calculated using Gauss' divergence theorem around the entire central U.S. region shown in Fig. 38 using data from the 30-km nest for the WRF simulations.
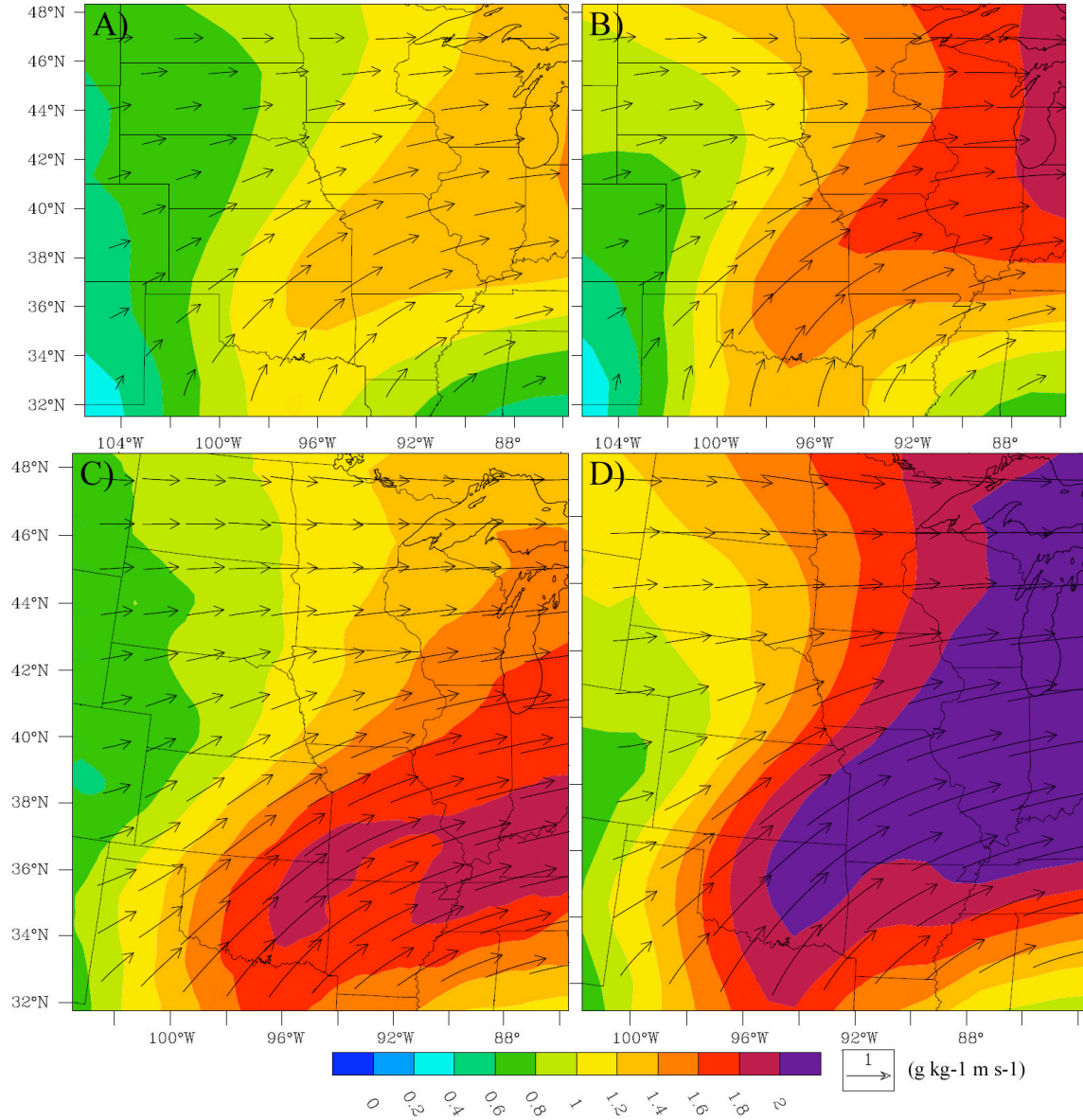
FIG. 38. 1990-1999 (A and C) and 2090-2099 (B and D) MJJA average transport of water vapor mixing ratio (g·kg⁻¹·m·s⁻¹) in the central U.S. from A and B) CCSM 3.0 and C and D) WRF-CCSM 30-km nest.
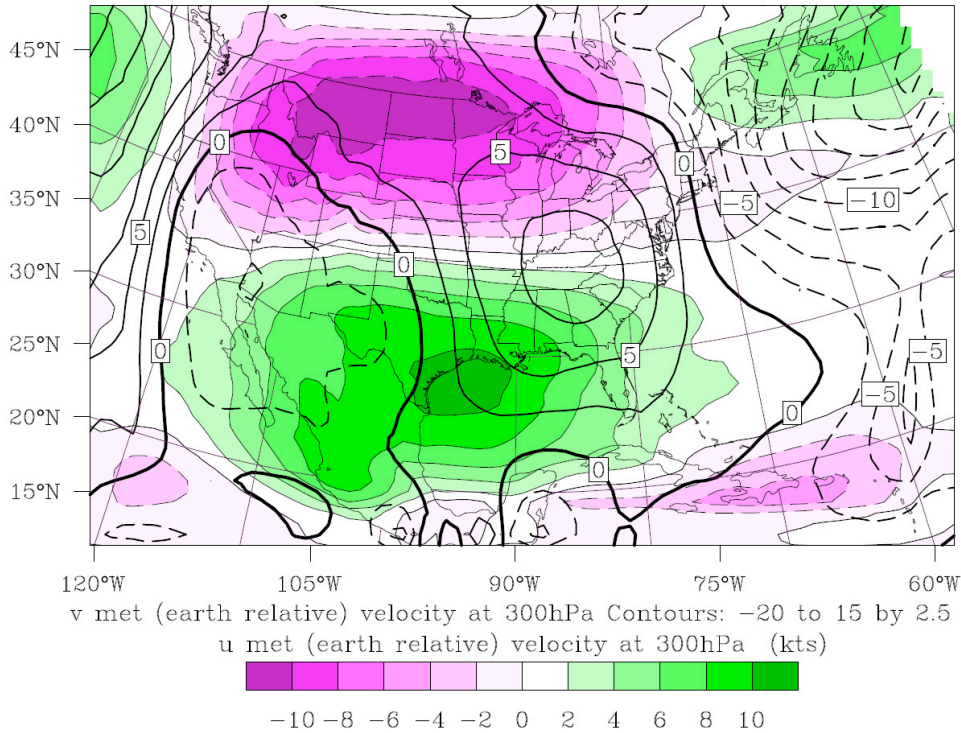
FIG. 39. NNRP minus WRF-NNRP difference for 1991-1995 MJJA average 300-hPa U and V wind components.

also appears to be a bias in the large-scale wave pattern between the NNRP and the WRF-NNRP. At most levels, this manifests itself as excessive ridging in the center of the domain. It is likely that this bias is due to the accumulation of errors at the boundaries, especially the eastern exit boundary, and then the propagation of those errors back into the domain. The latter would not likely be a problem with short-term simulations, but the large-scale bias does grow over time in the WRF and is clearly visible by the end of the first month. This problem is similar to one described by Miguez-Macho et al. (2005) in their month-long simulations using the Regional Atmospheric Modeling System (RAMS) forced by the NNRP. Though the difference shown in Fig. 39 is between the WRF-NNRP and the NNRP, the same processes creating this bias are likely present in the WRF-CCSM.

There is no easy solution to this problem, thus it remains unresolved in these experiments. However, it most likely similar and internally consistent between the 20th and 21st century simulations in the WRF-CCSM. That is, while there are biases likely caused by this

problem, they are contained in all of the WRF simulations in this study; present and future. The WRF still produces a better representation of precipitation than that from it's forcing parent system in the present, and the conditions from the CCSM 3.0 lead to a decrease in average MJJA precipitation in the late 21st century, and changes in other characteristics of precipitation, as previously shown.

8. Summary and Final Discussion

An analysis of late 20th and late 21st century warm-season precipitation from reanalyses, global climate models, and the WRF run as a nested regional climate model has been presented herein. In summary, these are some of the major findings and questions that have been answered by this work:

- The NARR provides the most realistic representation of some of the climatological characteristics of summertime precipitation in a conveniently gridded format compared to other commonly used reanalyses. It was found that this statement is only valid over U.S. land-based regions, and that care needs to be taken if using precipitation from the NARR over other North American land or water based regions. Because it is superior to other reanalyses, it was then used as the base for the comparison of GCMs and the WRF run as an RCM with reality.

- Global climate models analyzed in this study are not unskilled when it comes to simulating annual average U.S. precipitation, but do not adequately capture some of the major characteristics of U.S. warm-season precipitation. They fail to produce the secondary maximum in precipitation that occurs over the central U.S., and they are heavily biased towards producing many light precipitation events and few heavy precipitation events.

- The WRF is able to produce average precipitation fields that are better than those from the NNRP when the NNRP is used to drive the WRF. However, the WRF was found to be very sensitive to some aspects of its setup when used for long-term simulations. Some of the sensitivities found were not expected. This implies that anyone using the WRF model, even for shorter-term forecasts or case-studies, may have biases or errors in their simulations that are not obvious and due to their chosen WRF formulation.

- The WRF was also found to greatly improve on the characteristics of U.S. warm-season precipitation over that from a global climate model, when output from that model is supplied as initial and boundary conditions to the WRF. This is true for both the 30-km and 90-km WRF simulations. Specifically, the WRF-CCSM greatly improved on the magnitude of heavy 6h events and the frequency distribution of precipitation over the central U.S. The overall pattern and timing of precipitation was also much improved, but not to the same extent. The WRF also adds useful regional detail in the simulation of temperature.

- Given that the WRF is able to add valuable improvements to the simulation of warm-season precipitation for the present, it was then used to simulate the future of precipitation. Overall, decreases in average MJJA precipitation were projected over most of the U.S. by the end of the 21st century. Significant decreases in the frequency of all but the very heavy 6h precipitation events, significant increases in the frequency of those extreme events, increases in the intensity of both heavy precipitation events and in the general intensity of rain when it does fall, decreases in the number of 6h periods with rainfall, and an increase in the number of 6h periods without rainfall were also projected by the WRF-CCSM for the central U.S.

- Issues regarding the differences between the WRF-NNRP and the WRF-CCSM and their forcing reanalysis or GCM were also discussed. It was shown that the WRF-CCSM is subject to biases from the CCSM 3.0, like SSTs that are too cold and insufficient low-level moisture. Both the WRF-CCSM and the WRF-NNRP are also subject to internal biases, as illustrated. Despite this, they still produce reasonable warm-season climate simulations.

The ability of the WRF to simulate warm-season precipitation over the U.S. better than most current global climate models may be expected given its increase in resolution and the less simplistic nature of some of its parameterizations, but this may not have been the

101

end result. Simulation of warm-season precipitation is still a challenge, as discussed in section 1c . As noted in Christensen et al. (2007, pg. 889), using a regional model for the U.S. warm-season does not guarantee a better response just because it has a higher resolution.

Aside from being one of very few studies to utilize the WRF in this manner, given the published literature, it is also unique in some aspects of its analysis of changes in precipitation due to global warming. To the best of the author's knowledge, no study has been done that analyzes changes in precipitation in a warming climate using data at a higher temporal resolution than a daily average. Using 6 hourly data allows a better understanding of what might happen to events that have an even greater impact in a number of sectors, especially many hydrological applications: erosion, flooding, and flash flooding, for example. Furthermore, when broken down into smaller time periods, some types of precipitation events that may be heavy for a daily event may not be as intense as a 6h (or less) event relative to other potential 6h average events, and vice-versa. Using a finer time scale for analysis allows shorter, but important convective events to be better resolved in climatological analysis.

To the best of the author's knowledge, this is also the first study to specifically document where the switch between an increase in frequency and a decrease in frequency occurs in terms of the intensity/percentile of a given precipitation event, though this would also be an important point in hydrological applications. Here, it was around the 99.7th percentile, which is a very heavy and rather rare precipitation rate (approximately three 6h average events per decade per grid point). All rainfall events of intensities less than that were found to decrease in frequency. Though this study focused on the central U.S. for most parts of its analysis, documenting that there is a decrease in the frequency of the 90th and 95th percentile precipitation rates is still somewhat contrary to what other studies have found (again using daily average precipitation, at best). Most literature on this subject states that there will be a shift in the distribution to more frequent intense events without being

102

specific about where that shift occurs. Since a few studies have indicated that this shift in the frequency distribution can already be seen at some observation sites (e.g. Pryor et al. 2009), it would be interesting to know at what point in the distribution an increase in the frequency of intense events can already be observed in the central U.S., if at all.

As mentioned briefly in section 6b, the results from the WRF-CCSM for the late 21st century suggest an increase in the frequency of both droughts and flooding in the central U.S in MJJA. This is because of the increase in the number of dry days projected by the WRF-CCSM along with an increase in the intensity of precipitation when it does rain, which is also compounded by an increase in temperature. Longer, warmer dry periods with more evapotranspiration imply an increase in the frequency of drought, and an increase in precipitation intensity when it does rain points to an increase in runoff intensity, and therefore, more flooding events.

This, unfortunately, is another study where changes of this nature are only implied from changes in precipitation. Relatively few have tried to estimate potential future changes in surface hydrology. Much of what has been done has been global in scale, for very large river basins, and/or at a very coarse resolution (Nijssen et al. 2001, Arora and Boer 2001, Arnell 2005, Milly et al. 2005, Nohara et al. 2007). Studies that have analyzed streamflow and/or flooding in major global rivers have typically utilized GCM land surface parameterization generated runoff and some type of external flow routing model to calculate the discharge at the rivers' mouths, or the GCM data has been statistically downscaled to a resolution suitable for a more sophisticated hydrologic model (Arora et al. 1997, Nijssen et al. 2001, Milly et al. 2002, Vanrheenen et al. 2004). The temporal and spatial resolution of climate model data is usually low and inadequate for detailed hydrologic analysis, and as shown, GCMs don't necessarily produce the best representation of precipitation, especially during the U.S. summer. The precipitation simulations produced for this analysis, however, would be suitable for use in this type of study and for use in hydrologic models that can handle distributed precipitation information or simulate hydrologic variables at

points inside of a basin (i.e. models that can provide more than just basin average quantities, like distributed hydrological models). In this manner, more quantitative estimates could be made for potential future changes in regional flooding, for example. Since the impacts of runoff are seasonally dependent, however, full year simulations may be necessary to provide better estimates. This is just one area of possible future application. The production of realistic high resolution climate projections is also of relevance in climate change impact work, as well as in providing mitigation and adaptation policy guidance.

Reliable, detailed projections of future precipitation changes are, therefore, important. This requires an assessment of the uncertainty involved in the projections due to model deficiencies. It is also important to understand the underlying mechanisms of change in model simulations of the future. To a considerable extent, that has been done in this study.

Though it did produce precipitation simulations that were more realistic than those from a GCM, further work will be required to remove some of the internally rooted model bias found in the version of the WRF applied herein. There is also a potential error in radiation not previously mentioned in the simulations of the future. That is, the simulations for the future indirectly receive the impacts of changes in the concentration of various atmospheric constituents (e.g. greenhouse gases) through the initial and boundary conditions from the CCSM. Direct changes in these quantities in the WRF model are not included - i.e. concentrations are the same in the present as in the future in the WRF. This would lead to a gradual and slight cooling of the troposphere over time in the late 21st century simulations. However, this is likely balanced by the continual advection of a large-scale environment that includes the change in concentrations into the WRF from the CCSM boundary conditions. Further work will be needed to examine the degree to which this is balanced or not and to which the tropospheric warming in the WRF simulations may be underestimated because of this.

A greater number of simulated years per century would also help strengthen the analysis of extreme precipitation events completed in this study, since these events are rare and

few are produced per grid point per decade; they are even subject to great uncertainty in observational studies. Additionally, a greater ensemble of nested regional WRF simulations based on changes in WRF formulation would help quantify some of the uncertainty created due to internal model bias. Likewise, this analysis only used data from one global climate model and one emission scenario. Considering that the WRF is also subject to biases in the source of its forcing, it would be useful to expand this dataset to include the WRF nested within other global climate models. Along the same lines, future emissions are a great source of uncertainty, and utilizing more than one emissions scenario would at least provide a greater range of possibilities for future changes in precipitation. However, all of this is beyond the range of the current study and would require ample computational resources and storage capabilities.

A coordinated project that will address a number of these issues for the U.S. will be provided by NARCCAP. However, analysis from the model runs completed for that project are just beginning to surface and a useful quantity of results, in terms of addressing the above mentioned uncertainties, will probably not be available for another year or so. In a sense, this study is a personally-initiated preliminary contribution to NARCCAP, foreshadowing what the U.S., through NARCCAP, is trying to do. Thus, this current work is a significant contribution to a growing number of regional climate studies; it provides a well scrutinized ensemble member that can more completely address the impact of climate change on warm-season precipitation over the U.S. It is planned to continue further investigation along these lines.

References

Albritton, D. L., L. G. Meira Filbo, and coauthors, 2001: Climate Change 2001: The Scientific Basis. *Technical Summary*, Cambridge University Press, Cambridge, UK, 21–83.

Alexander, L. V., X. Zhang, T. C. Peterson, J. Caesar, B. Gleason, A. M. G. K. Tank, M. Haylock, D. Collins, B. Trewin, F. Rahimzadeh, A. Tagipour, K. R. Kumar, J. Revadekar, G. Griffiths, L. Vincent, D. B. Stephenson, J. Burn, E. Aguilar, M. Brunet, M. Taylor, M. New, P. Zhai, M. Rusticucci, and J. L. Vazquez-Aguirre, 2006: Global observed changes in daily climate extremes of temperature and precipitation. *J. Geophys. Res.*, **111**, D05 109.

Allen, M. R. and W. J. Ingram, 2002: Constraints on future changes in climate and the hydrologic cycle. *Nature*, **419**, 224–232.

AMS, 2000: *Glossary of Meteorology*. American Meteorological Society, Boston, MA, 855 pp.

Anderson, C. J., R. W. Arritt, E. S. Takle, Z. Pan, W. J. G. Jr., F. O. Otieno, R. D. Silva, D. Caya, J. H. Christensen, D. Lüthi, M. A. Gaertner, C. Gallardo, F. Giorgi, S. Y. Hong, C. Jones, H. M. H. Juang, J. J. Katzfey, W. M. Lapenta, R. Laprise, J. W. Larson, G. E. Liston, J. L. McGregor, R. A. P. Sr., J. O. Roads, and J. A. Taylor, 2003: Hydrological processes in regional climate model simulations of the central United States flood of June-July 1993. *J. Hydrometeorology*, **4**, 584–598.

Arakawa, A. and W. H. Schubert, 1974: Interaction of a cumulus cloud ensemble with the large-scale environment, Part I. *J. Atmos. Sci.*, **31**, 647–701.

Arnell, N., B. Bates, H. Lang, J. J. Magnuson, P. Mulholland, S. Fisher, C. Liu, D. McKnight, O. Starosolsky, and M. Taylor, 1996: Hydrology and freshwater ecology. *Climate Change 1995: Impacts, Adaptations, and Mitigation of Climate Change: Scientific-Technical Analyses. Contribution of Working Group II to the Second Assessment Report for the Intergovernmental Panel on Climate Change*, Watson, R. T., M. C. Zinyowera, and R. H. Moss, Eds., Cambridge University Press, 325–363.

Arnell, N. W., 2005: Implications of climate change for freshwater inflows to the Arctic Ocean. *J. Geophys. Res.*, **110**, D07 105.

Arora, V. K. and G. J. Boer, 2001: Effects of simulated climate change on the hydrology of major river basins. *J. Geophys. Res.*, **106**, 3335–3348.

Arora, V. K., F. H. S. Chiew, and R. B. Grayson, 1997: Surface hydrology in global climate models: how good is it? *Proceedings of the 24th International Hydrology and Water Resources Symposium*, Auckland, New Zealand, Institute of Engineers, 367–372.

Augustine, J. A. and F. Caracena, 1994: Lower-tropospheric precursors to nocturnal MCS development over the central United States. *Wea. Forecasting*, **9**, 116–135.

Baldwin, M. E., J. S. Kain, and M. P. Kay, 2002: Properties of the convection scheme in NCEP's Eta model that affect forecast sounding interpretation. *Wea. Forecasting*, **17**, 1063–1079.

Bechtold, P., J. P. Chaboureau, A. C. M. Beljaars, A. K. Betts, M. Köhler, M. Miller, and J. L. Redelsperger, 2004: The simulation of the diurnal cycle of convective precipitation over land in global models. *Quart. J. Roy. Meteor. Soc.*, **130**, 3119–3137.

Benestad, R. E., 2006: Can we expect more extreme precipitation on the monthly time scale? *J. Climate*, **19**, 630–637.

Betts, A. K., 1986: A new convective adjustment scheme. Part I: Observational and theoretical basis. *Quart. J. Roy. Meteor. Soc.*, **112**, 667–691.

———, 2004: Understanding hydrometeorology using global models. *Bull. Amer. Meteor. Soc.*, **85**, 1673–1688.

Betts, A. K. and C. Jakob, 2002: Study of diurnal cycle of convective precipitation over Amazonia using a single column model. *J. Climate*, **11**, 2881–2897.

Betts, A. K., P. Viterbo, and E. Wood, 1998: Surface energy and water balance for the Arkansas-Red River basin from the ECMWF reanalysis. *J. Climate*, **11**, 2881–2897.

Boville, B. A., P. J. Rasch, J. J. Hack, and J. R. McCaa, 2006: Representation of clouds and precipitation processes in the Community Atmosphere Model (CAM3). *J. Climate*, **19**, 2184–2198.

Bukovsky, M. S., J. S. Kain, and M. E. Baldwin, 2006: Bowing convective systems in a popular operational model: Are they for real? *Wea. Forecasting*, **21**, 307–324.

Bukovsky, M. S. and D. J. Karoly, 2007: A brief evaluation of precipitation from the North American Regional Reanalysis. *J. Hydrometeorology*, **8**, 837–846.

Carbone, R. E., J. D. Tuttle, D. A. Ahijevych, and S. B. Trier, 2002: Inferences of predictability associated with warm season precipitation episodes. *J. Atmos. Sci.*, **59**, 2033–2056.

Caya, D. and S. Binder, 2004: Internal variability of RCM simulations over an annual cycle. *Clim. Dynam.*, **22**, 33–46.

Chaboureau, J. P., P. Bechtold, M. Köhler, A. Beljaars, M. Miller, and J. L. Redelsperger, 2003: Evaluation of cumulus parameterizations in simulating the diurnal cycle of convective precipitation over land. *Quart. J. Roy. Meteor. Soc.*, **128**, 1–18.

Changnon, S. A., 2001: Thunderstorm rainfall in the conterminous United States. *Bull. Amer. Meteor. Soc.*, **82**, 1925–1940.

Christensen, J. H., B. Hewitson, A. Busuioc, A. Chen, X. Gao, I. M. Held, R. Jones, R. K. Kolli, W. T. Kwon, R. Laprise, V. M. Rueda, L. Mearns, C. G. Menéndez, J. Räisänen, A. Rink, A. Sarr, and P. Whetton, 2007: *Climate Change 2007: The Physical Science Basis. Contribution of Working Group I to the Fourth Assessment Report of the Intergovernmental Panel on Climate Change*, Cambridge University Press, Cambridge, United Kingdom and New York, NY, USA, Chap. Regional Climate Projections.

Collins, W. D., 2001: Parameterization of generalized cloud overlap for radiative calculations in general circulation models. *J. Atmos. Sci.*, **58**, 3224–3242.

Collins, W. D., C. M. Bitz, M. L. Blackmon, G. B. Bonan, C. S. Bretherton, J. A. Carton, P. Chang, S. C. Doney, J. J. Hack, T. B. Henderson, J. T. Kiehl, W. G. Large, D. S. McKenna, B. D. Santer, and R. D. Smith, 2006: The Community Climate System Model: CCSM3. *J. Climate*, **19**, 2122–2143.

Collins, W. D., J. K. Hackney, and D. P. Edwards, 2002: A new parameterization for infrared emission and absorption by water vapor in the National Center for Atmospheric Research Community Atmosphere Model. *J. Geophys. Res.*, **107**, D22.

Cook, K. H., E. K. Vizy, Z. S. Launer, and C. M. Patricola, 2008: Springtime intensification of the Great Plains low-level jet and Midwest precipitation in GCM simulations of the twenty-first century. *J. Climate*, **21**, 6321–6340.

Correia, J. and L. R. Leung, 2008: Large scale characteristics of NARCCAP generated severe weather environments from reanalysis and CCSM3 simulations using WRF. *Eos. Trans. AGU*, Fall Meet. Suppl., Abstract GC53A-0709, Vol. 89.

Cressman, G. P., 1959: An operational objective analysis system. *Mon. Wea. Rev.*, **87**, 367–374.

Dai, A., 1999: Recent changes in the diurnal cycle of precipitation over the United States. *Geophys. Res. Lett.*, **26**, 341–344.

———, 2006: Precipitation characteristics in eighteen coupled climate models. *J. Climate*, **19**, 4605–4630.

Dai, A., F. Giorgi, and K. E. Trenberth, 1999: Observed and model-simulated diurnal cycles of precipitation over the contiguous United States. *J. Geophys. Res.*, **104**, 6377–6402.

Davis, C. A., K. W. Manning, R. E. Carbone, S. B. Trier, and J. D. Tuttle, 2003: Coherence of warm-season continental rainfall in numerical weather prediction models. *Mon. Wea. Rev.*, **131**, 2667–2679.

DelGenio, A. D. and M. S. Yao, 1993: Efficient cumulus parameterization for long-term climate studies: The GISS scheme. *The Representation of Cumulus Convection in Numerical Models*, Emanuel, K. and D. Raymond, Eds., American Meteorological Society, No. 46 in AMS Meteor. Monograph, 181–184.

DelGenio, A. D., M. S. Yao, W. Kovari, and K. K. Lo, 1996: A prognostic cloud water parameterization for general circulation models. *J. Climate*, **9**, 270–304.

Delworth, T. L., A. J. Broccoli, A. Rosati, R. J. Stouffer, V. Balaji, J. A. Beesley, W. F. Cooke, K. W. Dixon, J. Dunne, K. A. Dunne, J. W. Durachta, K. L. Findell, P. Ginoux, A. Gnanadesikan, C. T. Gordon, S. M. Griffies, R. Gudgel, M. J. Harrison, I. M. Held, R. S. Hemler, L. W. Horowitz, S. A. Klein, T. R. Knutson, P. J. Kushner, A. R. Langenhorst, H. C. Lee, S. J. Lin, J. Lu, S. L. Malyshev, P. C. D. Milly, V. Ramaswamy, J. Russell, M. D. Schwarzkopf, E. Shevliakova, J. J. Sirutis, M. J. Spelman, W. F. Stern, M. Winton, A. T. Wittenberg, B. Wyman, F. Zeng, and R. Zhang, 2006: GFDL's CM2 global coupled climate models - Part 1: Formulation and simulation characteristics. *J. Climate*, **19**, 643–674.

Dickinson, R., R. Errico, F. Giorgi, and G. Bates, 1989: A regional climate model for the western United States. *Climatic Change*, **15**, 383–422.

Diffenbaugh, N. S., M. Ashfaq, B. Shuman, J. W. Williams, and P. J. Bartlein, 2006: Summer aridity in the United States: Response to mid-Holocene changes in insolation and sea surface temperature. *Geophys. Res. Lett.*, **33**, L22 712, doi: 10.1029/2006GL028 012.

Diffenbaugh, N. S., J. S. Pal, R. J. Trapp, and F. Giorgi, 2005: Fine-scale processes regulate the response of extreme events to global climate change. *Proc. Natl. Acad. Sci. U.S.A.*, **102 (44)**, 15 774–15 778, doi:10.1073/pnas.0506042 102.

Douville, H., F. Chauvin, S. Planton, J. F. Royer, D. Salas-Mélia, and S. Tyteca, 2002: Sensitivity of the hydrological cycle to increasing amounts of greenhouse gases and aerosols. *Clim. Dynam.*, **20**, 45–68.

Duffy, P. B., B. Govindasamy, J. P. Iorio, J. Milovich, K. R. Sperber, K. E. Taylor, M. F. Wehner, and S. L. Thompson, 2003: High-resolution simulations of global climate, Part 1: Present climate. *Clim. Dynam.*, **21**, 371–390.

Easterling, D. R., H. F. Diaz, A. V. Douglas, W. D. Hogg, K. E. Kunkel, J. C. Rogers, and J. F. Wilkinson, 2000a: Long-term observations for monitoring extremes in the Americas. *Clim. Dynam.*, **42**, 285–308.

Easterling, D. R., G. A. Meehl, C. Parmesan, S. A. Changnon, T. R. Karl, and L. O. Mearns, 2000b: Climate extremes: Observations, modeling, and impacts. *Science*, **289**, 2068–2074.

Easterling, D. R., T. W. R. Wallis, J. H. Lawrimore, and R. R. H. Jr., 2007: Effects of temperature and precipitation trends on U.S. drought. *Geophys. Res. Lett.*, **34**, L20 709.

Ek, M. B., K. E. Mitchell, Y. Lin, P. Grunmann, E. Rodgers, G. Gayno, and V. Koren, 2003: Implementation of the upgraded Noah land-surface model in the NCEP operational mesoscale Eta model. *J. Geophys. Res.*, **108 (8851)**, doi: 10.1029/2002JD003 296.

Fowler, H. J., S. Blenkinsop, and C. Tebaldi, 2007: Linking climate change modelling to impacts studies: recent advances in downscaling techniques for hydrological modeling. *Int. J. Climatol.*, **27**, 1547–1578.

Fowler, H. J. and M. Ekström, 2009: Multi-model ensemble estimates of climate change impacts on UK seasonal precipitation extremes. *Int. J. Climatol.*, **29**, 385–416.

Fowler, H. J., M. Ekström, C. G. Kilsby, and P. D. Jones, 2005: New estimates of future changes in extreme rainfall across the UK using regional climate model integrations. I. Assessment of control climate. *J. Hydrology*, **300**, 212–233.

Frei, C., R. Schöll, S. Fukutome, J. Schmidli, and P. L. Vidale, 2006: Future change of precipitation extremes in Europe: an intercomparison of scenarios from regional climate models. *J. Geophys. Res. Atmos.*, **111**, D06 105. DOI: 10.1029/2005JD005 965.

Frich, P., L. V. Alexander, P. Della-Marta, B. Gleason, M. Haylock, A. M. G. K. Tank, and T. Peterson, 2002: Observed coherent changes in climatic extremes during the second half of the twentieth century. *Clim. Res.*, **19**, 193–212.

Fritsch, J. M., R. J. Kane, and C. R. Chelius, 1986: The contribution of mesoscale convective weather systems to the warm-season precipitation in the United States. *J. Climate Appl. Meteor.*, **25**, 1333–1345.

Gallus, W. A. and J. F. Bresch, 2006: Comparison of impacts of WRF dynamic core, physics package, and initial conditions on warm season rainfall forecasts. *Mon. Wea. Rev.*, **134**, 2632–2641.

Garratt, J. R., P. B. Krummel, and E. A. Kowalczyk, 1993: The surface-energy balance at local and regional scales – a comparison of general-circulation model results with observations. *J. Climate*, **6**, 1090–1109.

Giorgi, F. and M. R. Marinucci, 1996: An investigation of the sensitivity of simulated precipitation to model resolution and its implications for climate studies. *Mon. Wea. Rev.*, **124**, 148–166.

Gleick, P. H., 2000: *Water: The Potential Consequences for Climate Variability and Change for the Water Resources of the United States*. National Water Assessment Group for the U.S. Global Change Research Program, USGS, Dept. of the Interior.

Groisman, P. Y., R. S. Bradley, and B. Sun, 2000: The relationship of cloud cover to near-surface temperature and humidity: comparison of GCM simulations with empirical data. *J. Climate*, **13**, 1858–1878.

Groisman, P. Y., T. R. Karl, D. R. Easterling, R. W. Knight, P. F. Jamason, K. J. Hennessy, R. Suppiah, C. M. Page, J. Wibig, K. Fortuniak, V. N. Razuvaev, A. Douglas, E. Førland, and P. M. Zhai, 1999: Changes in the probability of heavy precipitation: Important indicators of climatic change. *Climatic Change*, **42**, 243–283.

Groisman, P. Y., R. W. Knight, D. R. Easterling, T. R. Karl, G. C. Hegerl, and V. N. Razuvaev, 2005: Trends in intense precipitation. *J. Climate*, **18**, 1326–1350.

Groisman, P. Y., R. W. Knight, and T. R. Karl, 2001: Heavy precipitation and high streamflow in the contiguous United States: Trends in the Twentieth Century. *Bull. Amer. Meteor. Soc.*, **82**, 219–246.

Hack, J. J., 1994: Parameterization of moist convection in the National Center for Atmospheric Research Community Climate Model (CCM2). *J. Geophys. Res.*, **99**, 5551–5568.

Hammer, G. R. and P. M. Steurer, 1997: Data set documentation for Hourly Precipitation Data. NOAA/NCDC TD3240 Documentation Series, Ashville, NC.

Han, J. and J. O. Roads, 2004: U.S. climate sensitivity simulated with the NCEP regional spectral model. *Climatic Change*, **62**, 115–154.

Hane, C. E., M. E. Baldwin, H. B. Bluestein, T. M. Crawford, and R. M. Rabin, 2001: A case study of severe storm development along a dryline within a synoptically active environment. Part I: Dryline motion and an Eta model forecast. *Mon. Wea. Rev.*, **129**, 2183–2204.

Hasumi, H. and S. Emori, 2004: K-1 Coupled GCM (MIROC) Description. Tech. Report No. 1, 2 pp. [Available from http://www.ccsr.u-tokyo.ac.jp/kyosei/hasumi/MIROC/tech-repo.pdf].

Heideman, K. F. and J. M. Fritsch, 1988: Forcing mechanisms and other characteristics of significant summertime precipitation. *Wea. Forecasting*, **3**, 115–130.

Held, I. M. and B. J. Soden, 2006: Robust responses of the hydrological cycle to global warming. *J. Climate*, **19**, 5686–5699.

Hennessy, R. J., J. M. Gregory, and J. F. B. Mitchell, 1997: Changes in daily precipitation under enhanced greenhouse conditions. *Clim. Dynam.*, **13**, 667–680.

Higgins, R. W., J. E. Janowiak, and Y. P. Yao, 1996a: A gridded hourly precipitation data base for the United States (1963-1993). NCEP/Climate Prediction Center Atlas 1, National Centers for Environmental Prediction.

Higgins, R. W., K. C. Mo, and S. D. Schubert, 1996b: The moisture budget of the cental Unite States in spring as evaluated in the NCEP/NCAR and the NASA/DAO reanalyses. *Mon. Wea. Rev.*, **124**, 939–963.

Hong, S. Y., J. Dudhia, and S. H. Chen, 2004: A revised approach to ice microphysical processes for the bulk parameterization of clouds and precipitation. *Mon. Wea. Rev.*, **132**, 103–120.

Hong, S. Y., Y. Noh, and J. Dudhia, 2006: A new vertical diffusion package with an explicit treatment of entrainment processes. *Mon. Wea. Rev.*, **134**, 2318–2341.

Houghton, J. T. and coeditors, 2001: *Climate Change 2001: The Scientific Basis, Contribution of Working Group I to the Third Assessment Report of the Intergovernmental Panel on Climate Change*. Cambridge University Press, 881 pp.

IPCC, 2000: *Special Report on Emissions Scenarios*. Cambridge University Press, Cambridge, UK, 432 pp.

——, 2007: *Summary for Policymakers*. Cambridge University Press, Cambridge, United Kingdom and New York, NY, USA, 21 pp.

——, 2008: Climate Change and Water. *Technical Paper of the Intergovernmental Panel on Climate Change*, Bates, B. C., Z. W. Kundzewicz, S. Wu, and J. P. Palutikof, Eds., IPCC Secretariat, Geneva, 210 pp.

Iwashima, T. and R. Yamamoto, 1993: A statistical analysis of the extreme events: Long-term trend of heavy daily precipitation. *J. Meteorol. Soc. Japan*, **71**, 637–640.

Jakob, C. and A. P. Siebesma, 2003: A new subcloud model for mass-flux convection schemes: Influence on triggering, updraft properties, and model climate. *Mon. Wea. Rev.*, **131**, 2765–2778.

Janjić, Z. I., 1994: The step-mountain Eta coordinate model: Further developments of the convection, viscous sublayer, and turbulence closure schemes. *Mon. Wea. Rev.*, **122**, 927–945.

Kain, J. S., 2004: The Kain-Fritsch convective parameterization: An update. *J. Appl. Meteor.*, **422**, 170–181.

Kain, J. S. and J. M. Fritsch, 1992: The role of the convective "trigger function" in numerical forecasts of mesoscale convective systems. *Meteor. Atmos. Phys.*, **49**, 93–106.

Kållberg, P., A. Simmons, S. Uppala, and M. Fuentes, 2004: The ERA-40 Archive. ERA-40 Project Report Series, Vol. 17, ECMWF.

Kalnay, E., M. Kanamitsu, R. Kistler, W. Collins, D. Deaven, L. Gandin, M. Iredell, S. Saha, G. White, J. Woollen, Y. Zhu, A. Leetmaa, B. Reynolds, M. Chelliah, W. Ebisuzaki, W. Higgins, J. Janowiak, K. Mo, C. Ropelewski, J. Wang, R. Jenne, and D. Joseph, 1996: The NCEP/NCAR 40-Year reanalysis project. *Bull. Amer. Meteor. Soc.*, **77**, 437–471.

Kanamitsu, M., W. Ebisuzaki, J. Woollen, S. K. Yang, J. J. Hnilo, M. Fiorino, and G. L. Potter, 2002: NCEP-DOE AMIP-II Reanalysis (R-2). *Bull. Amer. Meteor. Soc.*, **83**, 1631–1643.

Karl, T. R. and R. W. Knight, 1998: Secular trends of precipitation amount, frequency, and intensity in the USA. *Bull. Amer. Meteor. Soc.*, **77**, 279–292.

Karl, T. R., R. W. Knight, and N. Plummer, 1995: Trends in high-frequency climate variability in the twentieth century. *Nature*, **377**, 217–220.

Kharin, V. V. and F. W. Zwiers, 2005: Estimating extremes in transient climate change simulations. *J. Climate*, **18**, 1156–1173.

Kharin, V. V., F. W. Zwiers, X. Zhang, and G. C. Hegerl, 2007: Changes in temperature and precipitation extremes in the IPCC ensemble of global coupled model simulations. *J. Climate*, **20**, 1419–1444.

Kiehl, J. T., J. J. Hack, G. B. Bonan, B. A. Boville, D. L. Williamson, , and P. J. Rasch, 1998: The National Center for Atmospheric Research Community Climate Model: CCM3. *J. Climate*, **11**, 1131–1149.

Kiktev, D., D. M. H. Sexton, L. Alexander, and C. K. Folland, 2003: Comparison of modeled and observed trends in indicies of daily climate extremes. *J. Climate*, **16**, 3560–3571.

Kunkel, K. E., K. Andsager, and D. R. Easterling, 1999: Long-term trends in extreme precipitation events over the conterminous United States and Canada. *J. Climate*, **12**, 2515–2527.

Le Treut, H. and Z. X. Li, 1991: Sensitivity of an atmospheric general circulation model to prescribed SST changes: feedback effects associated with the simulation of cloud optical properties. *Clim. Dynam.*, **5**, 175–187.

Leung, L. R. and Y. Qian, 2009: Atmospheric rivers induced heavy precipitation and flooding in the western U.S. simulated by the WRF regional climate model. *Geophys. Res. Lett.*, **36**, L03 820, doi:10.1029/2008GL036 445.

Leung, L. R., Y. Qian, and X. Bian, 2003: Hydroclimate of the Western United States based on observations and regional climate simulation of 1981-2000. Part I: Seasonal statistics. *J. Climate*, **16**, 1892–1911.

Li, J., R. A. Maddox, X. Gao, S. Sorooshian, and K. Hsu, 2003: A numerical investigation of storm structure and evolution during the July 1999 Las Vegas flash flood. *Mon. Wea. Rev.*, **131**, 2038–2059.

Liang, X. Z., H. I. Choi, K. E. Kunkel, Y. Dai, E. Joseph, J. X. L. Wang, and P. Kumar, 2005a: Development of the regional climate-weather research and forecasting (CWRF) Model: Surface boundary conditions. Illinois State Water Survey.

———, 2005b: Surface boundary conditions for mesoscale regional climate models. *Earth Interactions*, **9 (18)**, 1–28.

Liang, X. Z., K. E. Kunkel, and A. N. Samel, 2001: Development of a regional climate model for U.S. midwest applications. Part 1: Sensitivity to buffer zone treatment. *J. Climate*, **14**, 4363–4378.

Liang, X. Z., L. Li, A. Dai, and K. E. Kunkel, 2004a: Regional climate model simulation of summer precipitation diurnal cycle over the United States. *Geophys. Res. Lett.*, **31**, L24 208, doi:10.129/2004GL021 054.

Liang, X. Z., L. Li, K. E. Kunkel, M. Ting, and J. X. L. Wang, 2004b: Regional climate model simulation of U.S. Precipitation during 1982-2002. Part I: Annual cycle. *J. Climate*, **17**, 3510–3529.

Liang, X. Z., J. Pan, J. Zhu, K. E. Kunkel, J. X. L. Wang, and A. Dai, 2006: Regional climate model downscaling of the U. S. summer climate and future change. *J. Geophys. Res.*, **111**, D10 108.

Lin, X., D. A. Randall, and L. D. Fowler, 2000: Diurnal variability of the hydrological cycle and radiative fluxes: comparisons between observations and a GCM. *J. Climate*, **13**, 4159–4179.

Lin, Y., K. E. Mitchell, E. Rodgers, M. E. Baldwin, and G. I. DiMego, 1999: Test assimilations of the real-time, multi-sensor hourly precipitation analysis into the NCEP Eta model. *8th Conf. on Mesoscale Meteorology*, Boulder, CO, Amer. Meteor. Soc., 341–344.

Liu, S., W. Gao, X. Z. Liang, H. Zhang, and J. Slusser, 2006: Sensitivity of CWRF simulations of the China 1998 summer flood to cumulus parameterizations. *Proceeding of SPIE the International Society for Optical Engineering*, DOI:10.1117/12.676216, Vol. 6298, 62981I.

Lo, J. C. F., Z. L. Yang, and R. A. P. Sr., 2008: Assessment of three dynamical climate downscaling methods using the Weather Research and Forecasting (WRF) model. *J. Geophys. Res.*, **113**, D09 112, doi:10.1029/2007JD009 216.

McGuffie, K., A. Henderson-Sellers, N. Holbrook, Z. Kothavala, O. Balachova, and J. Hoekstra, 1999: Assessing simulations of daily temperature and precipitation variability with global climate models for present and enhanced greenhouse climates. *Int. J. Climatol.*, **19**, 1–26.

Mearns, L. O., R. Arritt, G. Boer, D. Caya, P. Duffy, F. Giorgi, W. Gutowski, I. Held, R. Jones, R. Laprise, L. R. Leung, J. Pal, J. Roads, L. Sloan, R. Stouffer, G. Takle, and W. Washington, 2005: North American Regional Climate Change Assessment Program. *16th Conference on Climate Variability and Change*, San Diago, CA, Amer. Meteor. Soc.

Meehl, G. A., J. M. Arblaster, and C. Tebaldi, 2005: Understanding future patterns of increased precipiation intensity in climate model simulations. *Geophys. Res. Lett.*, **32**, L18 719.

Meehl, G. A., T. F. Stocker, W. D. Collins, P. Friedlingstein, A. T. Gaye, J. M. Gregory, A. Kitoh, R. Knutti, J. M. Murphy, A. Noda, S. C. B. Raper, I. G. Watterson, A. J. Weaver, and Z. C. Zhao, 2007: *Climate Change 2007: The Physical Science Basis. Contribution of Working Group I to the Fourth Assessment Report of the Intergovernmental Panel on Climate Change*, Cambridge University Press, Cambridge, United Kingdom and New York, NY, USA, Chap. Global Climate Projections, 100.

Mesinger, F., G. DiMego, E. Kalnay, K. Mitchell, P. C. Shafran, W. Ebisuzaki, D. Jovic, J. Woollen, E. Rogers, E. H. Berbery, M. B. Ek, Y. Fan, R. Grumbine, W. Higgins, H. Li, Y. Lin, G. Manikin, D. Parrish, and W. Shi, 2006: North American regional reanalysis. *Bull. Amer. Meteor. Soc.*, **87**, 343–360.

Miguez-Macho, G., G. L. Stenchikov, and A. Robock, 2005: Regional climate simulations over North America: Interaction of local processes with improved large-scale flow. *J. Climate*, **18**, 1227–1246.

Milly, P. C. D., K. A. Dunne, and A. V. Vecchia, 2005: Global pattern of trends in streamflow and water availability in a changing climate. *Nature*, **438**, 347–350.

Milly, P. C. D., R. T. Wetherald, K. A. Dunne, and T. L. Delworth, 2002: Increasing risk of great floods in a changing climate. *Nature*, **415**, 514–517.

Mo, K. C., M. Chelliah, M. L. Carrera, R. W. Higgins, and W. Ebisuzaki, 2005: Atmospheric moisture transport of the United States and Mexico as evaluated in the NCEP Regional Reanalysis. *J. Hydrology*, **6**, 710–728.

Moorthi, S. and M. J. Suarez, 1992: Relaxed Arakawa-Schubert: A parameterization of moist convection for general circulation models. *Mon. Wea. Rev.*, **120**, 978–1002.

Nearing, M. A., V. Jetten, C. Baffaut, O. Cerdan, A. Couturier, M. Hernandez, Y. L. Bissonnais, M. H. Nichols, J. P. Nunes, C. S. Renschler, V. Souchère, and K. van Oost, 2005: Modeling response of soil erosion and runoff to changes in precipitation and cover. *Catena*, **61**, 131–154.

Nijssen, B., G. M. O'Donnell, A. F. Hamlet, and D. P. Lettenmaier, 2001: Hydrologic sensitivity of global rivers to climate change. *Climatic Change*, **50**, 143–175.

Nohara, D., A. Kitoh, M. Hosaka, and T. Oki, 2007: Impact of climate change on river runoff using multi-model ensemble. *J. Hydrometeorology*, in press.

NRC, 2003: *Understanding climate change feedbacks*. National Research Council Panel on Climate Change Feedbacks, National Academies Press, Washington D.C., 152 pp.

Oki, T. and S. Kanae, 2006: Global hydrological cycles and world water resources. *Science*, **313**, 1068–1072.

Pall, P., M. R. Allen, and D. A. Stone, 2007: Testing the Clausius-Clapeyron constraint on changes in extreme precipitation under CO_2 warming. *Clim. Dynam.*, **28**, 351–363.

Pan, D. M. and D. A. Randall, 1998: A cumulus parameterization with a prognostic closure. *Quart. J. Roy. Meteor. Soc.*, **124**, 949–981.

Pan, H. L. and W. S. Wu, 1994: Implementing a mass flux convective parameterization package for the NMC medium-range forecast model. *10th Conf. on Numerical Weather Prediction*, Portland, OR, Amer. Meteor. Soc., 96–98.

Pan, Z., R. W. Arritt, E. S. Takle, W. J. G. Jr., C. J. Anderson, and M. Segal, 2004: Altered hydrologic feedback in a warming climate introduces a "warming hole". *Geophys. Res. Lett.*, **31 (L17109)**, doi:10.1029/2004GL020 528.

Pan, Z., J. H. Christensen, R. W. Arritt, W. J. G. Jr., E. S. Takle, and F. Otieno, 2001: Evaluation of uncertainties in regional climate change simulations. *J. Geophys. Res.*, **106 (D16)**, 17 735–17 751.

Peterson, B. J., J. McClelland, R. Curry, R. M. Holmes, J. E. Walsh, and K. Aagaard, 2006: Trajectory shifts in the arctic and subarctic freshwater cycle. *Science*, **313**, 1061–1066.

Plummer, D. A., D. Caya, A. Frigon, H. Côté, M. Giguère, D. Paquin, S. Binder, R. Harvey, and R. de Elia, 2006: Climate and climate change over North America as simulated by the Canadian Regional Climate Model. *J. Climate*, **19**, 3112–3132.

Pryor, S. C., J. A. Howe, and K. E. Kunkel, 2009: How spatially coherent and statistically robust are temporal changes in extreme precipitation in the contiguous USA? *Int. J. Climatol.*, **29**, 31–45.

Randall, D. A., Harsvardhan, and D. A. Dazlich, 1991: Diurnal variability of the hydrologic cycle in a general circulation model. *J. Atmos. Sci.*, **48**, 40–62.

Randall, D. A., T. A. Wood, S. Bony, R. Colman, T. Fichefet, J. Fyfe, V. Kattsov, A. Pitman, J. Shukla, J. Srinivasan, R. J. Stouffer, A. Sumi, and K. E. Taylor, 2007: Climate Models and Their Evaluation. *Climate Change 2007: The Physical Science Basis. Contribution of Working Group I to the Fourth Assessment Report of the Intergovernmental Panel on Climate Change*, Solomon, S., D. Qin, M. Manning, Z. Chen, M. Marquis, K. B. Averyt, M. Tignor, and H. L. Miller, Eds., Cambridge University Press, Cambridge, United Kingdom and New York, NY, USA.

Rasch, P. J. and J. E. Kristjànsson, 1998: A comparison of the CCM3 model climate using diagnosed and predicted condensate parameterizations. *J. Climate*, **11**, 1587–1614.

Roads, J. O., S. C. Chen, A. K. Guetter, and K. P. Georgakakos, 1994: Large-scale aspects of the United States hydrologic cycle. *Bull. Amer. Meteor. Soc.*, **75**, 1589–1610.

Ross, R. J. and W. P. Elliott, 2001: Radiosonde-based Northern Hemisphere tropospheric water vapor trends. *J. Climate*, **14**, 1602–1612.

Rotstayn, L. D., 1997: A physically based scheme for the treatment of stratiform clouds and precipitation in large-scale models. I: Description and evaluation of microphysical processes. *Quart. J. Roy. Meteor. Soc.*, **123**, 1227–1282.

Ruiz-Barradas, A. and S. Nigam, 2005: Warm-season rainfall variability over the US Great Plains in observations, NCEP and ERA-40 reanalyses, and NCAR and NASA atmospheric model simulations. *J. Climate*, **18**, 1808–1830.

———, 2006: Great Plains hydroclimate variability: The view from the North American Regional Reanalysis. *J. Climate*, **19**, 3004–3010.

Salathé, E. P., Jr., R. Steed, C. F. Mass, and P. H. Zahn, 2008: A high-resolution climate model for the U.S. Pacific Northwest: Mesoscale feedbacks and local responses to climate change. *J. Climate*, **21**, 5708–5726.

Santer, B. D., C. Mears, F. J. Wentz, K. E. Taylor, P. J. Gleckler, T. M. L. Wigley, T. P. Barnett, J. S. Boyle, W. Brüggemann, N. P. Gillet, S. A. Klein, G. A. Meehl, T. Nozawa, D. W. Pierce, P. A. Stott, W. M. Washington, and M. F. Wehner, 2007: Indentification of human-induced changes in atmospheric moisture content. *Proc. Natl. Acad. Sci. U.S.A.*, **104**, 15 248–15 253.

Schmidt, G. A., R. Ruedy, J. E. Hansen, I. Aleinov, N. Bell, M. Bauer, S. Bauer, B. Cairns, V. Canuto, Y. Cheng, A. DelGenio, G. Faluvegi, A. D. Friend, T. M. Hall, Y. Hu, M. Kelley, N. Y. Kiang, D. Koch, A. A. Lacis, J. Lerner, K. K. Lo, R. L. Miller, L. Nazarenko, V. Oinas, J. Perlwitz, J. Perlwitz, D. Rind, A. Romanou, G. L. Russell, M. Sato, D. T. Shindell, P. H. Stone, S. Sun, N. Tausnev, D. Thresher, and M. S. Yao, 2006: Present day atmospheric simulations using GISS ModelE: Comparison to in-situ, satellite, and reanalysis data. *J. Climate*, **19**, 153–192.

Seager, R., M. Ting, I. Held, Y. Kushnir, J. Lu, G. Vecchi, H. P. Huang, N. Harnick, A. Leetmaa, N. C. Lau, C. Li, J. Velez, and N. Naik, 2007: Model projections of an imminent transistion to a more arid climate in southwestern North America. *Science*, **316**, 1181–1184.

Sillmann, J. and E. Roeckner, 2008: Indices for extreme events in projections of anthropogenic climate change. *Climatic Change*, **86**, 83–104.

Stephens, G. L. and T. D. Ellis, 2008: Controls of global-mean precipitation increases in global warming GCM experiments. *J. Climate*, **21**, 6141–6155.

Sun, B., P. Y. Groisman, and I. I. Mokhov, 2001: Recent changes in cloud type frequency and inferred increases in convection over the United States and the former USSR. *J. Climate*, **14**, 1864–1880.

Sun, Y., S. Solomon, A. Dai, and R. W. Portmann, 2006: How often does it rain? *J. Climate*, **19**, 916–934.

———, 2007: How often will it rain? *J. Climate*, **20**, 4801–4818.

Sundqvist, H., 1978: A parameterization scheme for nonconvective condensation including prediction of cloud water content. *Quart. J. Roy. Meteor. Soc.*, **104**, 677–690.

Sundqvist, H., E. Berge, and J. E. Kristjànsson, 1989: Condensation and cloud parameterization studies with a mesoscale numerical weather prediction model. *Mon. Wea. Rev.*, **117**, 1641–1657.

Suppiah, R. and K. J. Hennessy, 1998: Trends in total rainfall, heavy rainfall events, and number of dry events in Australia, 1910-1990. *Int. J. Climatol.*, **10**, 1141–1164.

Takle, E. S., W. J. G. Jr., R. W. Arritt, Z. Pan, C. J. Anderson, R. R. da Silva, D. Caya, S. C. Chen, F. Giorgi, J. H. Christensen, S. Y. Hong, H. M. H. Juang, J. Katzfey, W. M. Lapenta, R. Laprise, G. E. Liston, P. Lopez, J. McGregor, R. A. P. Sr., and J. O. Roads, 1999: Project to Intercompare Regional Climate Simulations (PIRCS): Description and initial results. *J. Geophys. Res.*, **104 (D16)**, 19 443–19 461.

Tebaldi, C., K. Hayhoe, J. M. Arblaster, and G. A. Meehl, 2006: Going to the extremes. *Climatic Change*, **79**, 185–211.

Tiedtke, M., 1989: A comprehensive mass flux scheme for cumulus parameterization in large-scale models. *Mon. Wea. Rev.*, **117**, 1779–1800.

———, 1993: Representation of clouds in large-scale models. *Mon. Wea. Rev.*, **121**, 3040–3061.

Trenberth, K. E., 1998: Atmospheric moisture residence times and cycling: implications for rainfall rates and climate change. *Climatic Change*, **39**, 667–694.

Trenberth, K. E., A. Dai, R. M. Rasmussen, and D. B. Parsons, 2003: The changing character of precipitation. *Bull. Amer. Meteor. Soc.*, **84**, 1205–1217.

Trenberth, K. E. and C. J. Guillemot, 1998: Evaluation of the atmospheric moisture and hydrological cycle in the NCEP/NCAR reanalyses. *Clim. Dynam.*, **14**, 213–231.

Tselioudis, G. and W. B. Rossow, 2006: Climate feedback implied by observed radiation and precipitation changes with midlatitude storm strength and frequency. *Geophys. Res. Lett.*, **33**, L02 704.

Vanrheenen, N. T., A. W. Wood, R. N. Palmer, and D. P. Lettenmaier, 2004: Potential implications of PCM climate change scenarios for Sacramento-San Joaquin River Basin hydrology and water resources. *Climatic Change*, **62**, 257–281.

Vecchi, G. A. and B. J. Soden, 2006: Global warming and the weakening of the tropical circulation. *J. Climate*, **20**, 4316–4340.

von Storch, H. and F. W. Zwiers, 1999: *Statistical Analysis in Climate Research*. Cambridge University Press, Cambridge, UK, 484 pp.

Vorosmarty, C. J., P. Green, J. Salisbury, and R. B. Lammers, 2000: Global water resources: vulnerablility from climate change and population growth. *Science*, **289**, 284–288.

Wang, J. and X. Zhang, 2008: Downscaling and projection of winter extreme daily precipitation over North America. *J. Climate*, **21**, 923–937.

Wang, W., D. Barker, J. Bray, C. Bruyère, M. Duda, J. Dudhia, D. Gill, and J. Michalakes, 2007: *ARW Version 2 Modeling System User's Guide*. Mesoscale and Microscale Meteorology Division, National Center for Atmospheric Research.

Watterson, I. G., 2006: The intensity of precipitation during extratropical cyclones in globa warming simulations: a link to cyclone intensity? *Tellus*, **58A**, 82–97.

West, G. L., W. J. Steenburge, and W. Y. Y. Chen, 2006: Spurious grid-scale convection in the North American Regional Reanalysis. *Mon. Wea. Rev.*, **135**, 2168–2184.

Willett, K. M., N. P. Gillet, P. D. Jones, and P. W. Thorne, 2007: Attribution of observed surface humidity changes to human influence. *Nature*, **449**, 710–712.

Xie, S., K. M. Xu, R. T. Cederwall, P. Bechtold, A. D. DelGenio, S. A. Klein, D. G. Cripe, S. J. Ghan, D. Gregory, S. F. Iacobellis, S. K. Krueger, U. Lohmann, J. C. Petch, D. A. Randall, L. D. Rotstayn, R. C. J. Somerville, Y. C. Sud, K. V. Salzen, G. K. Walker, A. Wolf, J. J. Yio, G. J. Zhang, and M. Zhang, 2002: Intercomparison and evaluation of cumulus parameterizations under summertime midlatitude continental conditions. *Quart. J. Roy. Meteor. Soc.*, **128**, 1095–1135.

Zhang, G. J. and N. A. McFarlane, 1995: Sensitivity of climate simulations to the parameterization of cumulus convection in the Canadian Climate Centre general circulation model. *Atmos. -Ocean*, **33**, 407–446.

Zhang, M., W. Lin, C. S. Bretherton, J. J. Hack, and P. J. Rasch, 2003: A modified formulation of fractional stratiform condensation rate in the NCAR Community Atmospheric Model (CAM2). *J. Geophys. Res.*, **108**, doi:10.1029/2002JD002 523.

Appendix: The Sensitivity of Precipitation to Convective Parameterization

Additional simulations were completed using the WRF-CCSM with the BMJ convective parameterization scheme in place of the KF convective parameterization. These simulations were not included in the main document for two key reasons. First, a full decade of simulations for the late 20th and 21st centuries has not been completed, making a thorough comparison difficult. Second, simulations using the BMJ scheme do not show as much of an improvement over the CCSM compared to those using the KF parameterization. Although the latter point was made in section 4, this appendix will briefly expand on the differences between the simulations using the KF and BMJ schemes in MJJA for a full 5-year period in the late 20th and 21st centuries.

As Fig. 40 demonstrates, similar problems exist in the pattern of 1991-1995 MJJA average precipitation from the WRF-CCSM using the BMJ scheme, as were present in just the 1991 MJJA average (see simulation I in Figs. 18 and 19). Mainly, too little precipitation is produced over the FL peninsula. Compared to Fig. 20, the KF scheme counterpart to Fig. 40, this is the most obvious problem. Though not particularly apparent without a more detailed color-scale, there is also more precipitation in the Southwest, along the Appalachians, off the Southeastern seaboard, and less precipitation over the Gulf of Mexico in the simulations using the BMJ CPS. The bulk of these differences are statistically significant over most of their extent (not shown).

More variation is seen in some of the details regarding the type of precipitation produced in these simulations, as illustrated in Fig. 41 for the central U.S. Here, the frequency of precipitation is less in the simulations using the BMJ for all but the lightest 6h average events (Fig. 41, panels a, b, and c). Peculiarly, much of this difference is caused by a change in the character of the distribution of precipitation produced by the convective parameterization. As panels d-f of Fig. 41 show, the simulations using the BMJ scheme have more frequent light convective precipitation components, but the contributions by the convective scheme are much less frequent in many other categories. It is obvious, therefore,
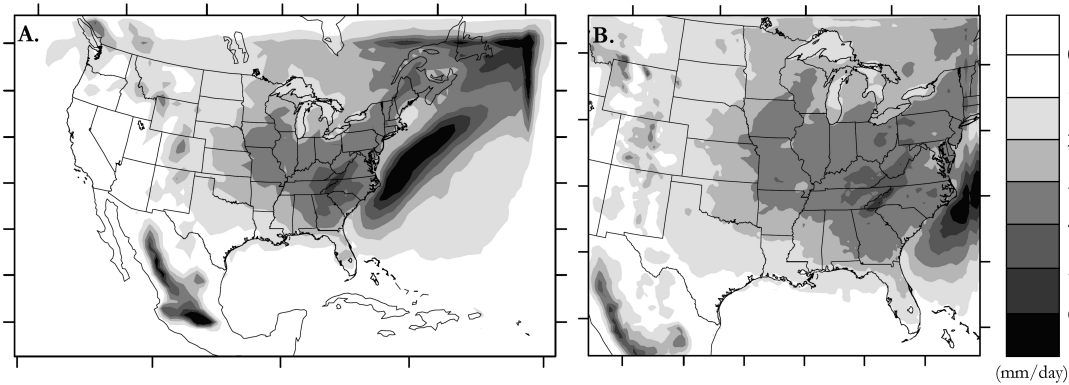
120

FIG. 40. 1991-1995 MJJA average precipitation rate (mm/day) from A) WRF-CCSM (BMJ) 90-km parent domain, B) WRF-CCSM (BMJ) 30-km inner nest.

that the central U.S. very heavy to extreme precipitation events occurring in the simulations using the BMJ scheme are produced primarily by resolved precipitation (as shown for the 30-km simulations; the 90-km simulations illustrate similar trends over the entire domain (not shown)).

It is difficult to assess the sensitivity of precipitation projections with only 5 simulation years available in the late 21st century. Interannual variability is more likely to play a role in influencing the differences between the late 20th and 21st century periods. However, some interesting sensitivities have been noted and are briefly described below.

It must first be noted that on average, simulated warm-season precipitation over the U.S. is less from 2091-2095 than it is from 2090-2099. That is, the second-half of the 2090's is wetter than the first-half in both sets of WRF-CCSM simulations; therefore, the differences projected in Fig. 42 are stronger[18]. The projected differences in average warm-season precipitation are, however, reasonably similar. Except for a small part of the Southwest, there are decreases in precipitation over most of the U.S. Trends in the same simple statistics used in section 6.b between 1991-1995 and 2091-2095 over the central U.S. are also similar. Both sets of simulations indicate a decrease in the number of 6h wet periods by about 34% and an increase of around 10% in the number of dry periods. Despite an increase in water vapor content over the central U.S., both also contain a decrease in the S6II. When

---

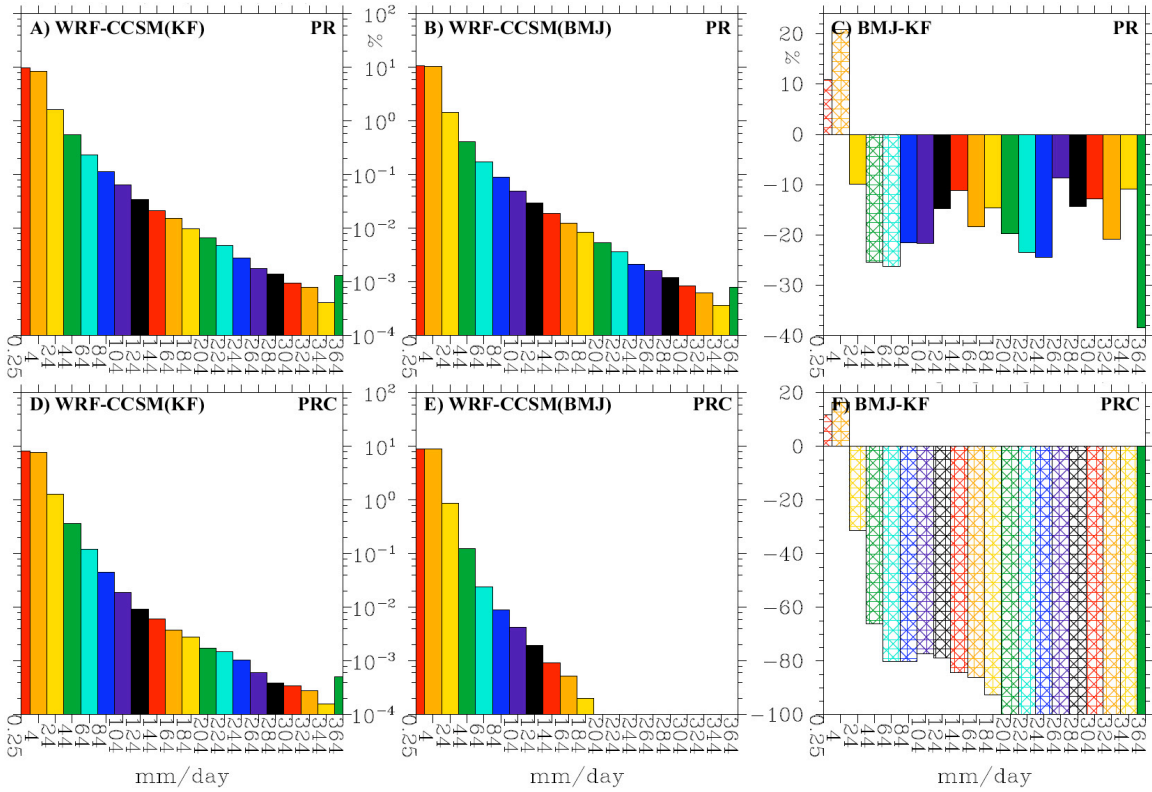[18]The 1991-1995 period is comparable to the 1990-1999 period

FIG. 41. A-C) 1991-1995 MJJA frequency distribution for 6h average precipitation rates (PR, mm/day) from the WRF-CCSM using A) the KF scheme and B) the BMJ scheme: C) is the percent difference between B) and A). D-F) As in A-C), but for the convective precipitation component only (PRC). All panels are from the 30-km simulations for the region outlined in Fig. 22, panel b: the central U.S. Hatching indicates that the difference is significant at the 10% level.
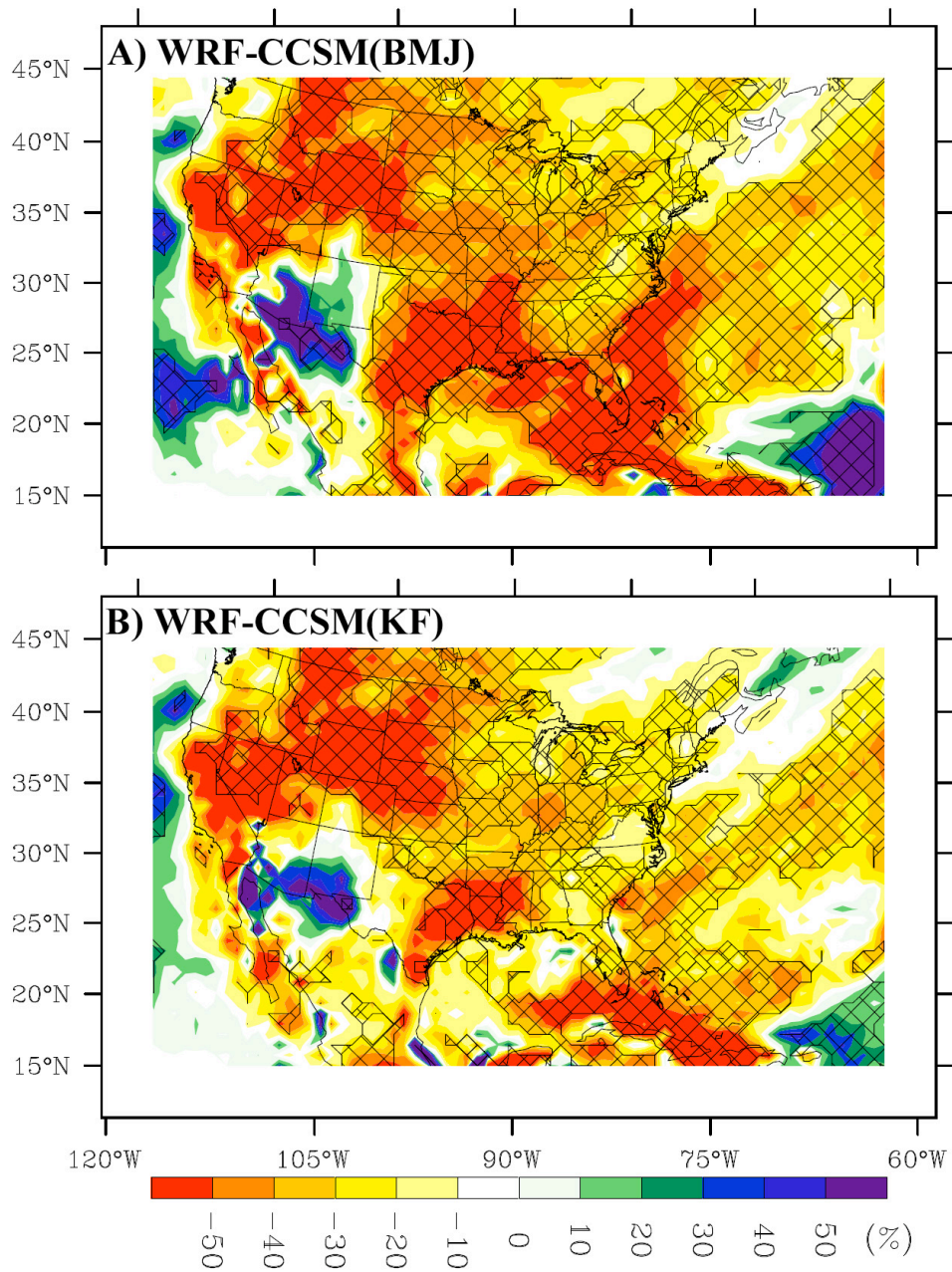
FIG. 42. Percent difference between 2091-2095 and 1991-1995 MJJA average precipitation from the 90-km WRF-CCSM domain using A) the BMJ CPS and B) the KF CPS. Hatching indicates that the difference is significant at the 10% level.

it rains in the simulations using the BMJ scheme, it is about 15% less intense, and in the simulations using the KF scheme it is about 7% less intense. There is still an increase in the frequency of the extreme precipitation events in the WRF-CCSM using the KF scheme though (Fig. 43a). This is not the case in the simulations using the BMJ CPS (Fig. 43c); in these there is a strong decrease in the frequency of all precipitation events. Given an increase in atmospheric moisture content, a decrease in the intensity of precipitation and a decrease in the frequency of *all* precipitation categories is not intuitive and the cause remains unexplained at this time. There is, at least, an increase in the frequency of heavy *convective* precipitation (Fig. 43d), though not of a large enough magnitude to offset the decrease in the frequency of resolved precipitation[19].

A complete explanation for the behavior of the BMJ scheme has not been determined. It is assumed that the difference in adjustment techniques used in each scheme accounts for the differences (see section 4.a.1 for more details on the convective parameterizations). The general environment simulated in the WRF, especially in the central U.S., combined with the reference profile-type adjustment used in the BMJ scheme must not be conducive to heavy precipitation production. It may also be that the scheme is unable to trigger with a high enough frequency in the simulated environment; thus, resolved precipitation is produced to remove excess moisture and instability from the atmosphere.

Since the simulations using the KF CPS show more improvement in the pattern of warm-season precipitation and in the production of intense precipitation events, it was chosen for use in the bulk of this work. The simulations using the KF CPS also contain fewer instances of resolved precipitation; therefore, it could be said that the model using the KF CPS is entering "failure mode" less often in terms of the removal of instability from the atmosphere through the CPS. It is unclear at this time how often grid-point storms are

---

[19]A similar comparison can be made between Fig. 43, panels a and b, but in this case, an increase in the frequency of heavy convective precipitation is responsible, in part, for the increase in the frequency of total extreme precipitation events. This comparison, though not shown, is even stronger between the 1990-1999 and 2090-2099 periods. In that case, changes in frequency in the central U.S. are clearly due to changes in convective precipitation.
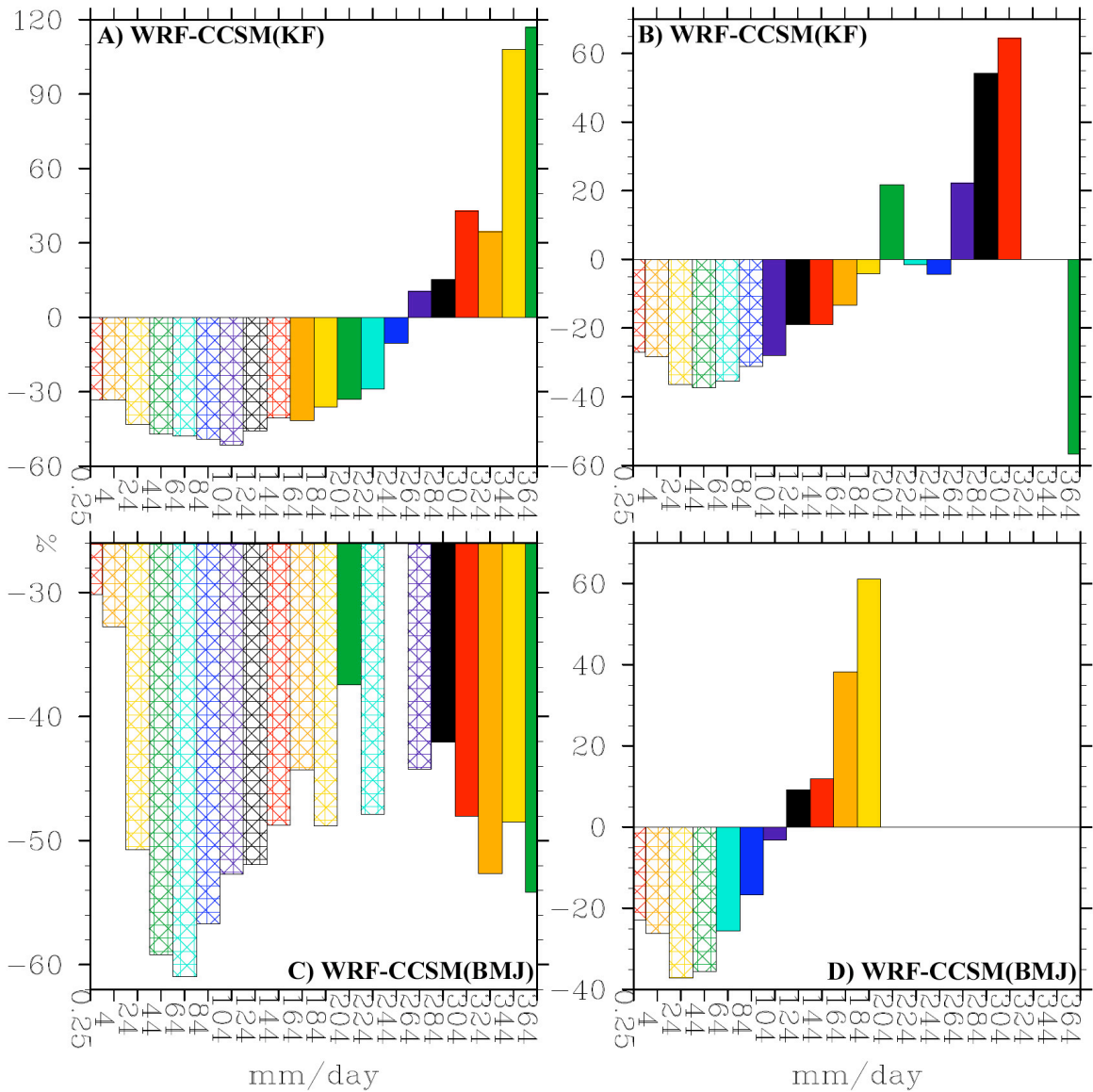
FIG. 43. Percent difference between 2090-2099 and 1990-1999 MJJA 6h average precipitation rate frequency distribution from the WRF-CCSM 30-km nest for the region shown in Fig. 25c (central U.S. only). A) Total precipitation from the WRF-CCSM using the KF CPS. B) As in A), but for convective precipitation only. C) As in A), but using the BMJ CPS. D) As in A), but for convective precipitation only. Hatching indicates that the difference is significant at the 10% level.

produced in the simulations, but given the smooth frequency distributions for convective and total precipitation from the simulations using the KF CPS, it is clear that grid-point storms do not make up an extraordinarily disproportionate amount of the heavy to extreme 6h average precipitation events in the central U.S.

Though not comprehensive, this appendix was added because it does clearly show that choice of convective parameterization will influence predictions of precipitation on a climatological scale. Clearly, this is an area where further research is warranted.